NASA TECHNICAL NOTE

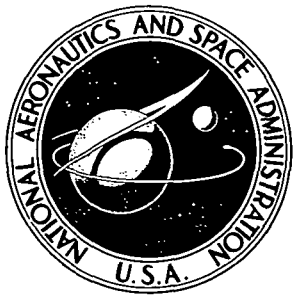

NASA TN D-7906

NASA TN D-7906

PERFORMANCE OF AN ISOLATED TWO-DIMENSIONAL VARIABLE-GEOMETRY WEDGE NOZZLE WITH TRANSLATING SHROUD AND COLLAPSING WEDGE AT SPEEDS UP TO MACH 2.01

Donald L. Maiden

Langley Research Center
Hampton, Va. 23665

NATIONAL AERONAUTICS AND SPACE ADMINISTRATION • WASHINGTON, D. C. • APRIL 1975

1. Report No.	2. Government Accession No.	3. Recipient's Catalog No.
NASA TN D-7906		

4. Title and Subtitle	5. Report Date
PERFORMANCE OF AN ISOLATED TWO-DIMENSIONAL VARIABLE-GEOMETRY WEDGE NOZZLE WITH TRANSLATING SHROUD AND COLLAPSING WEDGE AT SPEEDS UP TO MACH 2.01	April 1975
	6. Performing Organization Code
7. Author(s)	8. Performing Organization Report No.
Donald L. Maiden	L-9976
	10. Work Unit No.
9. Performing Organization Name and Address	505-04-11-01
NASA Langley Research Center Hampton, Va. 23665	11. Contract or Grant No.
	13. Type of Report and Period Covered
12. Sponsoring Agency Name and Address	Technical Note
National Aeronautics and Space Administration Washington, D.C. 20546	14. Sponsoring Agency Code

15. Supplementary Notes

16. Abstract

A wind-tunnel investigation has been conducted to determine the aeropropulsion performance (thrust-minus-drag) of a single-engine, variable-geometry, two-dimensional (2-D) wedge nozzle with simulated translating-shroud and collapsing-wedge mechanisms. The investigation was conducted statically and at Mach numbers from 0.60 to 2.01 at an angle of attack of 0° and at varied jet total-pressure ratios up to 21, depending on the Mach number. The results indicate that the isolated aeropropulsion performance of a variable-geometry two-dimensional wedge nozzle is competitive with axisymmetric nozzles at transonic and supersonic speeds, but the isolated performance is slightly inferior for static take-off and low subsonic speeds. With the use of a simple tertiary-air ejector, the static take-off performance was increased.

17. Key Words (Suggested by Author(s))	18. Distribution Statement
2-D nozzle Nozzle integration Vectoring nozzle Thrust-reversing nozzle	Unclassified – Unlimited New Subject Category 01

19. Security Classif. (of this report)	20. Security Classif. (of this page)	21. No. of Pages	22. Price*
Unclassified	Unclassified	75	$4.25

*For sale by the National Technical Information Service, Springfield, Virginia 22151

PERFORMANCE OF AN ISOLATED TWO-DIMENSIONAL VARIABLE-GEOMETRY WEDGE NOZZLE WITH TRANSLATING SHROUD AND COLLAPSING WEDGE AT SPEEDS UP TO MACH 2.01

Donald L. Maiden
Langley Research Center

SUMMARY

An investigation has been conducted to determine the aeropropulsion performance (thrust-minus-drag) of a single-engine, variable-geometry, two-dimensional (2-D) wedge nozzle with simulated translating-shroud and collapsing-wedge mechanisms. The investigation was conducted statically and at Mach numbers from 0.6 to 1.20 at an angle of attack of 0^{o} in the Langley 16-foot transonic tunnel and at a Mach number of 2.01 at an angle of attack of 0^{o} in the Langley 4-foot supersonic pressure tunnel. The jet total-pressure ratio was varied up to 21 depending on Mach number.

The results of this investigation indicate that the isolated aeropropulsion performance of a variable-geometry two-dimensional wedge nozzle is competitive with axisymmetric nozzles at transonic and supersonic flight Mach numbers, but the isolated performance is slightly inferior (1 percent to 2 percent of the ideal thrust) for static take-off and low subsonic Mach numbers. With the use of a simple tertiary air ejector, the static take-off performance of the two-dimensional wedge nozzle was increased about 1 percent of the ideal thrust.

INTRODUCTION

Airplanes that operate at subsonic and supersonic speeds require propulsion-exhaust nozzles with variable geometry for high performance over a wide range of engine-power settings. Because of the high internal performance attainable with axisymmetric nozzles, this type of nozzle has been used in past and current aircraft designs. However, many airplane aft-end drag problems arise with present-day multiengine configurations because of the complex aft-end flow field and the "round" geometry of the nozzles. Such problems arise especially if the horizontal-tail surfaces are mounted on booms which extend aft of the nozzle exits. (See ref. 1.) Generally, multiengine airplane designs result in a large boattailed "gutter" interfairing, or base region between the nozzles. These regions, as well as the nozzle boattail, are subject to adverse interference effects, especially if the external flow separates from the afterbody near the nozzle exits. The flow interference

created by horizontal and vertical tails can induce flow separation over a large section of the nozzle boattail, and thereby increase the aft-end drag. (See ref. 2.)

Two-dimensional (2-D) wedge nozzles, properly integrated with the airframe, offer improved aeropropulsion performance (thrust-minus-drag performance) by eliminating the large boattail gutter between the engine nacelles, and/or the booms and the nozzles. Figure 1 illustrates this concept integrated with a twin-engine configuration. In addition, the two-dimensional wedge nozzle is inherently better suited for inflight thrust vectoring (with supercirculation lift if properly integrated with the airframe, as discussed in ref. 3) and inflight thrust reversing than are conventional axisymmetric nozzle designs. The wedge centerbody can be used as a carry-through structure for the horizontal tails to reduce weight; it also can be used with cooling air to suppress significantly infrared radiation when compared with conventional nozzles.

Because of the potential advantages offered by two-dimensional wedge nozzles, a program has been initiated at the Langley Research Center to evaluate experimentally the advantages to be derived from the use of this type of nozzle. As a part of this program, an investigation of a single-engine configuration has been conducted in the Langley 16-foot transonic and 4-foot supersonic tunnels. One purpose of the investigation was to determine the internal-external aerodynamic performance of a single-engine two-dimensional wedge nozzle with simulated translating-shroud and collapsing-wedge mechanisms throughout the speed range up to a Mach number of 2.01. Another purpose of the investigation was to determine whether the performance of the two-dimensional wedge nozzle is competitive with that of other nozzle types.

SYMBOLS

A	area
A_b	effective annular area between metal bellows and surrounding sleeve, m^2
A_{base}	cross-sectional area of wedge centerbody at truncation station, m^2
A_e	nozzle-exit area, m^2
$A_{e,x}$	area of theoretically fully expanded flow at wedge tip, m^2
A_m	model maximum cross-sectional area, m^2
$A_{m,wedge}$	wedge maximum cross-sectional area, m^2

A_{noz}	nozzle-duct internal cross-sectional area, m^2
A_t	nozzle-throat area, m^2
$A_{turbine}$	simulated turbine cross-sectional area, m^2
$C_{F,i}$	ideal thrust coefficient, F_i/qA_m
D	duct internal diameter, m
D_f	external skin-friction drag of model between stations 67.31 cm and 126.75 cm, positive downstream, N
D_t	throat diameter, m
$F_{a,ap}$	total nozzle-pressure axial force (pressure drag for $\alpha = 0^o$) on portion of model aft of station 126.75 cm, positive downstream, N
$F_{a,n}$	total nozzle axial force (drag at $\alpha = 0^o$) on portion of model aft of station 126.75 cm positive downstream, N
F_{bal}	axial force indicated by balance, positive downstream, N
F_i	ideal isentropic gross thrust, N
F_j	gross thrust, positive upstream, N
L_D	transition duct length from circular cross section to two-dimensional throat, m
L_p	wedge length from leading edge to throat, m
M	free-stream Mach number
$\dot{m}_i$	ideal mass-flow rate, kg/sec
$\dot{m}_j$	measured nozzle-mass flow rate, kg/sec
n	order of elliptical equation (see fig. 6(a))

$p_{b,d}$	pressure acting on downstream bellows, Pa
$p_{b,u}$	pressure acting on upstream bellows, Pa
p_{cav}	model internal-cavity pressure, Pa
$p_{t,j}$	jet total pressure, Pa
p_{∞}	free-stream static pressure, Pa
q	free-stream dynamic pressure, Pa
r	radius, m
r_t	nozzle-throat radius, m
x	distance along center line from leading edge of wedge, m (see fig. 6(b))
Y	lateral distance from plane passing through nozzle crown line and center line, m (see fig. 6(a))
Z	vertical distance from plane passing through nozzle maximum half-breadth line and center line, m (see fig. (6a))
z	distance from center line to surface of wedge, m (see fig. 6(b))
α	angle of attack, deg
β	local boattail angle, deg
β_c	nozzle-chord boattail angle, deg

Abbreviations:

ASME	American Society of Mechanical Engineers
C-D	converging-diverging
$\mathfrak{C}_L$	center line

CRN crown line (see fig. 6)

DPR design pressure ratio based on one-dimensional flow theory

EPR engine-pressure ratio (stagnation to free stream)

L.E. leading edge

MHB maximum half breadth (see fig. 6)

APPARATUS AND METHODS

Wind Tunnels

This investigation was conducted in the Langley 16-foot transonic tunnel and in the Langley 4-foot supersonic pressure tunnel. The Langley 16-foot transonic tunnel is a single-return, continuous-flow, atmospheric wind tunnel with a slotted octagonal test section. The test-section airspeed is continuously variable between Mach numbers of 0.20 and 1.30. A detailed description of the 16-foot transonic tunnel is given in reference 4. The Langley 4-foot supersonic pressure tunnel is a single-return, continuous-flow wind tunnel with a stagnation-pressure range of 27.58 kPa to 206.84 kPa and a stagnation-temperature range from 310 K to 322 K. By the use of flexible tunnel-nozzle walls fitted to a calibrated contour, the tunnel Mach number can be varied from 1.25 to 2.20. A brief description of the Langley 4-foot supersonic pressure tunnel is given in reference 5.

Model and Support System

General arrangement.- Shown in figure 2 are photographs of the air-powered nacelle model with a two-dimensional wedge nozzle installed in the 16-foot transonic tunnel and in the 4-foot supersonic pressure tunnel. The overall model arrangement, illustrated in detail in figure 3, is composed of four major sections:

	Model station, cm
Nose forebody	0 to 67.31
Low pressure plenum	67.31 to 104.01
Instrumentation	104.01 to 126.75
Nozzle	126.75 to 167.10

In this test, the nose forebody section was nonmetric and all the other major sections are part of the metric nacelle. The fixed forebody provided a smooth transition from the circular nose to the rectangular maximum cross-sectional area of the model; the area occurred forward of the metric break. The metric break is illustrated in figure 2

by the double stripe lines. A low-friction teflon seal was inserted in the metric break to eliminate cross flow through the metric-nonmetric interface and to stabilize the cavity-pressure variation without transmission of the axial force at the metric-nonmetric interface.

Internal air supply.- Inside the model, dry high-pressure air, at a stagnation temperature of about 300 K, entered the high-pressure plenum in the nose-forebody through six supply lines in the support strut. The high-pressure air was then introduced, perpendicular to the model axis, into the low-pressure plenum which was supported by the balance as shown in figure 3. The decelerated airflow in the low-pressure plenum was diffused by the bullet fairing over the balance. The airflow was then straightened forward of the instrumentation section by a 75-percent open-area baffle plate constructed of aluminum with holes having a length-to-diameter ratio of 2.5. The air passed through the instrumentation section, where the stagnation conditions were measured, and was exhausted through the test nozzle (illustrated in fig. 2 by the single stripe line).

Force balance-air system.- Air passage from the high-pressure plenum to the low-pressure plenum was through eight sonic nozzles equally spaced around the axis of the high-pressure plenum. Since the high-pressure air was introduced radially to the model axis and an opposing nozzle cancels each jet impingement, the resultant forces and moments were minimal. Therefore, the balance measured only the gross thrust developed by the rearward acceleration of the air and the external aerodynamic forces. The low-pressure plenum was sealed by a set of flexible metal bellows having similar spring constants. The sealing served to compensate the axial forces caused by pressurization.

Model support system.- The model was supported in the tunnel by a sting-strut support with the nose of the model attached to the strut as shown in figures 2 and 3. The center line of the model was located on the wind-tunnel center line with the center line of the sting, which supports the strut, 55.88 cm below that level. (See fig. 3.) The sting portion of the support system was 5.08 cm by 10.16 cm in cross section with the top and bottom capped by half cylinders of 2.54 cm radius. The strut blade was 5 percent thick with a 50.8-cm chord in the streamwise direction. The strut-blade leading and trailing edges were swept 45°. Only the strut support was used in the 4-foot supersonic tunnel installation.

Nozzle configurations.- The component parts of the two-dimensional wedge nozzle are shown by photographs in figure 4. The various nozzle configurations tested are shown in figure 5. The dry-power nozzle configurations (fig. 5(a)) had an external area ratio $A_{e,x}/A_t$ equal to 3.61. These nozzle configurations were tested statically and transonically with internal area ratios equal to 1.05 and 1.53. The afterburner-power configurations (fig. 5(b)) had an external area ratio equal to 1.68. These nozzle configurations were tested statically, transonically, and supersonically with internal area ratios equal to 1.03

and 1.12 with the exception of the truncated-wedge configurations, which generally were not tested above M = 0.9. In addition, an internal area ratio of 1.22 was tested at a Mach number of 2.01.

The design features are shown in figure 6. Figure 6(a) illustrates an overview of the general design features of the two-dimensional wedge nozzle tested in this investigation. The main features of this design are the wedge-centerbody geometry illustrated in figure 6(b) and the nozzle internal area distribution shown in figure 6(c). Figure 6(d) presents the nozzle-duct cross-sectional geometry at several axial locations.

The wedge design was independent of the internal area distribution consideration. The blunt parabolic-profile nose of the wedge centerbody was selected to provide a shallow local slope as the throat station is approached and to minimize the stagnation-temperature concentration at the leading edge of the wedge in a full-scale exhaust nozzle. The 10° half-angle of the wedge was selected to provide higher thrust-minus-drag nozzle performance at transonic speeds with a 10° half-angle as compared with a 15° boattail wedge. The longer wedge surface may also be used for thrust-reversing or thrust-vectoring flaps if so desired. The dry-power wedge cross-sectional area represented 42.3 percent of the maximum nozzle area to allow minimum cowl boattail angles.

The internal area distribution in the nozzle includes the upstream duct transition from a circular cross section to a circumscribed "square" cross section with large rounded corners at the wedge leading-edge station as shown in figure 6(d). The duct transition from round to "square" continues to the throat section shown in figures 6(a) and 6(d). The section downstream of the throat has constant geometry; therefore, the exit area is dependent only on the wedge half-angle. The transition geometry was selected from the data of reference 6 which indicates the optimum transition in a similar nozzle to be $L_D/D = 1.10$ and $L_p/D = 0.50$.

A constant internal area distribution in the transition upstream of the wedge nose was used to minimize the total-pressure loss in the exhaust flow caused by the drastic change in the duct geometry. This distribution was accomplished by reducing the internal area of the duct at the crown line of the nozzle; the reduction resulted in a two-dimensional ramp on the top and bottom of the duct. (See fig. 6(a).) The two-dimensional ramps also serve to divert laterally the exhaust flow entering the converging section of the nozzle, and thereby fill in the corners of the two-dimensional throat to minimize corner losses. Since the sidewalls remain virtually unaltered, the wedge centerbody installation and operation is simplified.

The area distribution of the nozzle from the wedge-nose station to the throat station was designed as a parabolic distribution allowing the necessary area convergence to choke the nozzle at the throat. (See fig. 6(c).) The rationale for the parabolic distribution was

to minimize the local slopes upstream of the throat in order to reduce the risk of flow separation from the 10° wedge surface as the flow is turned down the wedge.

The cowl external profile was designed as a circular-arc boattail angle of 12° to the cowl-exit center line in the vertical plane. (See fig. 6(d).) The vertical profile blends smoothly into the horizontal profile of a 5° circular-arc boattail which reflexes along the sidewall half breadth into a 0° boattail at the wedge trailing edge. A higher cowl boattail angle to the cowl-exit center line in the vertical profile is necessary to turn the exhaust flow down the wedge at forward speeds.

Instrumentation

A six-component strain-gage balance was used to measure the forces and moments on that part of the model downstream of the metric break. (See fig. 3.) Individual pressure transducers were used to determine the jet total pressure and tare pressures (such as internal cavity and differential bellows pressures). A total of 12 total pressures, 15 internal-cavity pressures, and 2 bellows pressures were measured. A thermocouple was used to measure the jet total temperature, and an electronic turbine flowmeter was used to measure the mass flow of the high pressure air. The strut angle of attack was measured by a calibrated electrical potentiometer.

Tests

Tests were conducted in the Langley 16-foot transonic tunnel at Mach numbers from 0 to 1.20. Tests were also conducted in the Langley 4-foot supersonic pressure tunnel statically and at a Mach number of 2.01 at a stagnation pressure of 124.1 Pa and a stagnation temperature of 316.5 K. The angle of attack was restricted to a constant value of 0° during the entire investigation. The Reynolds number based on the model length varied from approximately 18.3×10^6 at $M = 0.6$ to 21.9×10^6 at $M = 1.2$ in the Langley 16-foot transonic tunnel and was approximately 20.8×10^6 at $M = 2.01$ in the Langley 4-foot supersonic pressure tunnel. The ratio of jet total pressure to free-stream static pressure was varied from jet-off to approximately 21 depending on Mach number. The boundary-layer transition on the model was fixed by a 0.254-cm strip of No. 100 grit, 2.54 cm from the nose in accordance with the techniques described in references 7 and 8.

Data Reduction

The wind-tunnel data recorded on magnetic tape were used to compute standard force and pressure coefficients. All force data in this report are referenced to the body axes through the center line of the model. The model angle of attack has been corrected for flow angularity and deflection of the model support caused by aerodynamic-thrust loading.

The basic performance parameter used for the presentation of results is the aeropropulsion thrust ratio $\frac{F_j - F_{a,n}}{F_i}$, which is the ratio of the actual nozzle thrust minus the nozzle axial force (drag) to the ideal nozzle thrust where

$$F_j - F_{a,n} = F_{bal} + (p_{cav} - p_\infty)A_m + (p_{b,d} - p_{b,u})A_b + \Delta K_b + D_f$$

In the foregoing expression, the term F_{bal} is the axial force indicated by the balance, corrected for weight tares and balance interactions. The term $(p_{cav} - p_\infty)A_m$ is a tare-force correction for a pressure difference between the inside and outside of the model. The cavity pressure was measured at 15 locations within the model, and the average pressure was assumed to act on the maximum cross-sectional area A_m. The term $(p_{b,d} - p_{b,u})A_b$ is a bellows dynamic-tare correction which by design should be essentially 0. However, when the internal velocities are high, a small pressure difference between the ends of the bellows exists. In this investigation, the maximum bellows dynamic-tare correction was less than 0.5 percent of the ideal thrust. The term ΔK_b is a bellows static-tare correction which also by design should be 0. However, differences in the spring constants of the forward and aft bellows can cause a slight tare force as the bellows is pressurized. In this investigation the bellows static-tare correction was essentially 0 in the 16-foot transonic tunnel test and less than 0.5 percent of the ideal thrust in the 4-foot supersonic pressure tunnel test. The term D_f is the calculated skin friction on the constant cross-section portion of the model between the metric break at station 67.31 cm and the nozzle station 126.75 cm. For static tests where $M = 0$, the external nozzle axial force $F_{a,n}$ is 0 and the aeropropulsion thrust ratio reduces to F_j/F_i, or the internal performance thrust ratio.

The effect of external flow was determined by subtracting the aeropropulsion thrust ratio $\frac{F_j - F_{a,n}}{F_i}$ from the average internal-performance thrust ratio F_j/F_i obtained from several static runs. The resulting term $F_{a,n}/F_i$ is the magnitude (in percent of ideal thrust) of the effect of the external flow on the external axial force and the internal nozzle performance.

In an attempt to aid performance estimates on aircraft with this type of nozzle installed, all friction drag on the external wetted area of the nozzle has been subtracted and the performance is presented as the ratio of thrust minus axial pressure force to ideal thrust $\frac{F_j - F_{a,ap}}{F_i}$. This term reflects only the external pressure drag and the internal performance. The wedge and internal sideplate friction drag was charged to the nozzle performance.

Data Accuracy

To check the operation of the force-balanced airflow system and the resulting tare corrections, an axisymmetric convergent nozzle (configuration 3 of ref. 9) was tested statically to determine whether the system would repeat the static internal performance determined in reference 9. The "reference" convergent-nozzle internal contour was essentially an ASME long-throat nozzle with a throat area of 45.16 cm^2. The result of the convergent-nozzle static performance test is shown in figure 7. The data indicate that the static internal performance F_j/F_i and the mass-flow repeatability were within 0.5 percent above the jet total-pressure ratio of 2.0 and agreed well with the data from reference 9. The reference convergent nozzle was tested randomly throughout the investigation to verify the data repeatability of the system.

RESULTS AND DISCUSSION

Since the external flow affects the internal performance of plug- and ejector-type nozzles, a complete evaluation of these nozzle types must be made at the flight Mach number and the engine operating-pressure ratio. The internal performance F_j/F_i is important for static take-off condition, but the aeropropulsion performance, or thrust minus-drag of the nozzle, must be determined to evaluate plug and ejector nozzles at forward flight speeds. This evaluation is for the two-dimensional wedge nozzle. The following discussion involves internal performance for static take-off conditions and aeropropulsion performance for forward flight speeds.

Static Take-Off Performance

The static internal-performance characteristics of several two-dimensional wedge nozzle configurations are shown in figure 8. The parameters, the mass-flow ratio $\dot{m}_j/\dot{m}_i$ and the thrust ratio F_j/F_i are shown as a function of the jet total-pressure ratio $p_{t,j}/p_\infty$ for all configurations except the tertiary-air ejector configurations. At $p_{t,j}/p_\infty = 2.5$, peak thrust ratios of about 0.968 and 0.985 were achieved for the unshrouded dry and unshrouded afterburner-power nozzles, respectively. Truncating the dry and afterburner-power nozzles reduced the peak thrust ratios to about 0.945 and 0.977 at $p_{t,j}/p_\infty = 2.5$. The wedge truncation represented only 24 percent of the aft sloping wedge measured along the nozzle center line, but represented a base-area ratio $A_b/A_{m,wedge}$ of 25 percent for the dry, and 43 percent of the afterburner-power nozzle. Similar reductions in the internal performance were shown in reference 10 for a truncated, axisymmetric 15^o cone plug nozzle with similar base to maximum plug-area ratios.

Generally, shrouding the wedge to achieve a higher internal area distribution causes a shift in the peak performance of the nozzle to higher jet total-pressure ratios consistent

with convergent-divergent nozzle design. However, as shown in figure 8(c) for the dry-power nozzle with an internal area ratio of 1.53 and a design pressure ratio of 6.50, a significant decrease in the internal performance is shown as the pressure ratio is increased from about 5.0 to 6.0. This static-performance decrease is probably caused by shock-wave-induced separation on the wedge as a result of the shroud shock impingement on the wedge surface. If most of the wedge tip was separated, the performance of the shrouded wedge would be equivalent to the shrouded truncated wedge at the pressure ratio of 6.0. An inspection of figures 8(c) and 8(d) reveals that the performances are the same.

Figure 9 presents the effect of a tertiary-air ejector on two-dimensional wedge-nozzle static performance. Although the tertiary-air ejector design was not optimum, the data in figure 9 indicate that static internal-thrust performance can be increased up to a jet total-pressure ratio of about 3.0 for both the dry and the afterburner power nozzles. This performance increase is significant because the ejector could also be used in a closed down position to form a shroud to obtain high internal area ratios for high performance at supersonic flight. Incorporating the tertiary-air ejector with this type of two-dimensional wedge nozzle also has attractive structural design features.

Aeropropulsion Performance

Figure 10 presents the variation of the mass-flow ratio with the jet total-pressure ratio at several Mach numbers for the dry and afterburner-power nozzle configurations. Deviation in the mass-flow ratio was generally less than 1 percent for the dry-power configurations and less than 0.5 percent for the afterburner power configurations. These deviations reflect the total accuracy of flow, area, and test condition measurement and should affect thrust-ratio measurements negligibly.

Figures 11 and 12 present the variation of the thrust-minus-axial force ratio with the jet total-pressure ratio at several Mach numbers for the dry and afterburner power nozzles, respectively. Internal-area ratios of 1.05 and 1.53 (shroud translated aft) were tested with and without a wedge truncation of 24 percent. The data in figure 11 indicate that for all test Mach numbers the highest aeropropulsion performance was achieved with the nontruncated baseline nozzle. As expected, the internal area ratio of 1.05 provided the highest aeropropulsion performance up to a jet total-pressure ratio of about 4 at which the performance of the 1.53 internal area ratio became superior. The data in figure 11 also indicate that the 24-percent wedge truncation has an adverse effect on the nozzle aeropropulsion performance with losses incurred of up to 4 percent of the ideal thrust. About 2 percent of this loss is attributed to lower internal performance (see fig. 8), and the remainder is attributed to external flow effects.

The same cowl and translated-shroud length tested with the dry power wedge (see fig. 6) were tested with the afterburner wedge resulting in internal area ratios of 1.03

and 1.12. A longer shroud, resulting in an internal area ratio of 1.22, was tested at a Mach number of 2.01. Only small changes in the internal area ratio were possible with shroud translation as a result of the low boattail angle of the afterburner power wedge. The data in figure 12 indicate very little change in the aeropropulsion performance with Mach number for changes in the internal area ratio from 1.03 to 1.12 with the exception of $M = 2.01$. However, at the higher pressure ratios, slightly higher aeropropulsion performance was achieved for the 1.12 internal area ratio. This higher performance indicates that shroud translation could still be beneficial. The highest aeropropulsion gain (about 2.4 percent of F_i) using the translated shroud with $A_e/A_t = 1.22$ was noted at $M = 2.01$ as shown in figure 12(c). Also shown in figure 12(c) is a representative aeropropulsion performance value for a convergent-divergent nozzle with an area ratio of 1.6. Adverse effects from wedge truncation, although not as severe as with the dry power wedge, still persist with the afterburner wedge.

External flow effects.- The external flow effects on the nozzle wedge and cowl axial-force ratio $F_{a,n}/F_i$ are shown in figure 13 for the dry power nozzle and in figure 14 for the afterburner power nozzle. It should be noted that the term $F_{a,n}$ contains cowl drag and wedge forces as noted in the section "Data Reduction." The data of figures 13 and 14 show that increasing the jet total pressure decreases the cowl and wedge axial force (drag). Most of the drag reduction and/or the increased internal performance is probably the result of favorable jet interference on the wedge boattail surface with the higher boattailed and larger projected-area, dry power wedge showing the greatest effect. The beneficial jet effect is also observed for the truncated-wedge configurations. However, at the jet pressure ratios below about 5, the truncated-wedge configurations exhibit higher drag forces and can be as much as 4 percent of the ideal thrust above the drag forces on the nontruncated-wedge configurations. An observation from these data is that at supersonic speeds it is most important to have small external boattailing on the wedge centerbody and to avoid any wedge truncation.

The variation of the thrust-minus-axial pressure-force ratio $\frac{F_j - F_{a,ap}}{F_i}$ with the jet total-pressure ratio for the dry and the afterburner-power nozzles at several Mach numbers is presented in figures 15 and 16, respectively. As discussed in the section "Data Reduction," the term $\frac{F_j - F_{a,ap}}{F_i}$ does not include the nozzle external-friction drag. The results of figures 15 and 16 are similar to those discussed for figures 11 and 12, respectively, and are presented for reference.

The variation of the aerodynamic ideal thrust coefficient with the jet total-pressure ratio for all configurations is presented in figure 17 for all test Mach numbers. These data are presented for reference only.

Figure 18 presents a schedule of the total-pressure ratio with the flight Mach number for a typical low-bypass turbofan engine. Reference to these data is made in figures 19 to 22.

Figure 19 presents the variation of the thrust-minus-drag ratio with Mach number. These data were obtained from the straight-line fairings of the basic data. Since the peak aeropropulsion performance $\frac{F_j - F_{a,n}}{F_i}$ for the dry power nozzle was attained at jet total-pressure ratios either lower with $(A_e/A_t = 1.05)$ or higher (with $A_e/A_t = 1.53$) than the engine operating pressure-ratio schedule of figure 18, the aeropropulsion performance values shown in figure 19 are not optimized. The values can be improved by matching the internal area ratio of the nozzle to the design area ratios for the engine-operating pressure-ratio schedule (EPR). For example, at $M = 0.60$ the EPR is about 3.4 which requires the internal area ratio to be about 1.14; at $M = 0.90$ the EPR is about 4.15 which requires an internal area ratio of about 1.24. A maximum internal area ratio of about 1.3 appears to be sufficient for subsonic-transonic flight speeds. The data in figure 19 indicate that, even in the off-design case, moderately high values of nozzle thrust-minus-axial force can be obtained with a horizontal wedge nozzle with a translating shroud. It can be noticed that as the Mach number and the engine pressure ratio increase, it is desirable to increase A_e/A_t by shroud translation. In actual operation, the nozzle shroud would be continuously variable from minimum to maximum A_e/A_t, and thus performance could be optimized at each flight condition. This performance can be approximated by fairing a line through the maximum performance points of each A_e/A_t tested; these points are shown in figure 19. In addition, the data in figure 19 show that severe aeropropulsion losses can be incurred with only a small truncation of the wedge.

Figure 20 presents the variation of the thrust-minus-axial pressure force with Mach number at the scheduled pressure ratio. The results of this figure are similar to the the results discussed for figure 19.

Convergent nozzle comparison.- Figure 21 presents the dry power, two-dimensional wedge nozzle and the axisymmetric convergent nozzle performance (from ref. 9) for the jet total-pressure ratio schedule given in figure 18. The axisymmetric convergent nozzle was chosen as a reference nozzle because of its predictable performance and because it had been previously tested on the air-powered model used in this investigation. It should be noted that these comparisons are not direct comparisons because of the differences in the internal area ratio A_e/A_t and the differences in the closure area ratio $\frac{A_m - A_e}{A_m}$ between the convergent and the two-dimensional wedge nozzles. The effects of these differences are discussed in the following comparisons.

For static take-off, the most directly comparable condition, the convergent nozzle performance is about 2 percent of the ideal thrust higher than that of the two-dimensional

wedge nozzle tested. The 2-percent loss in performance encountered with the two-dimensional wedge nozzle is attributed to friction losses on the large internal wetted area, to a small loss of stagnation pressure at the throat caused by the intersection of boundary layers in the corners of the nozzle throat, and to flow separation on the 10^{o} wedge boattail. The 2-percent performance loss can be reduced, as has been shown in figure 9, with the use of a tertiary-air ejector. An increase of about 1 percent of the ideal thrust was achieved with a simple tertiary-air ejector. The ram drag on this type of tertiary-air ejector would cancel the performance gain at or about $M = 0.2$. (See ref. 11.) Therefore, a blow-in-door type of tertiary-air ejector may be a more promising solution to the low two-dimensional wedge-nozzle static performance. The two-dimensional geometry minimizes the adverse effects on nozzle performance as was encountered with earlier axisymmetric blow-in-door ejector installations with interfairings and horizontal-tail booms surrounding the nozzle. (See ref. 1.)

For subsonic speeds, the isolated dry power nozzle performance of the two-dimensional wedge nozzle tested is slightly inferior to the reference convergent nozzle up to approximately $M = 0.85$. Above this Mach number the transonic drag rise and increased nozzle underexpansion losses of the convergent nozzle significantly lower its performance as is shown by the $M = 0.90$ data in figure 21. If the convergent nozzle geometry were changed to convergent-divergent with $A_e/A_t = 1.05$ (equivalent to the baseline two-dimensional nozzle geometry), the resulting axisymmetric C-D nozzle performance should be about 0.5 percent higher than the convergent-nozzle performance shown at $M = 0.90$ for the scheduled pressure ratio. However, it should be noted that the closure area ratio $\frac{A_m - A_e}{A_m}$ of the reference axisymmetric convergent nozzle is lower than that of the two-dimensional wedge nozzle. This condition means that the two-dimensional nozzle tested was charged with more closure area (boattailing) than the reference convergent nozzle. If the closure area ratio of the axisymmetric convergent nozzle were increased to that of the two-dimensional wedge nozzle, the performance should be lower (estimated 0.5 percent of ideal thrust) than the convergent-nozzle performance shown at $M = 0.90$ for the scheduled pressure ratio. These offsetting penalties indicate that the comparisons at $M = 0.90$ in figure 21 are reasonable. These comparisons show that the isolated aeropropulsion performance of the two-dimensional wedge nozzle is competitive with axisymmetric nozzles at transonic Mach numbers less than 1.0. Another interesting observation is that, although the static ($M = 0$) performances of the baseline two-dimensional wedge with $A_e/A_t = 1.05$ or 1.53 are the same at a pressure ratio of 4.15 (as shown in fig. 8), the effect of the external flow (forward speed) is to increase the aeropropulsion performance of the $A_e/A_t = 1.53$ nozzle (with translated shroud) as shown in figure 21 for $M = 0.90$ at the scheduled pressure ratio of 4.15. At $M = 1.20$ the aeropropulsion value for the reference convergent nozzle was computed, subtracting

the theoretical flat-plate friction drag at $M = 1.20$ and the boattail pressure drag from reference 9 from the theoretical internal performance of a convergent nozzle. The isolated nozzle aeropropulsion performance of the two-dimensional wedge nozzle with $A_e/A_t = 1.05$ is shown in figure 21, at $M = 1.20$, to be slightly lower than the convergent-nozzle performance. A significant increase of 2.5 percent was achieved at $M = 1.20$ by translating the shroud to achieve $A_e/A_t = 1.53$ for the dry-power, two-dimensional wedge nozzle.

Figure 22 presents the afterburner-power, two-dimensional wedge nozzle, the axisymmetric convergent nozzle (from ref. 12), and the convergent-divergent nozzle (from ref. 13) aeropropulsion performance at the scheduled jet total-pressure ratios. A similar argument as was discussed for figure 21 is made against direct comparisons with the data of figure 22; however, the difference in the geometrical closure area ratios is less with these axisymmetric nozzle comparisons.

For static acceleration take-off, the most directly comparable condition, the convergent nozzle performance is about 0.5 percent of the ideal thrust higher than that of the two-dimensional wedge nozzle tested. The 0.5-percent loss in performance encountered with the two-dimensional nozzle is attributed mainly to friction force on the large internal wetted area and to a small loss of stagnation pressure at the throat caused by the intersection of boundary layers in the corners of the nozzle throat. As was shown for the dry-power nozzle, the static internal performance of the two-dimensional wedge nozzle was increased almost 1 percent of the ideal thrust with the use of a tertiary-air ejector.

At flight speeds the isolated nozzle afterburner-power performance of the two-dimensional wedge nozzle is slightly inferior to the convergent nozzle until a Mach number slightly higher than 0.60 is attained. At transonic speeds the aeropropulsion performance of the two-dimensional wedge afterburner-power nozzle is superior to that of the convergent nozzle. At $M = 2.01$, the aeropropulsion performance of a convergent-divergent nozzle with a 5° conical boattail and an A_e/A_t of approximately 1.6 was calculated using one-dimensional flow theory and boattail drag measurements from reference 13. Because of the shallow boattail of the afterburner wedge, large values of the internal area ratio cannot be achieved. However, with a moderately long shroud translation an internal area ratio of 1.22 can be obtained. The data in figure 22 at $M = 2.01$ indicate that high values of the aeropropulsion performance can be obtained with relatively low internal area ratios for a two-dimensional wedge nozzle. Hence it is concluded that the two-dimensional wedge nozzle isolated performance can be competitive with the axisymmetric convergent-divergent aeropropulsion performance at supersonic-flight Mach numbers.

CONCLUSIONS

A wind-tunnel investigation has been conducted in the Langley 16-foot transonic and 4-foot supersonic pressure tunnels on a two-dimensional variable-geometry wedge nozzle with a collapsible wedge and a translating shroud. The investigation was conducted statically and at flight speeds up to $M = 2.01$ at an angle of attack of 0°. The jet total-pressure ratio of the simulated exhaust was varied up to 21 depending on Mach number.

The results of the investigation indicate the following:

1. The aeropropulsion isolated performance of a variable-geometry two-dimensional wedge nozzle is competitive with axisymmetric nozzles at transonic and supersonic Mach numbers.

2. For static take-off and low subsonic Mach numbers, the aeropropulsion performance of the variable-geometry two-dimensional wedge nozzle is slightly inferior (1 percent to 2 percent of ideal thrust) to a convergent nozzle. However, with the use of a simple tertiary-air ejector, the static take-off performance of the two-dimensional wedge nozzle was increased about 1 percent of the ideal thrust in this investigation.

3. Truncation of the wedge centerbody to achieve a shorter nozzle can result in significantly lower nozzle performance. A 24-percent wedge truncation of the baseline 10° boattail wedge resulted in a 2-percent loss in the aeropropulsion performance at flight Mach numbers.

Langley Research Center,
National Aeronautics and Space Administration,
Hampton, Va., February 12, 1975.

REFERENCES

1. Runckel, Jack F.: Interference Between Exhaust System and Afterbody of Twin-Engine Fuselage Configurations. NASA TN D-7525, 1974.

2. Galigher, Lawrence L.: Performance of Various Twin-Nozzle Afterbody Configurations of an Air Superiority Fighter-Type Model at Mach Numbers From 0.6 to 2.5. AEDC-TR-72-17, U.S. Air Force, Feb. 1972.

3. Capone, Francis J.: Supercirculation Effects Induced by Vectoring a Partial-Span Rectangular Jet. AIAA Paper No. 74-971, Aug. 1974.

4. Corson, Blake W., Jr.; Runckel, Jack F.; and Igoe, William B.: Calibration of the Langley 16-Foot Transonic Tunnel With Test Section Air Removal. NASA TR R-423, 1974.

5. Schaefer, William T., Jr.: Characteristics of Major Active Wind Tunnels at the Langley Research Center. NASA TM X-1130, 1965.

6. Goetz, G. F.; and Petit, J. E.: Integrated Nozzle Development Program, Transition Study Test Report. No. D180-15443 (Contract No. N00140-73-C0027), Boeing Co.

7. Braslow, Albert L.; and Knox, Eugene C.: Simplified Method for Determination of Critical Height of Distributed Roughness Particles for Boundary-Layer Transition at Mach Numbers From 0 to 5. NACA TN 4363, 1958.

8. Braslow, Albert L.; Hicks, Raymond M.; and Harris, Roy V., Jr.: Use of Grit-Type Boundary-Layer-Transition Trips on Wind-Tunnel Models. NASA TN D-3579, 1966.

9. Reubush, David E.; and Runckel, Jack F.: Effect of Fineness Ratio on the Boattail Drag of Circular-Arc Afterbodies Having Closure Ratios of 0.50 With Jet Exhaust at Mach Numbers up to 1.30. NASA TN D-7192, 1973.

10. Berrier, Bobby L.: Effect of Plug and Shroud Geometry Variables on Plug-Nozzle Performance at Transonic Speeds. NASA TN D-5098, 1969.

11. Maiden, Donald L.; and Mercer, Charles E.: Performance Characteristics of a Single-Engine Fighter Model Fitted With an In-Flight Thrust Reverser. NASA TN D-6460, 1971.

12. Reubush, David E.: Effects of Fineness and Closure Ratios on Boattail Drag of Circular-Arc Afterbody Models With Jet Exhaust at Mach Numbers up to 1.30. NASA TN D-7163, 1973.

13. Compton, William B., III: Jet Effects on the Drag of Conical Afterbodies at Supersonic Speeds. NASA TN D-6789, 1972.

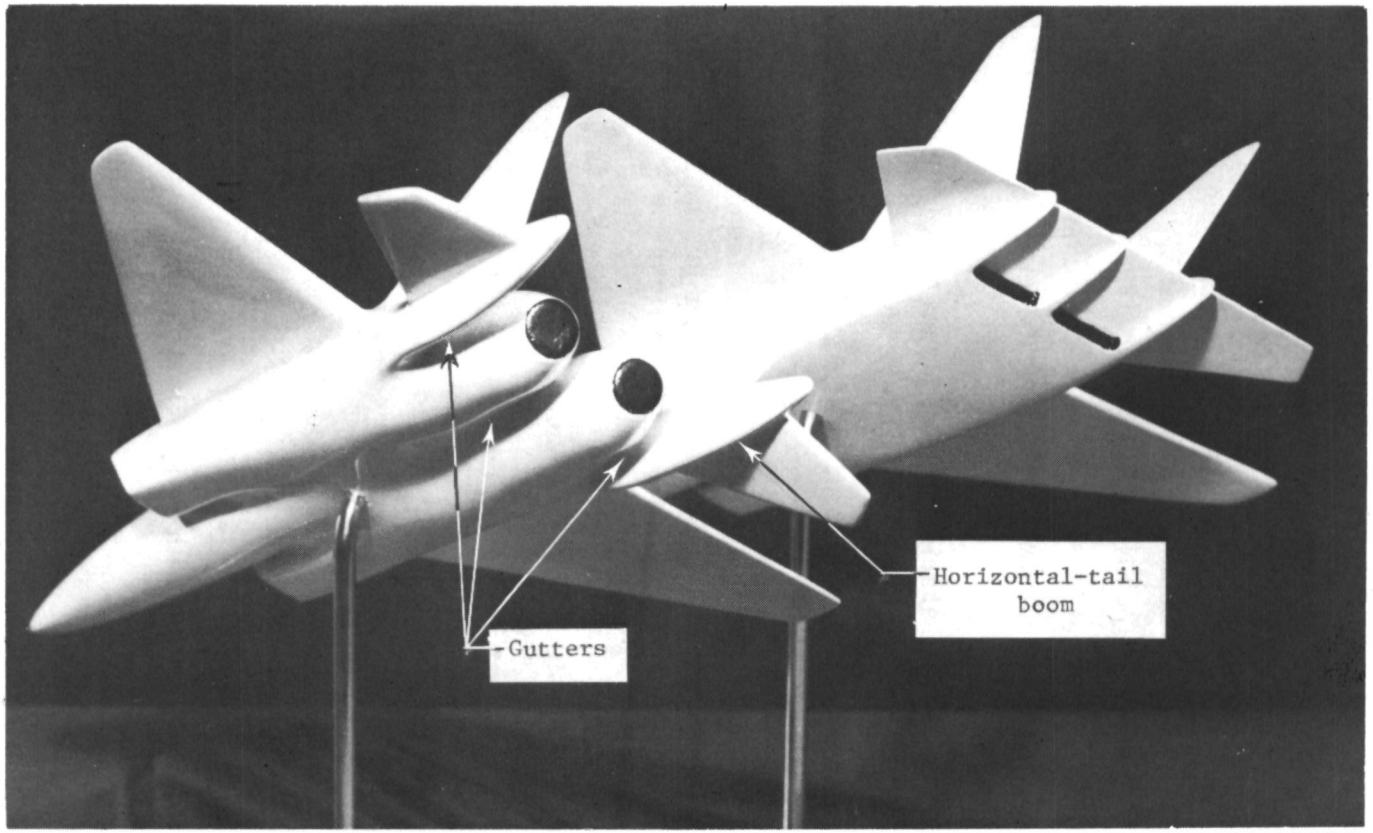

L-74-3691.1

Figure 1.- Conventional axisymmetric nozzle integration and two-dimensional wedge-nozzle integration concept.

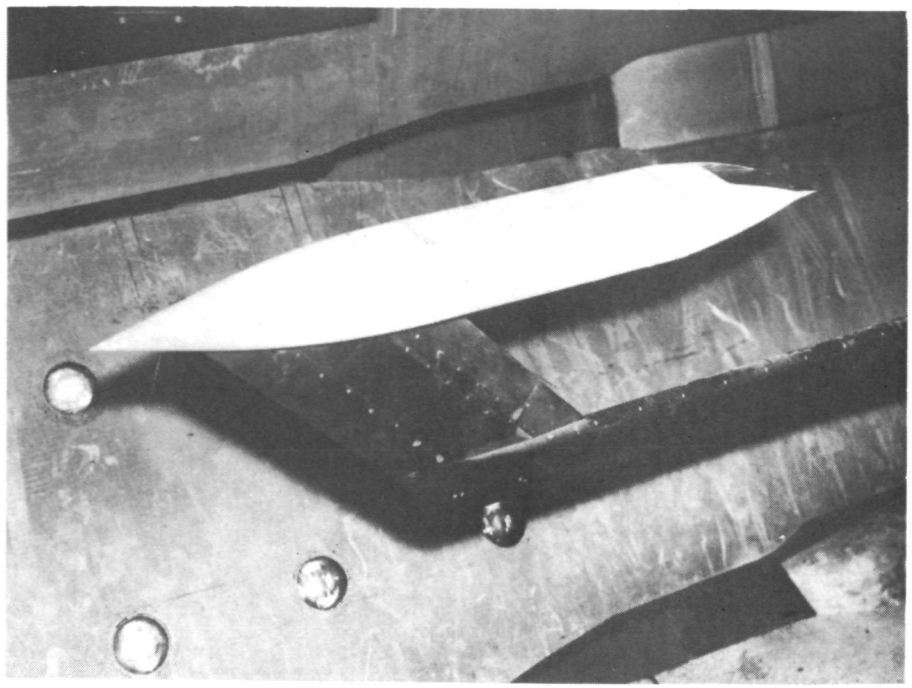

L-74-3220

(a) Langley 16-foot transonic tunnel.

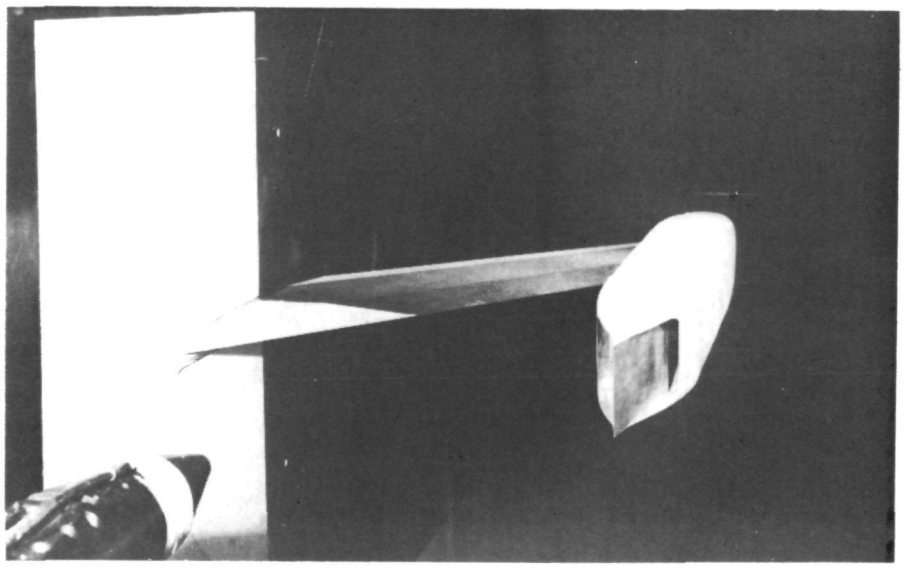

L-74-4332

(b) Langley 4-foot supersonic pressure tunnel.

Figure 2.- Isolated air-powered nacelle installations.

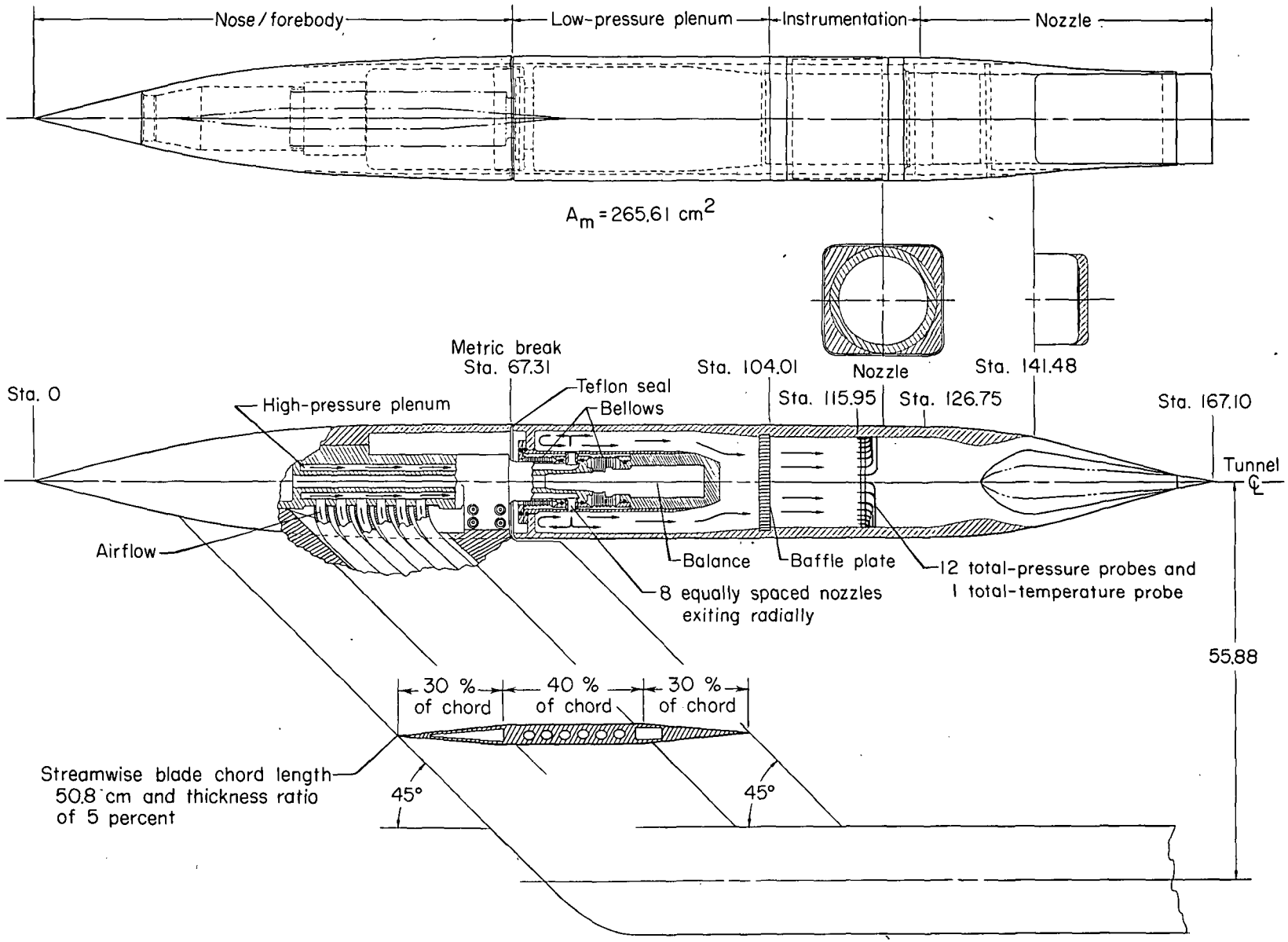

Figure 3.- Sketch of air-powered nacelle model with two-dimensional wedge nozzle installed. All dimensions are in centimeters unless otherwise noted.

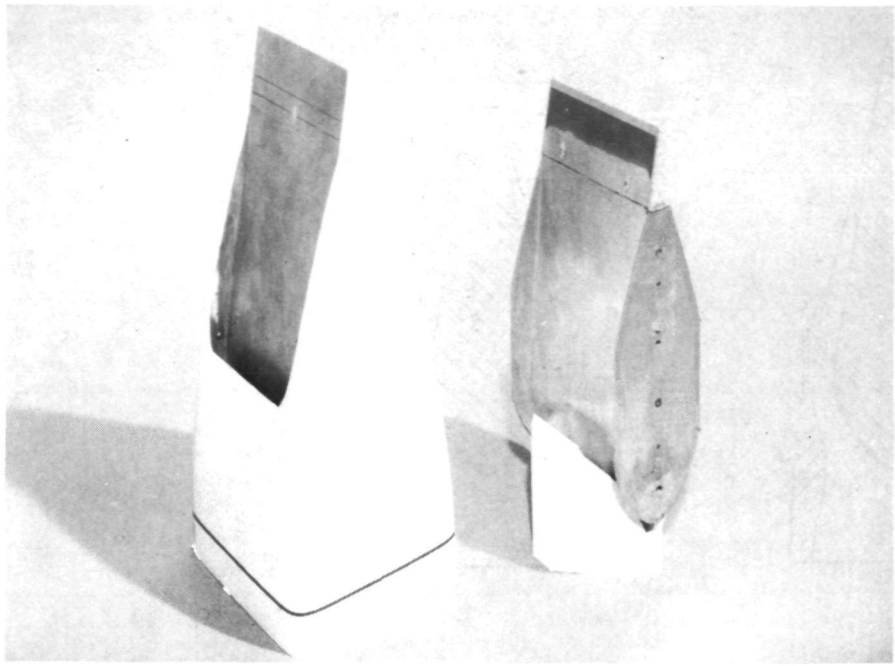

L-74-3261

(a) Three-quarter side view without shrouds.

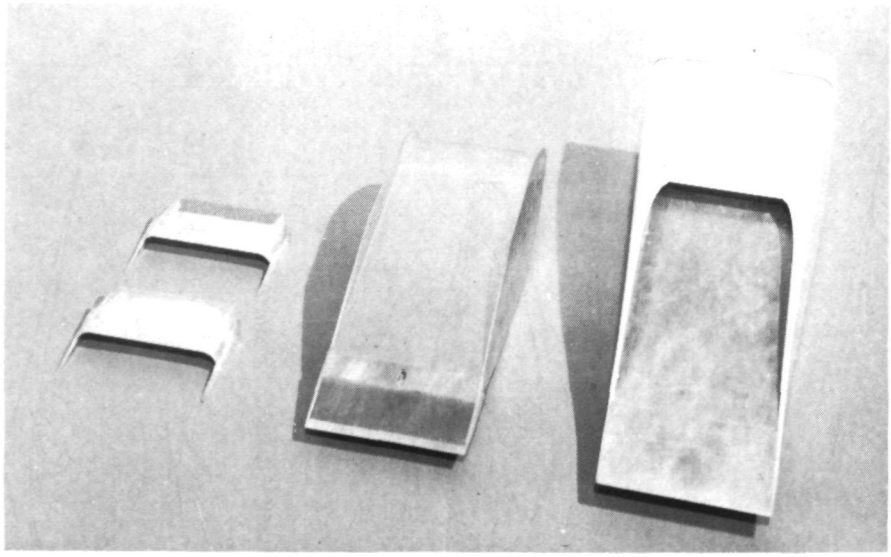

L-74-3257

(b) Three-quarter rear view.

Figure 4.- Nozzle component parts. Dry-power wedge installed.

Baseline

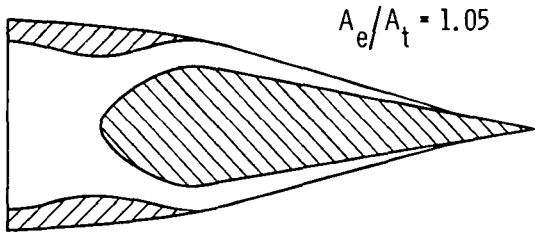

Short translated shroud

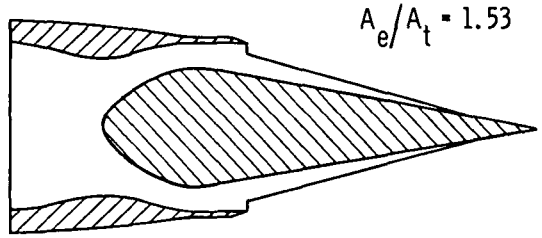

Truncated

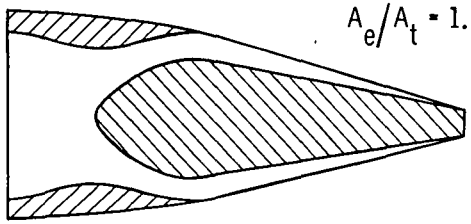

Truncated, short translated shroud

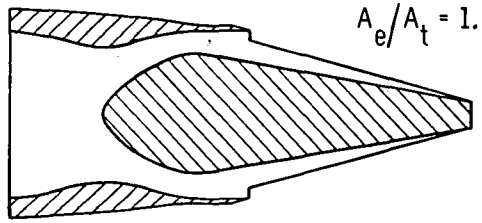

Tertiary-air ejector (static test only)

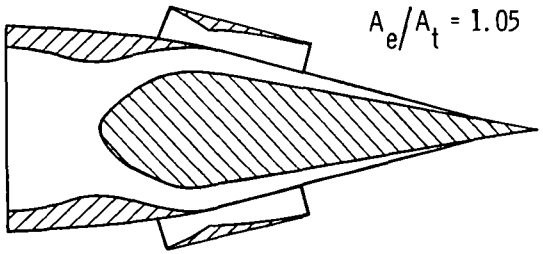

(a) Dry-power configurations. $A_{e,x}/A_t = 3.61$.

Figure 5.- Sketch of two-dimensional wedge-nozzle configurations of the test.

Baseline

$A_e/A_t = 1.03$

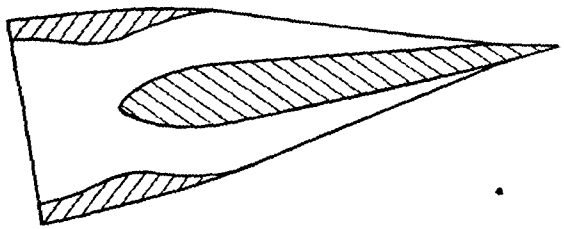

Truncated

$A_e/A_t = 1.03$

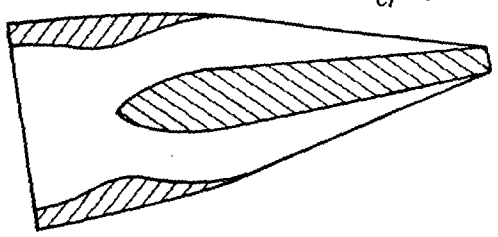

Tertiary-air ejector

$A_e/A_t = 1.03$

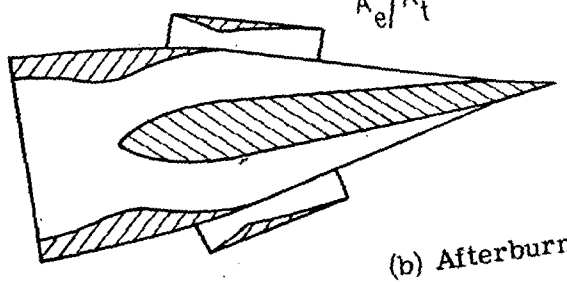

Short translated shroud

$A_e/A_t = 1.12$

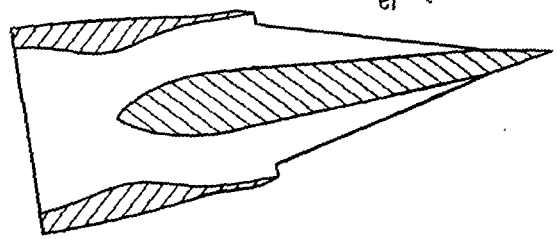

Truncated, short translated shroud

$A_e/A_t = 1.12$

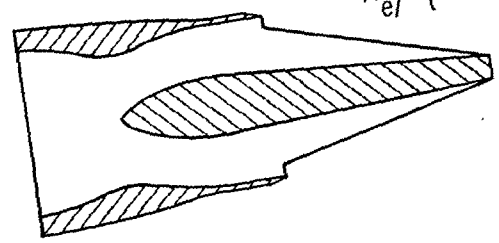

Long translated shroud (only M = 2.01 data)

$A_e/A_t = 1.22$

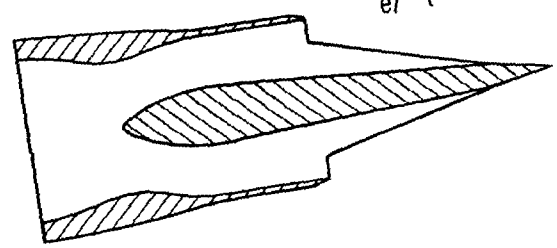

(b) Afterburner-power configurations. $A_{e,x}/A_t = 1.68$.

Figure 5.- Concluded.

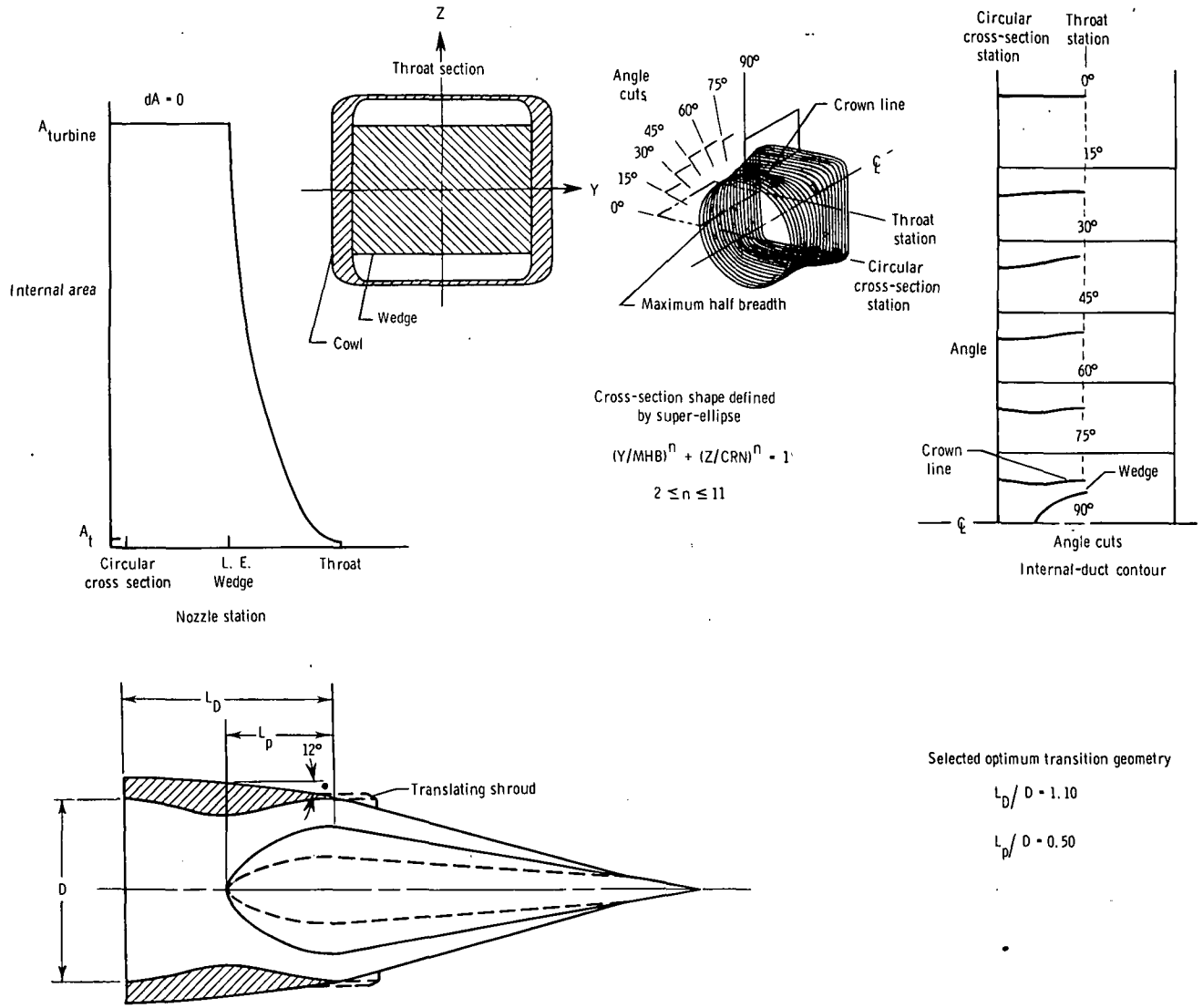

(a) General design overview.

Figure 6.- Wedge-nozzle concept with collapsing two-dimensional horizontal wedge and translating shroud.

Dry-wedge coordinates	
x	z
0	0
.693	1.321
1.387	2.032
2.080	2.540
2.774	3.048
3.467	3.353
4.161	3.708
4.854	3.962
5.547	4.204
6.241	4.382
6.934	4.470
7.628	4.394
8.321	4.428
33.436	0

Afterburner-wedge coordinates	
x	z
0	0
.693	.838
1.387	1.270
2.080	1.575
2.774	1.839
3.467	2.080
4.161	2.230
4.854	2.392
5.547	2.484
6.241	2.532
6.934	2.532
7.628	2.478
27.122	1.115
33.436	0

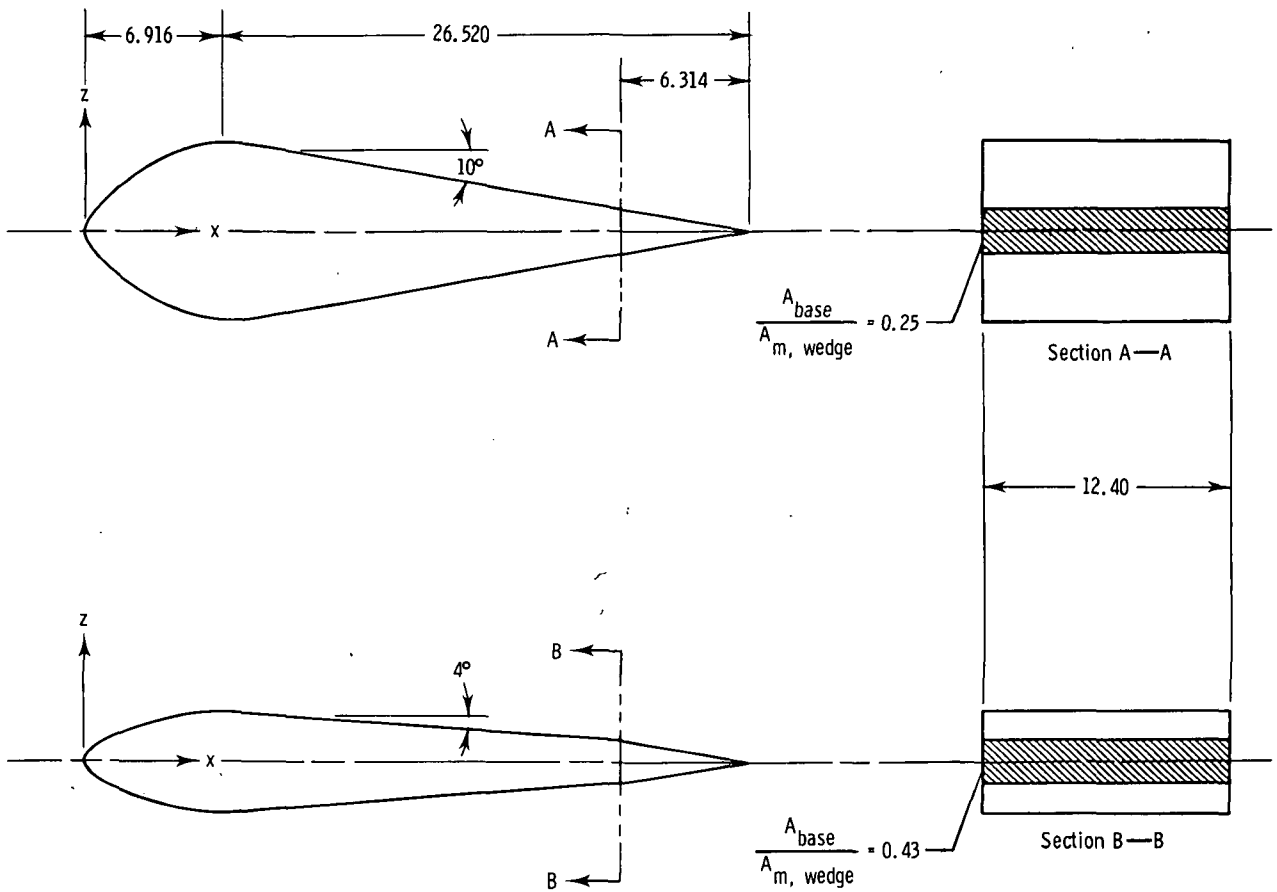

(b) Two-dimensional wedge geometry.

Figure 6.- Continued.

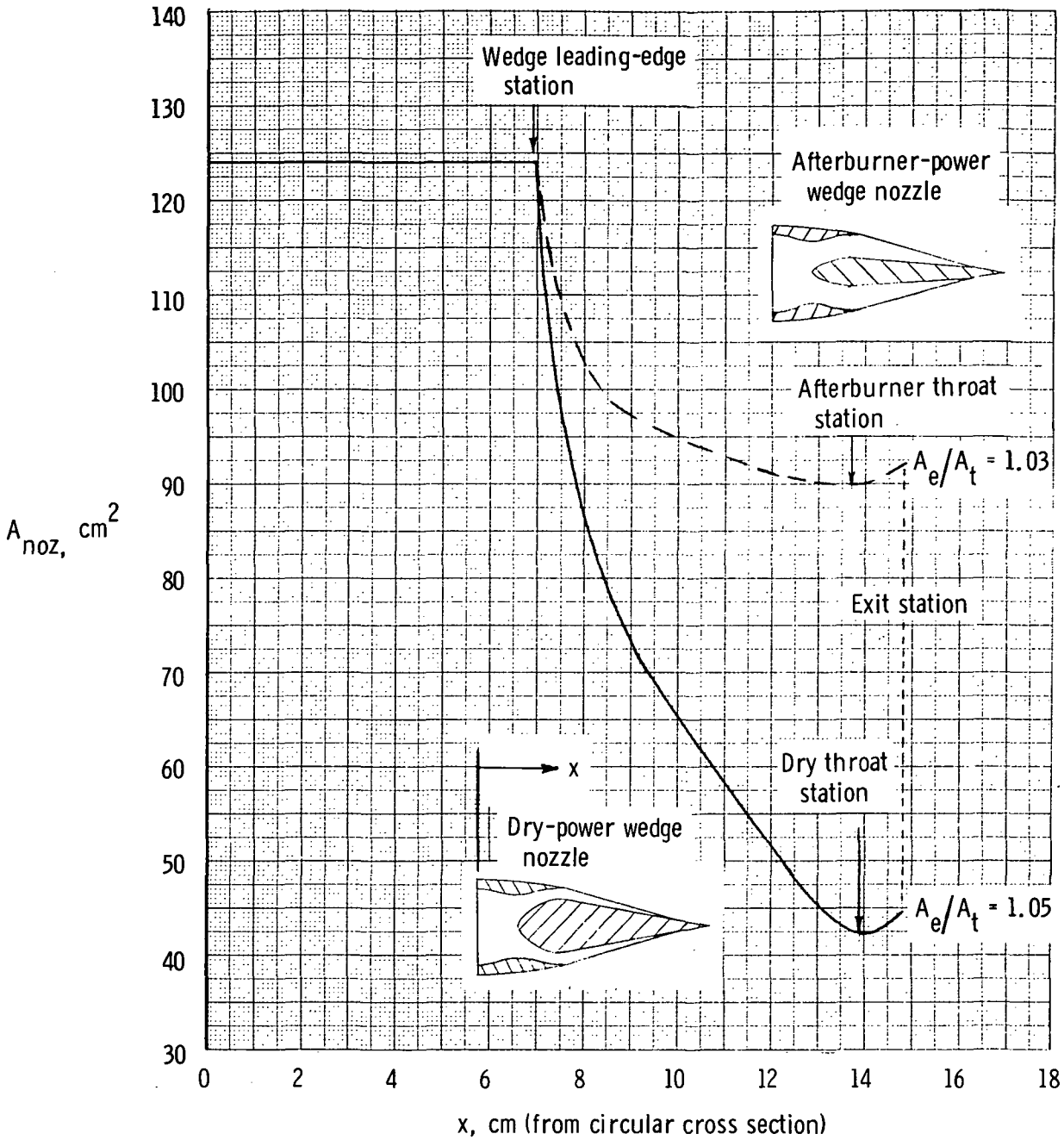

(c) Nozzle area distribution.

Figure 6.- Continued.

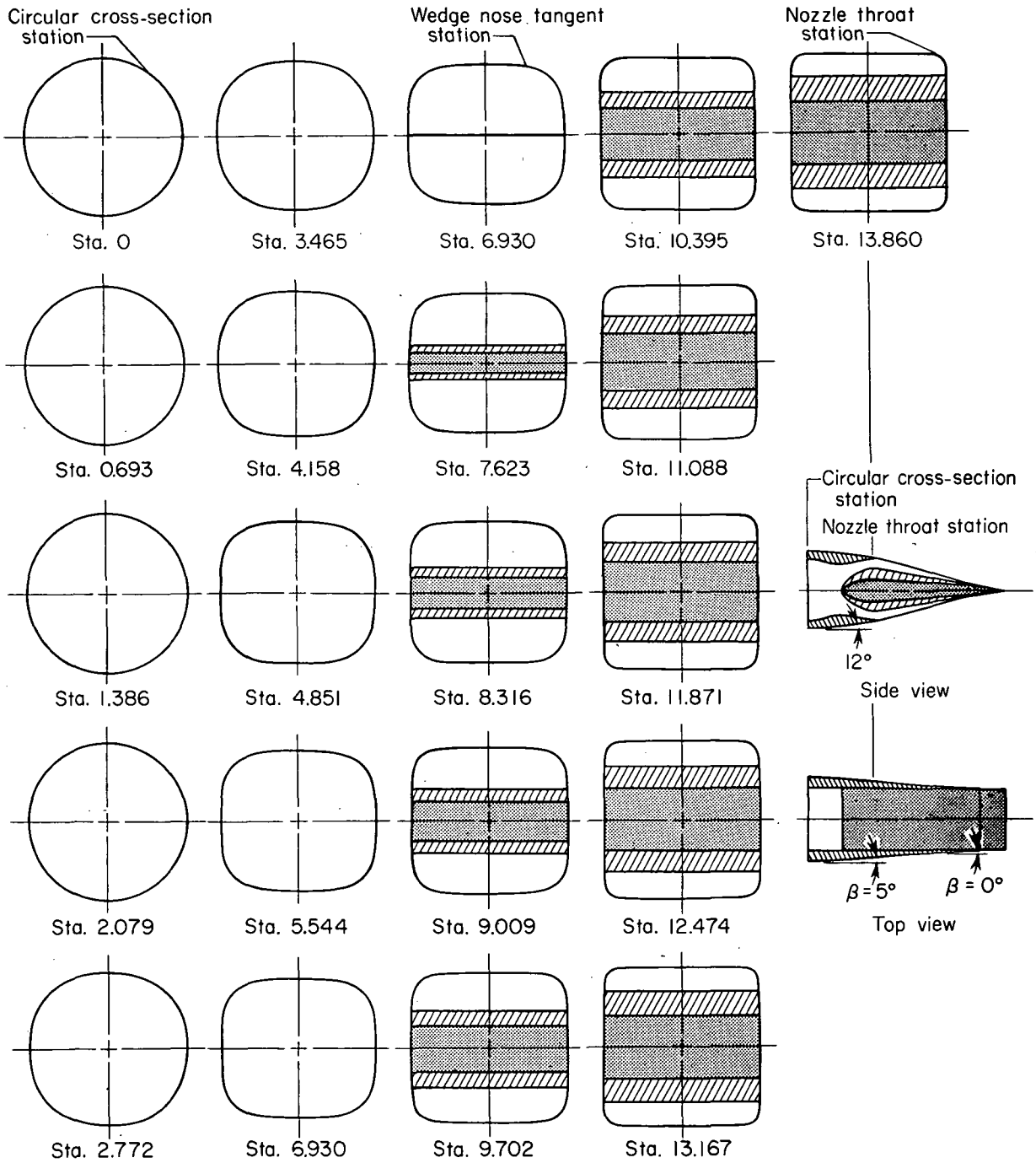

(d) Duct-wedge cross sections.

Figure 6.- Concluded.

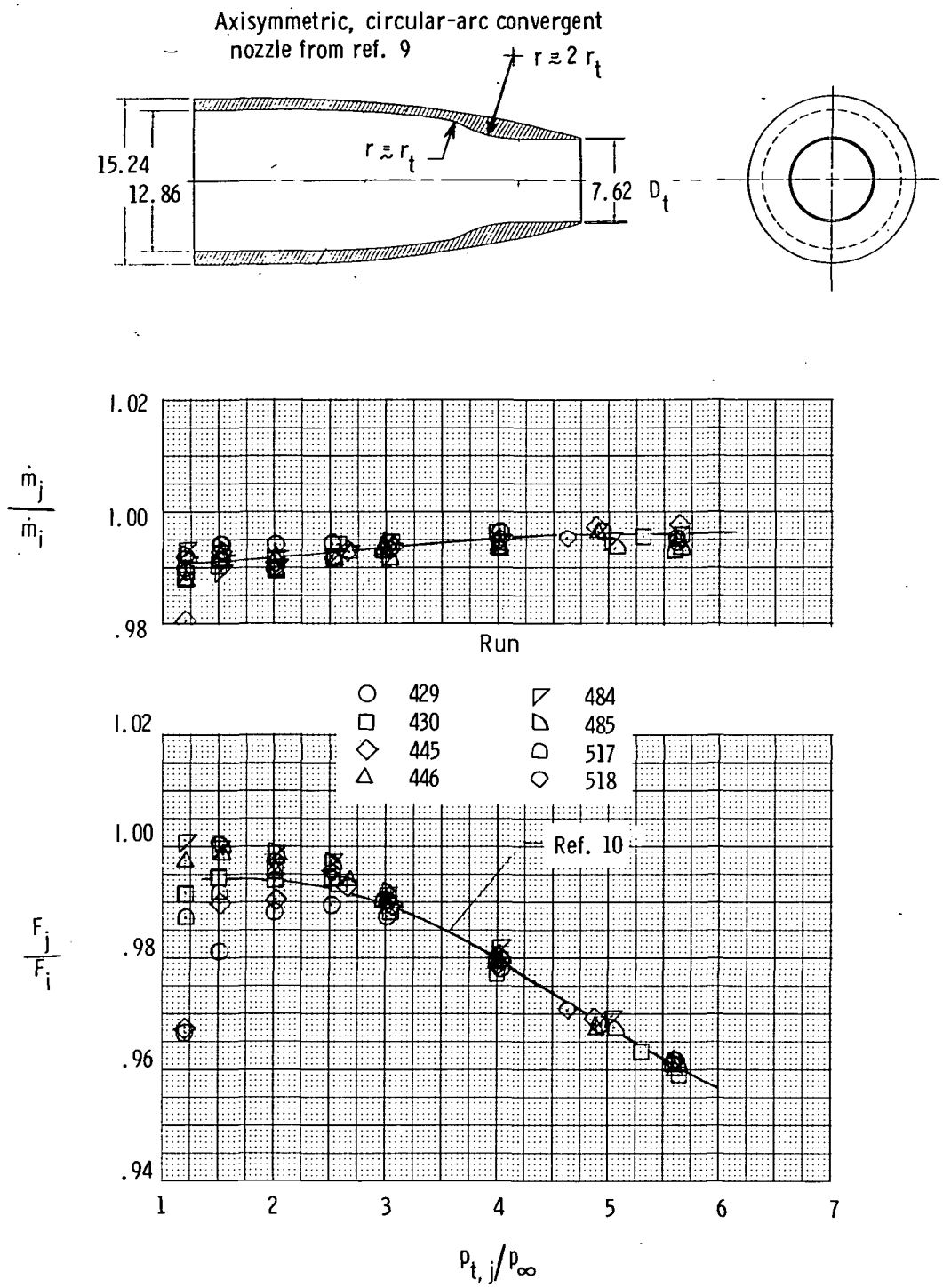

(a) 16-foot transonic-tunnel installation.

Figure 7.- Static performance of convergent nozzle used as calibration for air-powered nacelle. All dimensions are in centimeters.

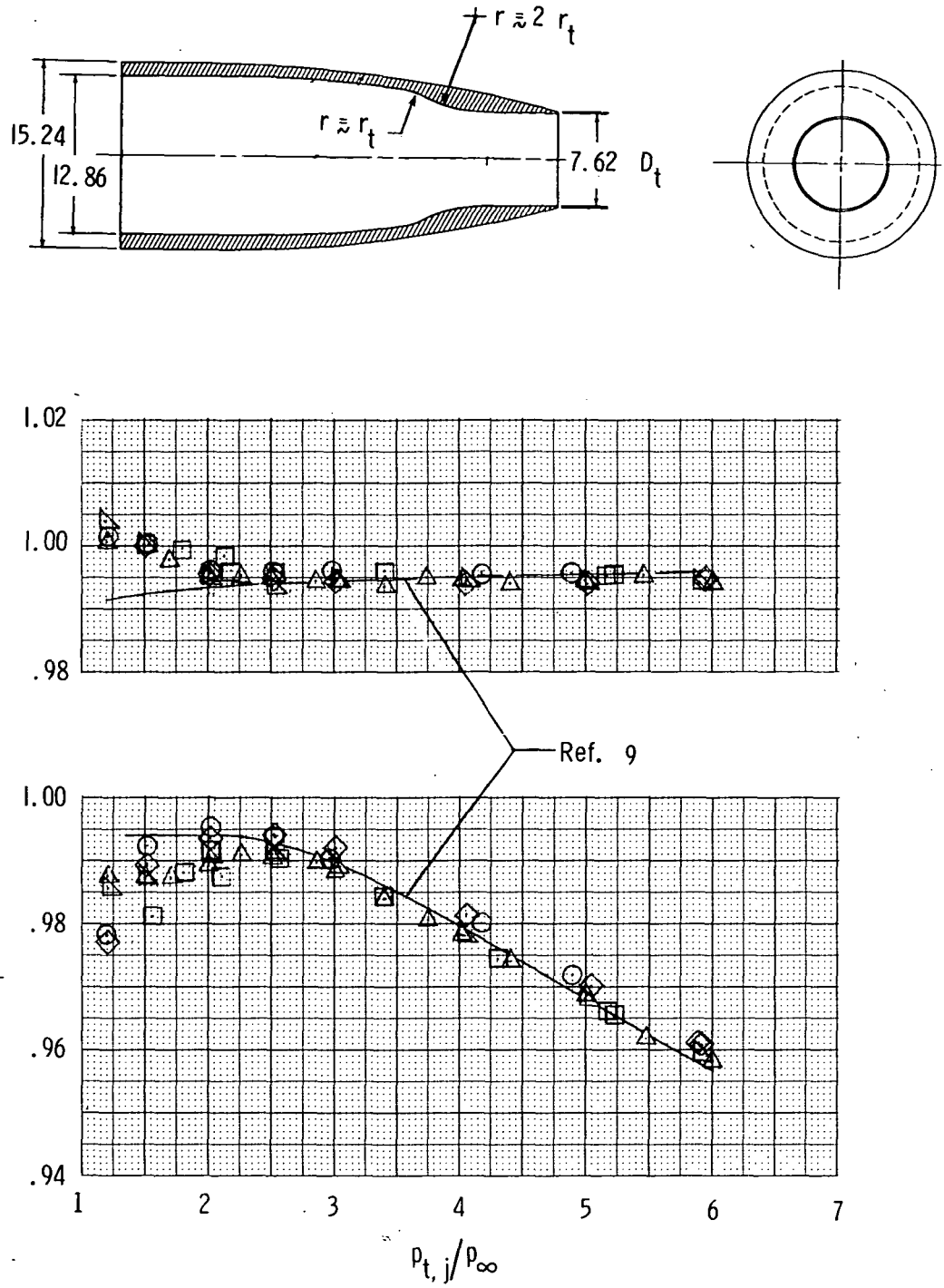

(b) 4-foot supersonic pressure tunnel installation.

Figure 7.- Concluded.

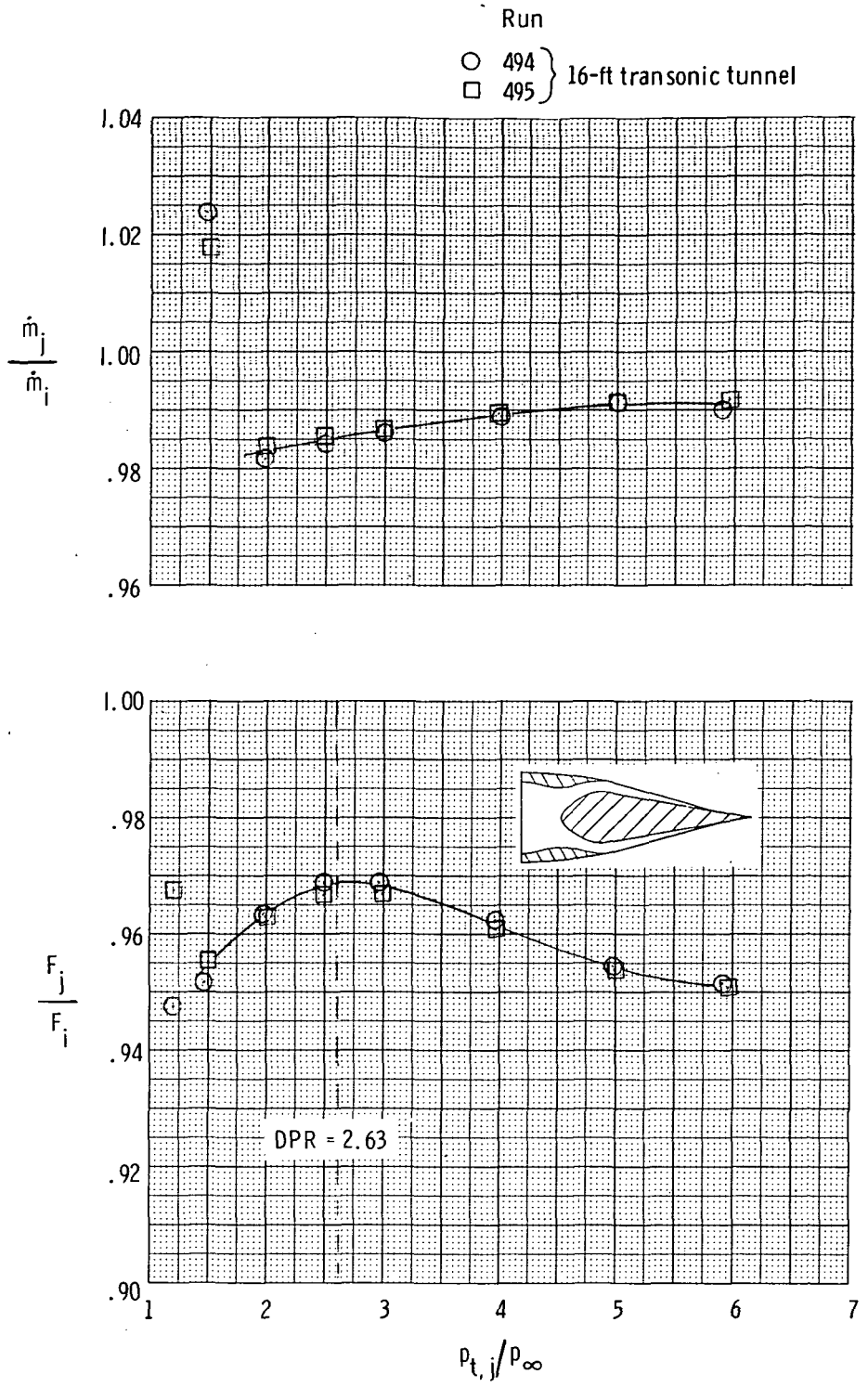

(a) Dry-power nozzle. $A_e/A_t = 1.05$.

Figure 8.- Static performance characteristics of several two-dimensional wedge configurations.

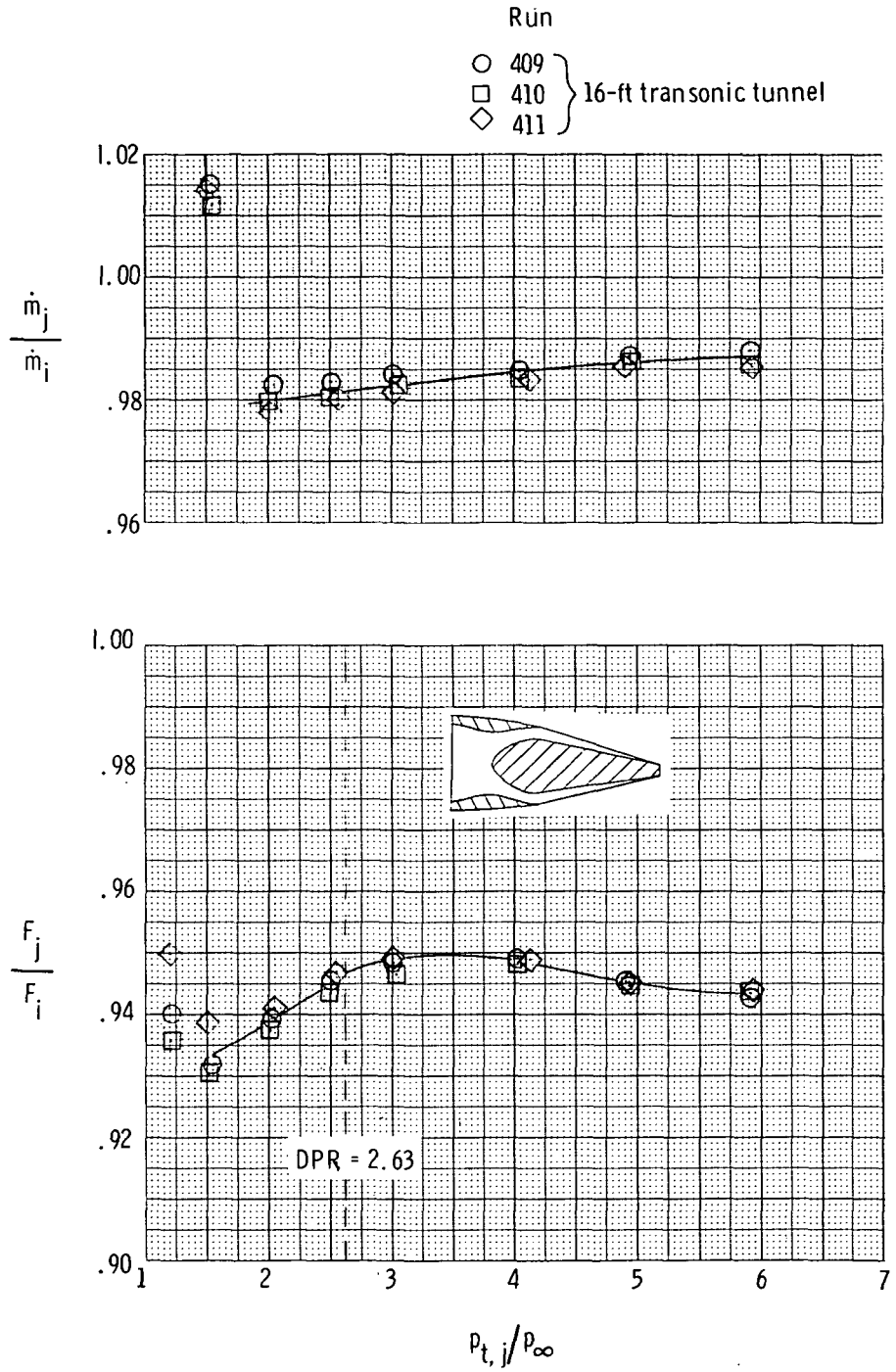

(b) Truncated wedge dry-power nozzle. $A_e/A_t = 1.05$.

Figure 8.- Continued.

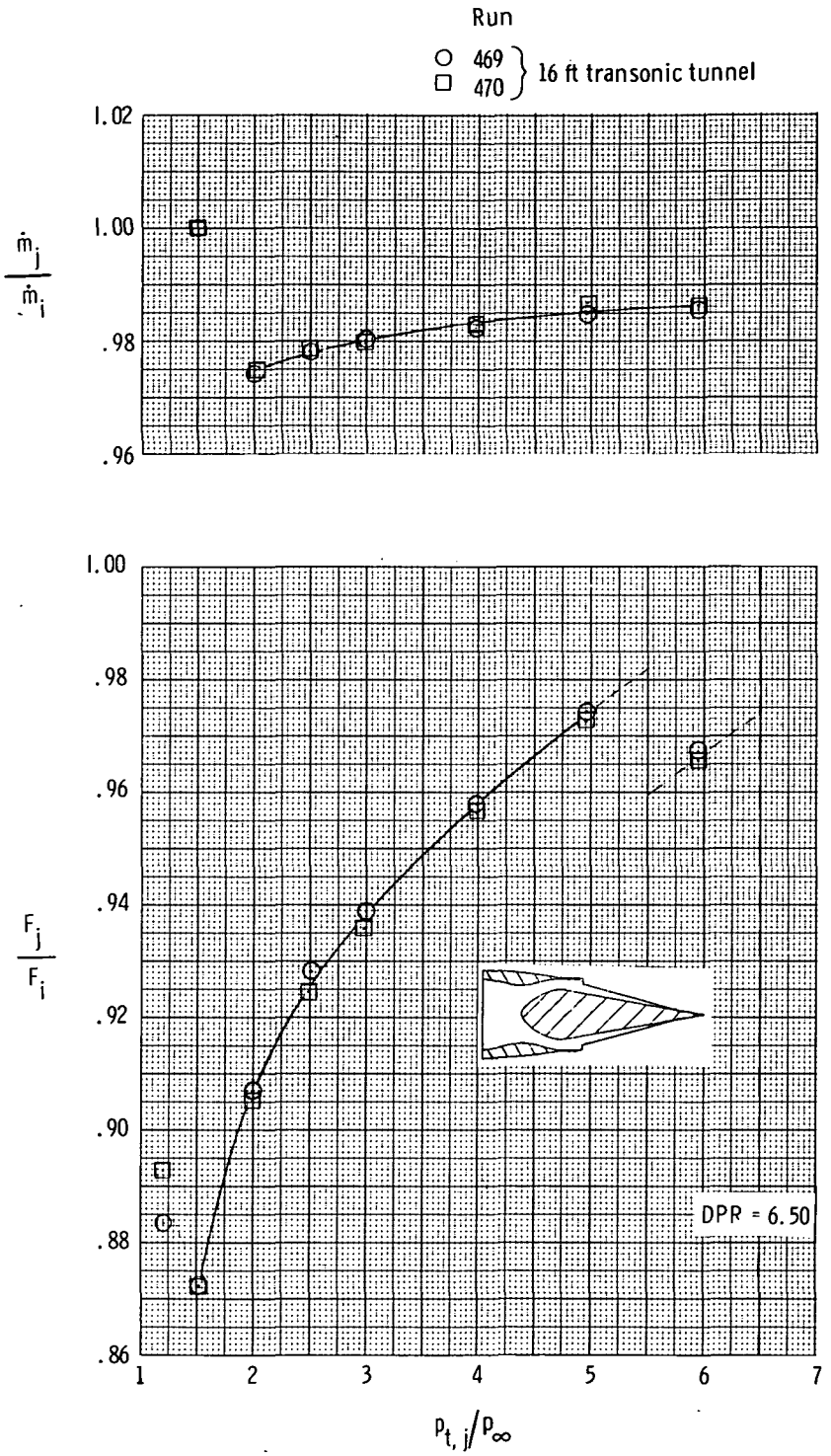

(c) Dry-power nozzle. $A_e/A_t = 1.53$.

Figure 8.- Continued.

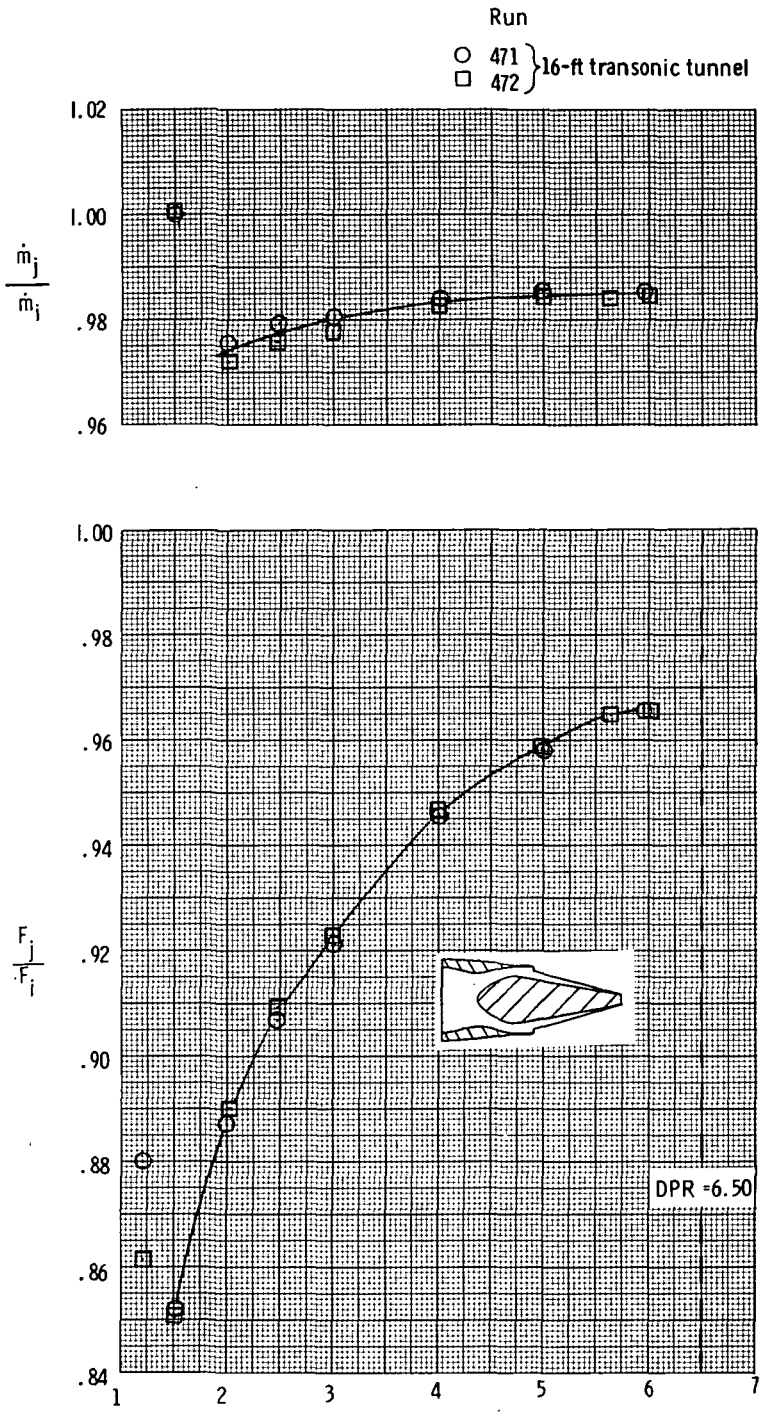

(d) Truncated dry-power nozzle. $A_e/A_t = 1.53$.

Figure 8.- Continued.

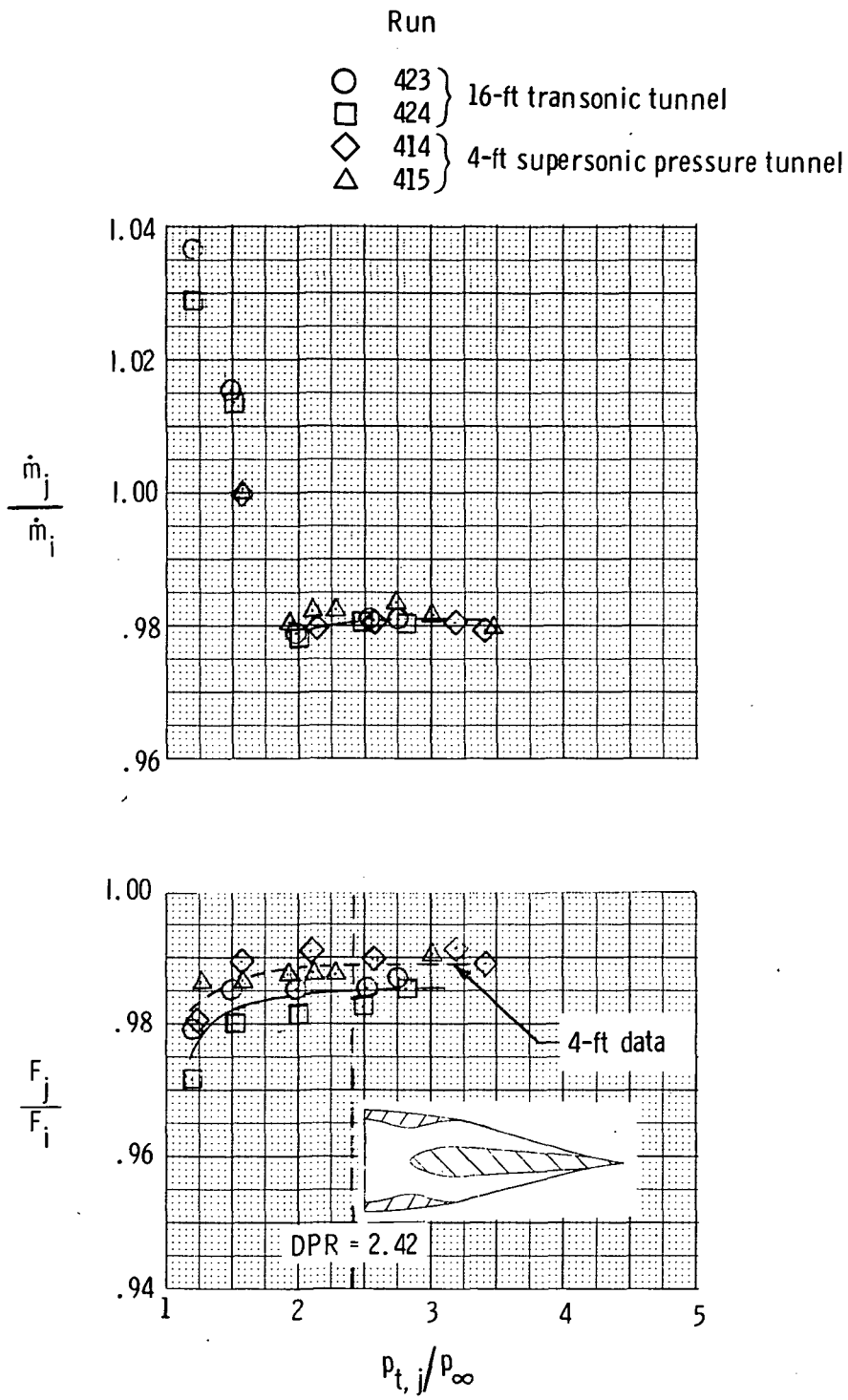

(e) Afterburner power nozzle. $A_e/A_t = 1.03$.

Figure 8.- Continued.

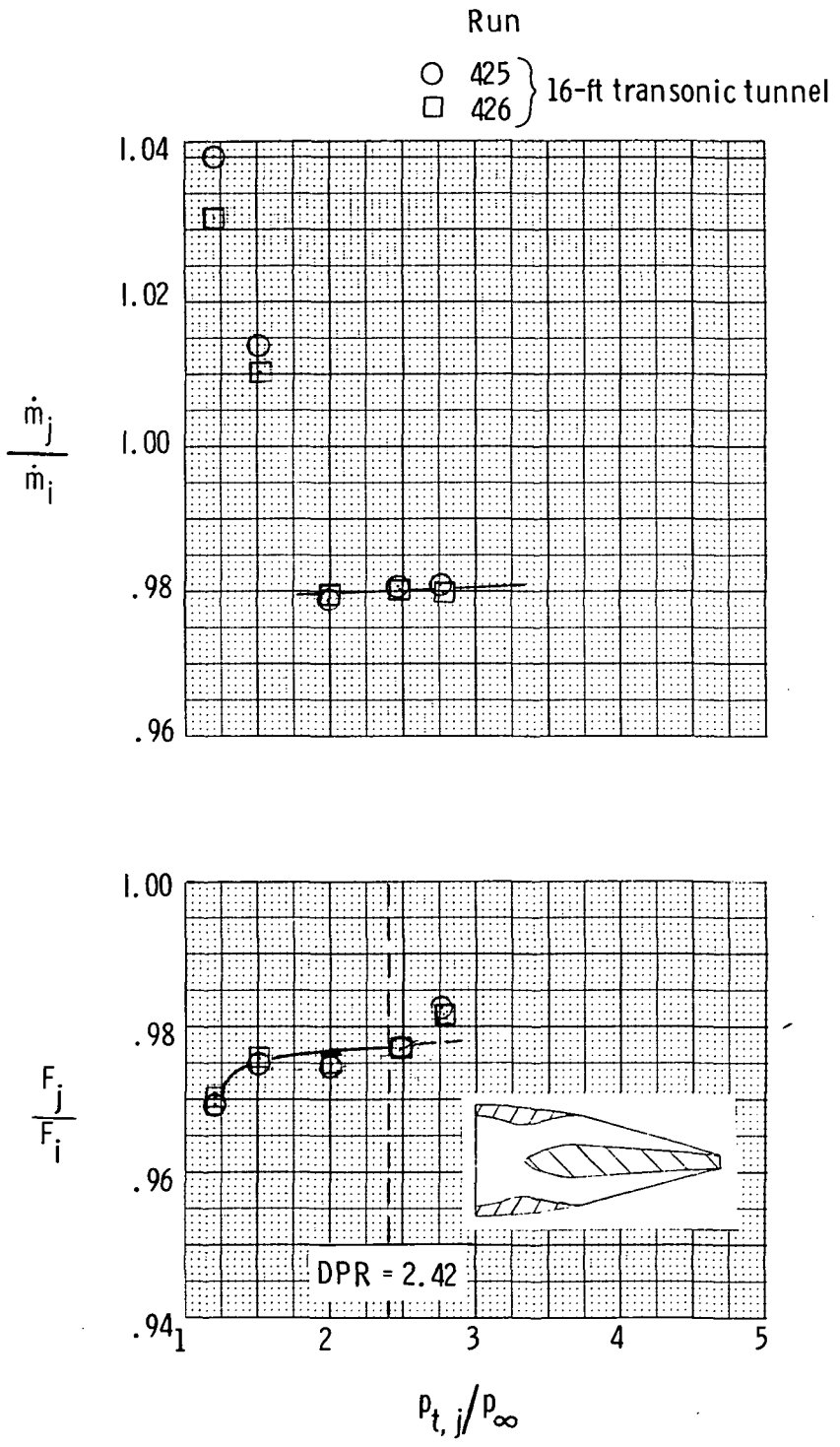

(f) Truncated afterburner-power nozzle. $A_e/A_t = 1.03$.

Figure 8.- Continued.

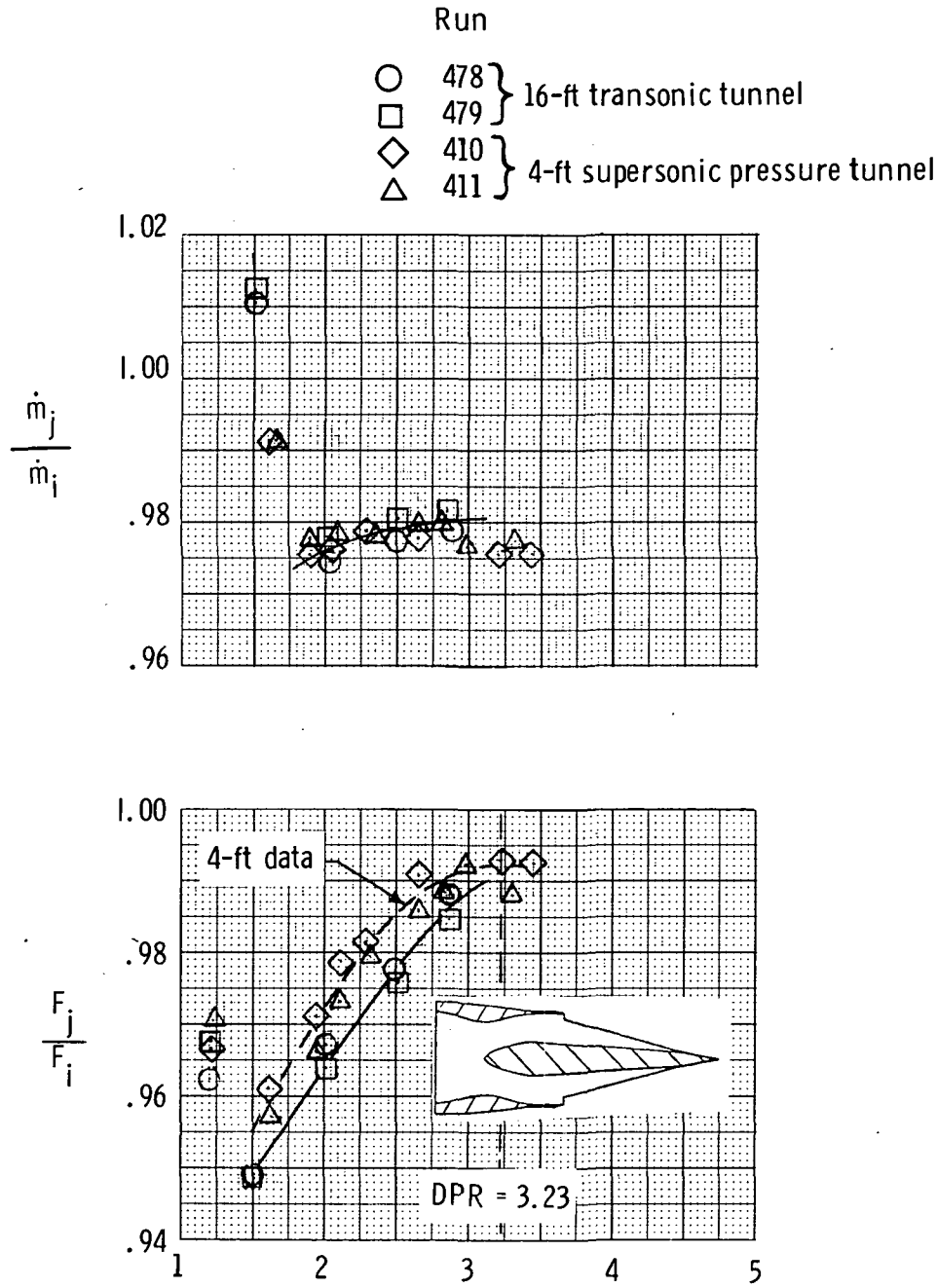

(g) Afterburner-power nozzle. $A_e/A_t = 1.12$.

Figure 8.- Continued.

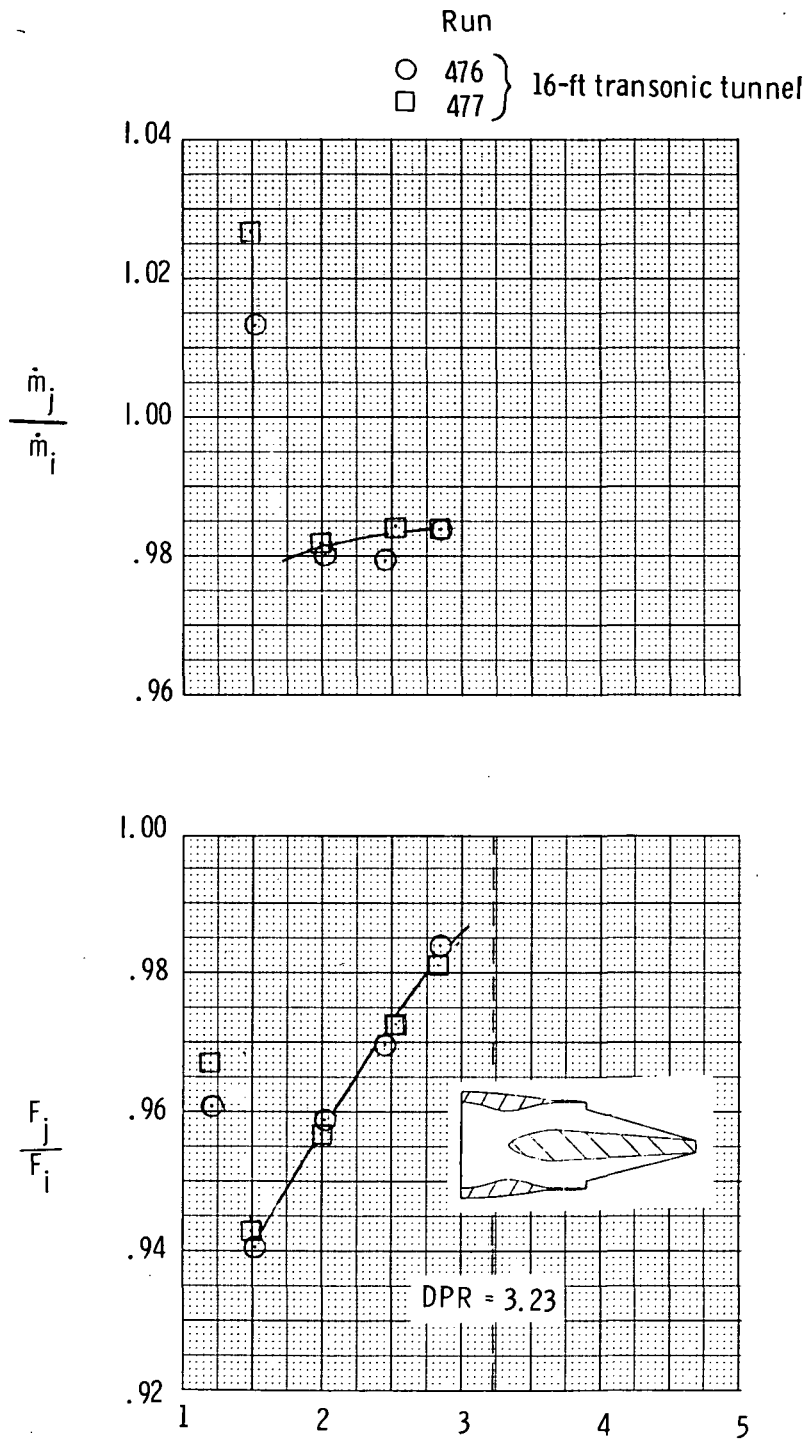

(h) Truncated afterburner-power nozzle. $A_e/A_t = 1.12$.

Figure 8.- Continued.

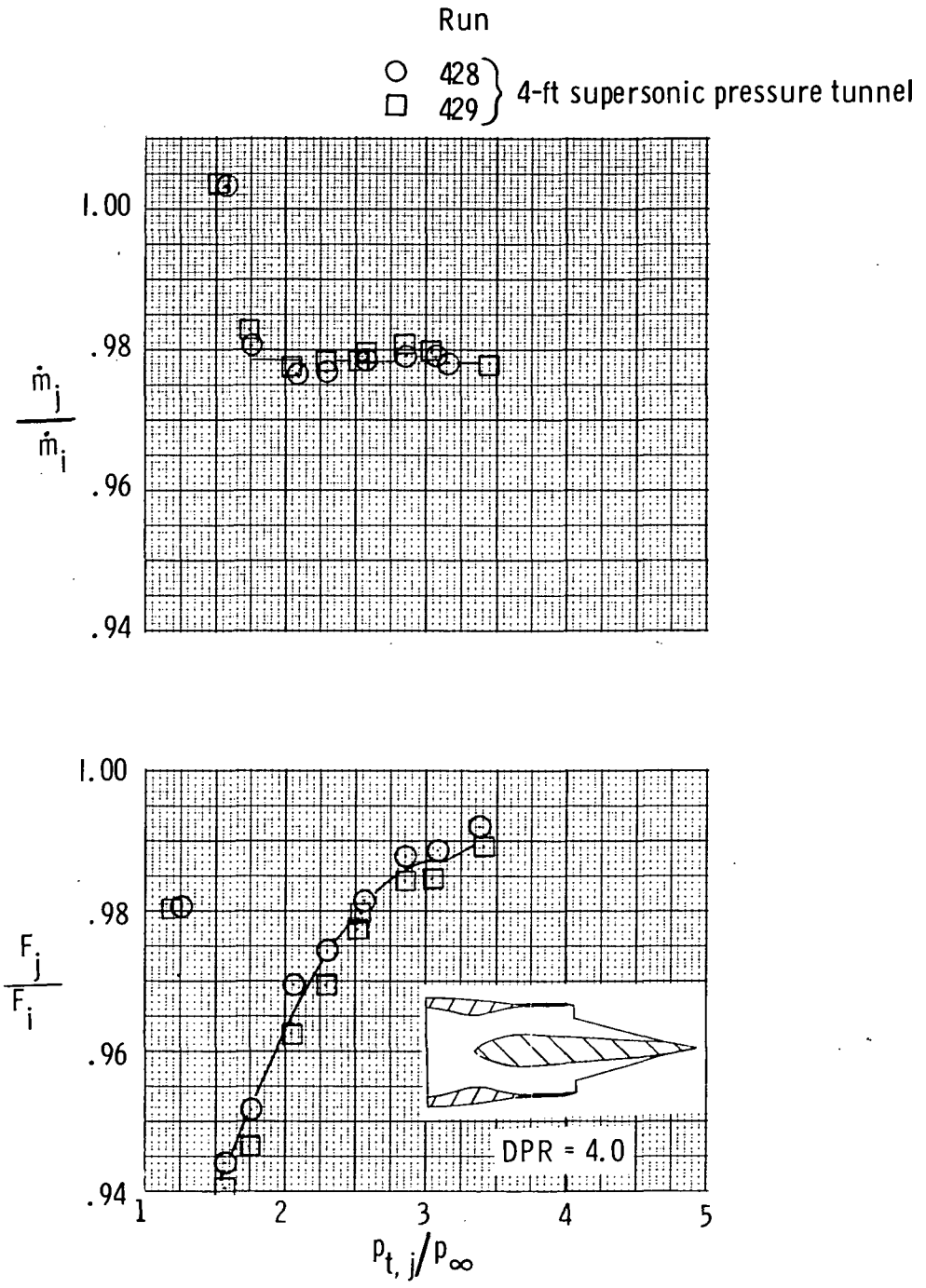

(i) Afterburner nozzle. $A_e/A_t = 1.22$.

Figure 8.- Concluded.

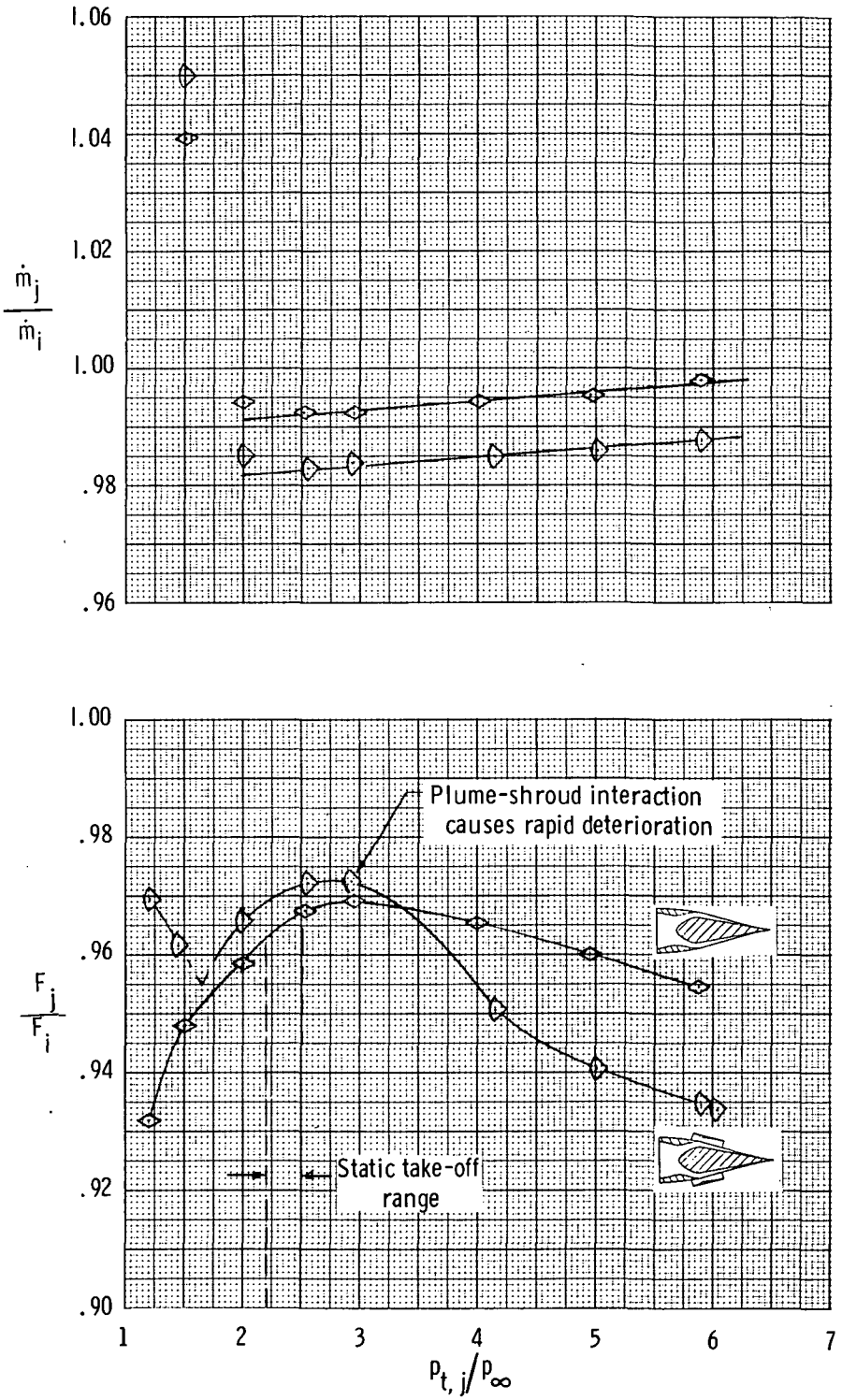

(a) Dry-power nozzle. $A_e/A_t = 1.05$.

Figure 9.- Effect of tertiary-air ejector on two-dimensional wedge nozzle static performance.

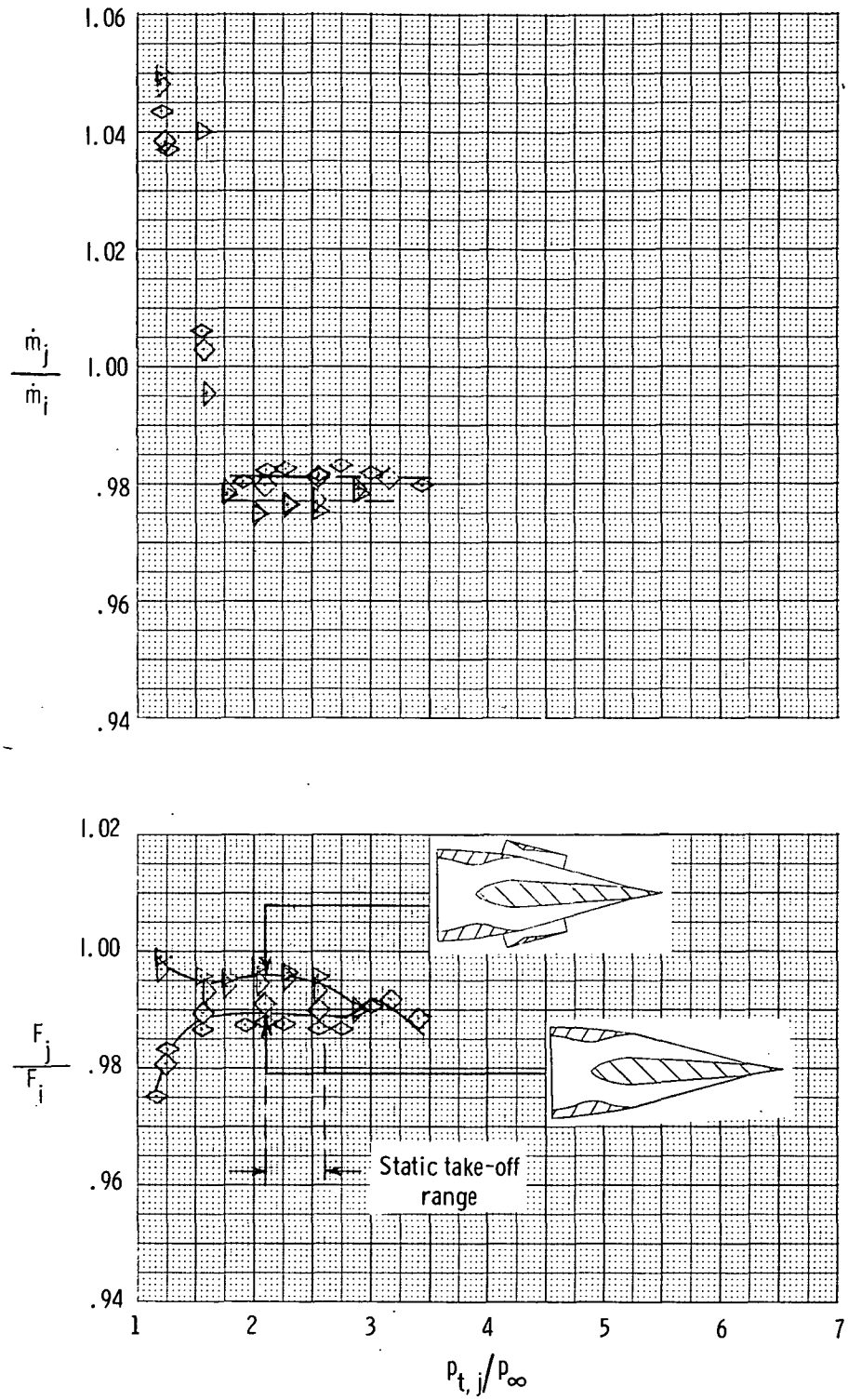

(b) Afterburner-power nozzle. $A_e/A_t = 1.03$.

Figure 9.- Concluded.

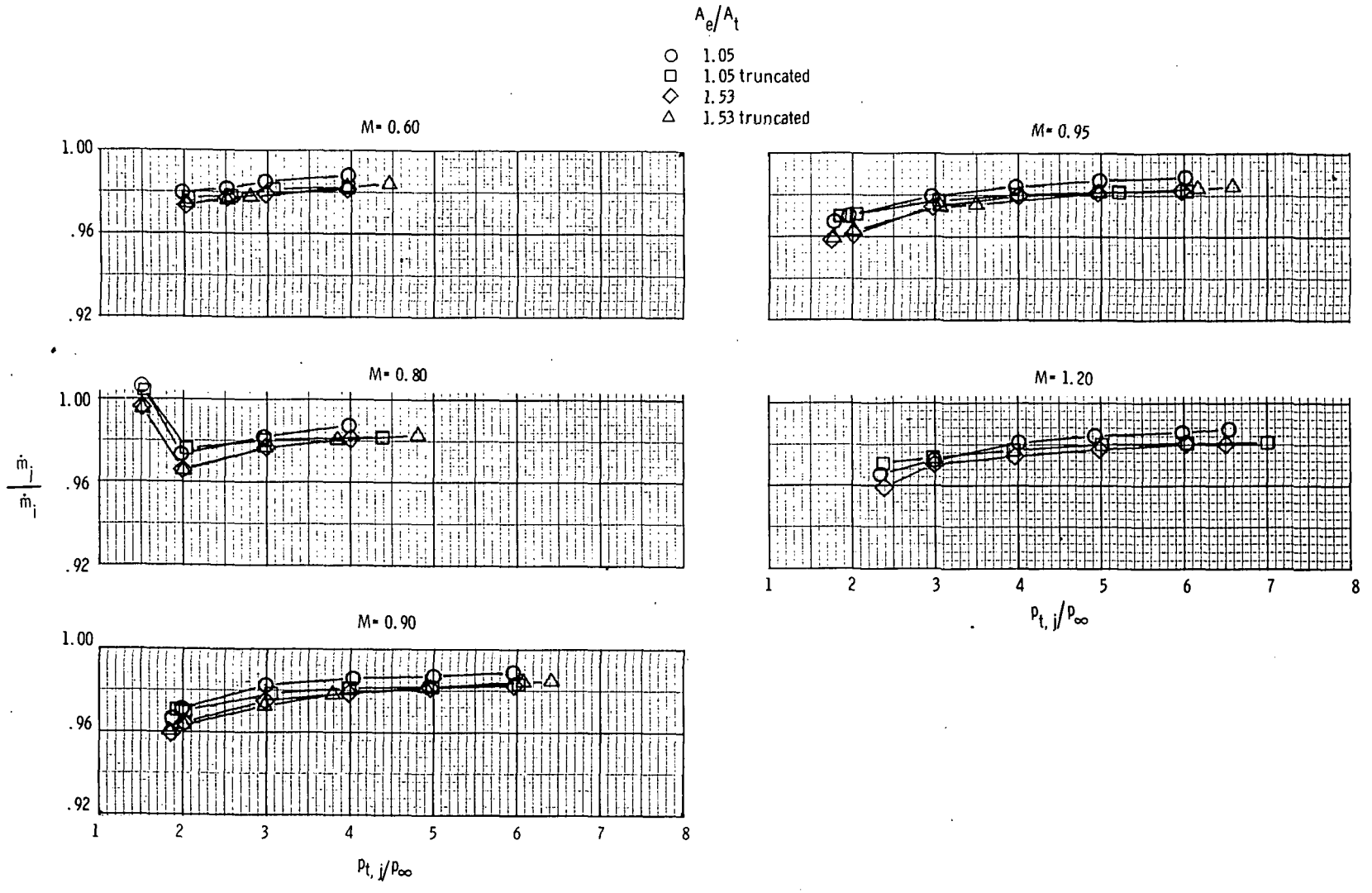

(a) Dry-power nozzle configurations.

Figure 10.- Variation of mass-flow ratio with jet total-pressure ratio for several Mach numbers.

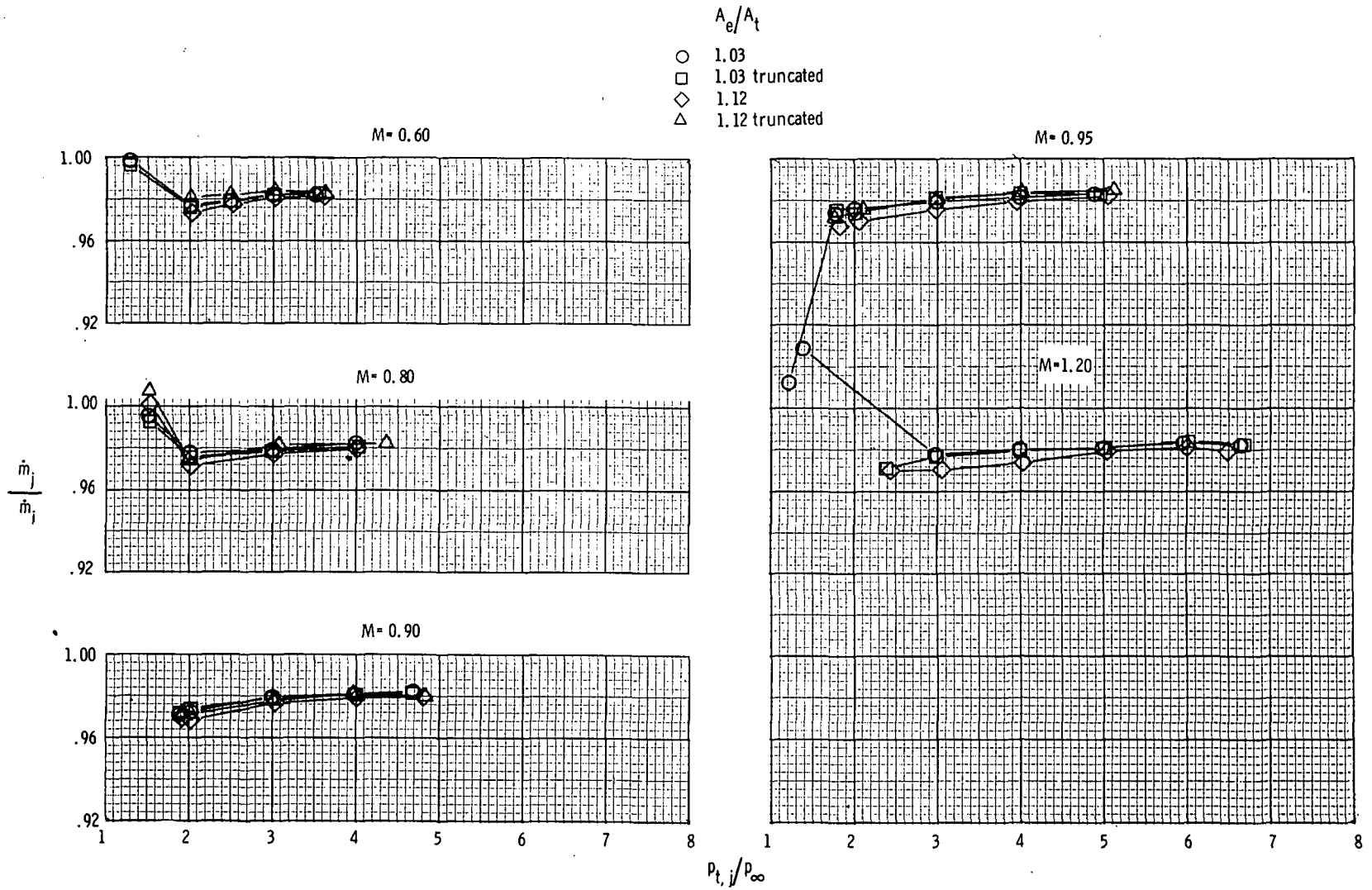

(b) Afterburner-power configurations.

Figure 10.- Continued.

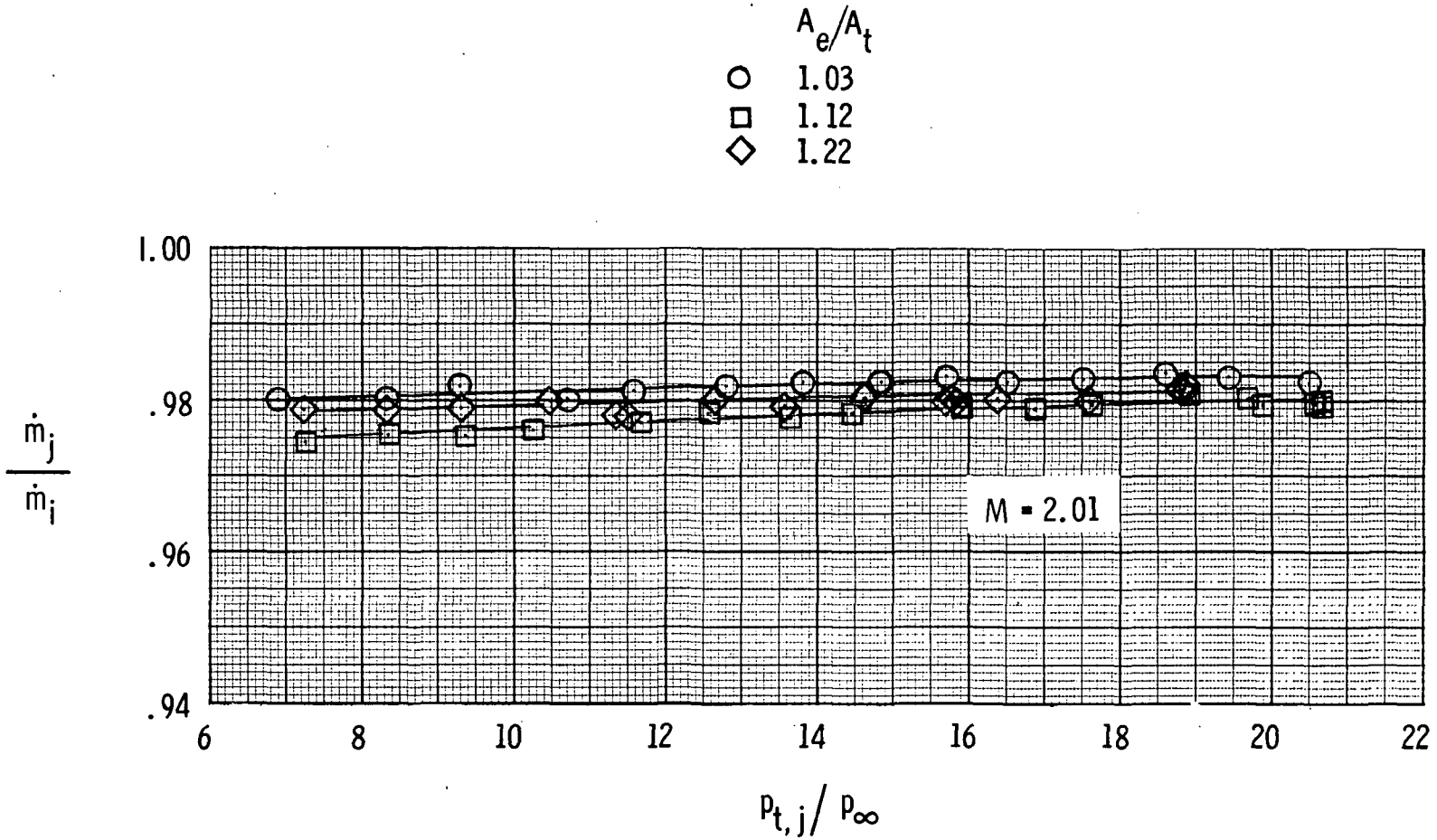

(b) Concluded.

Figure 10.- Concluded.

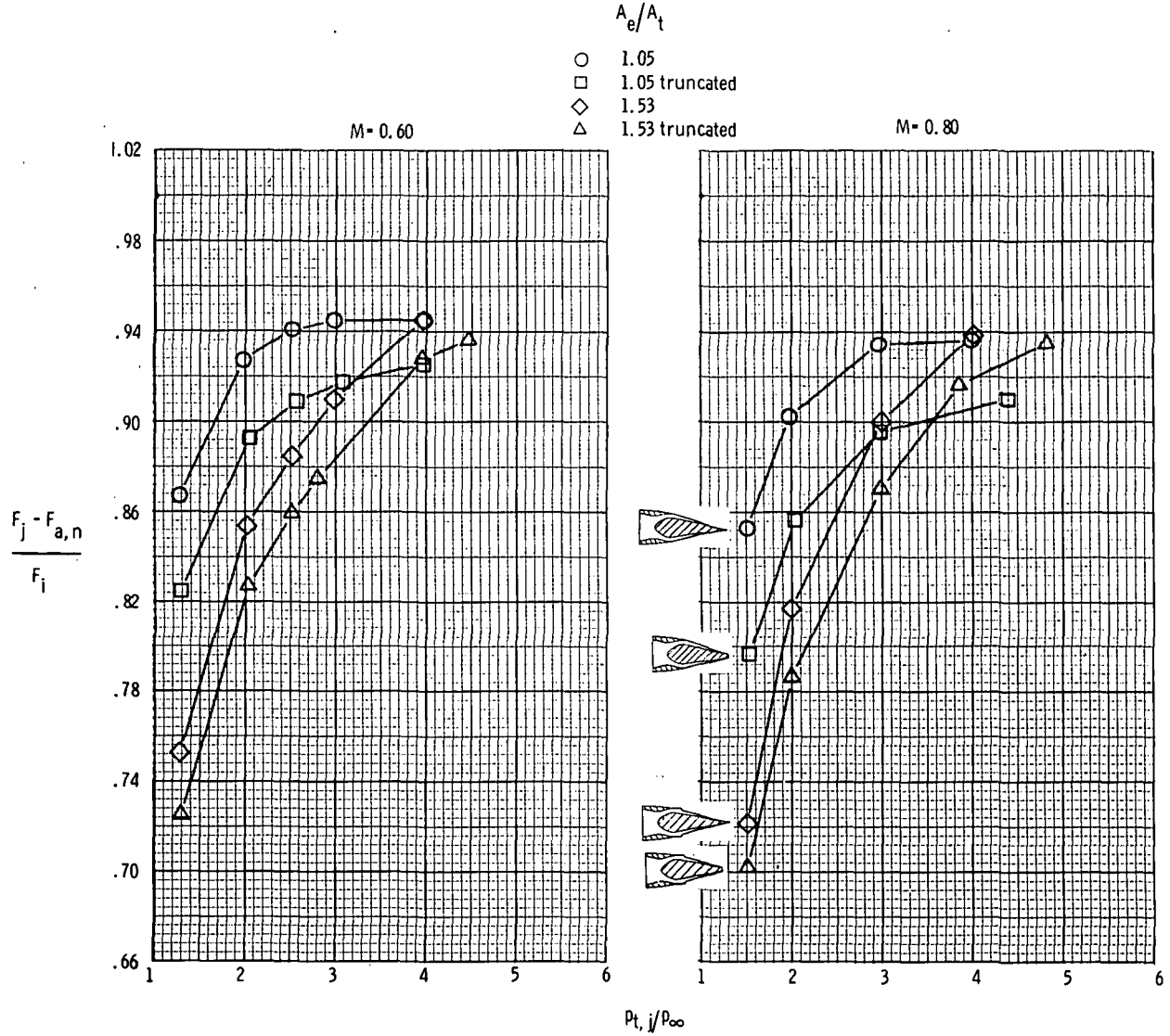

(a) M = 0.60 and 0.80.

Figure 11.- Variation of thrust-minus-axial-force ratio with jet total-pressure ratio for dry-power nozzle at several Mach numbers. $\alpha = 0^o$.

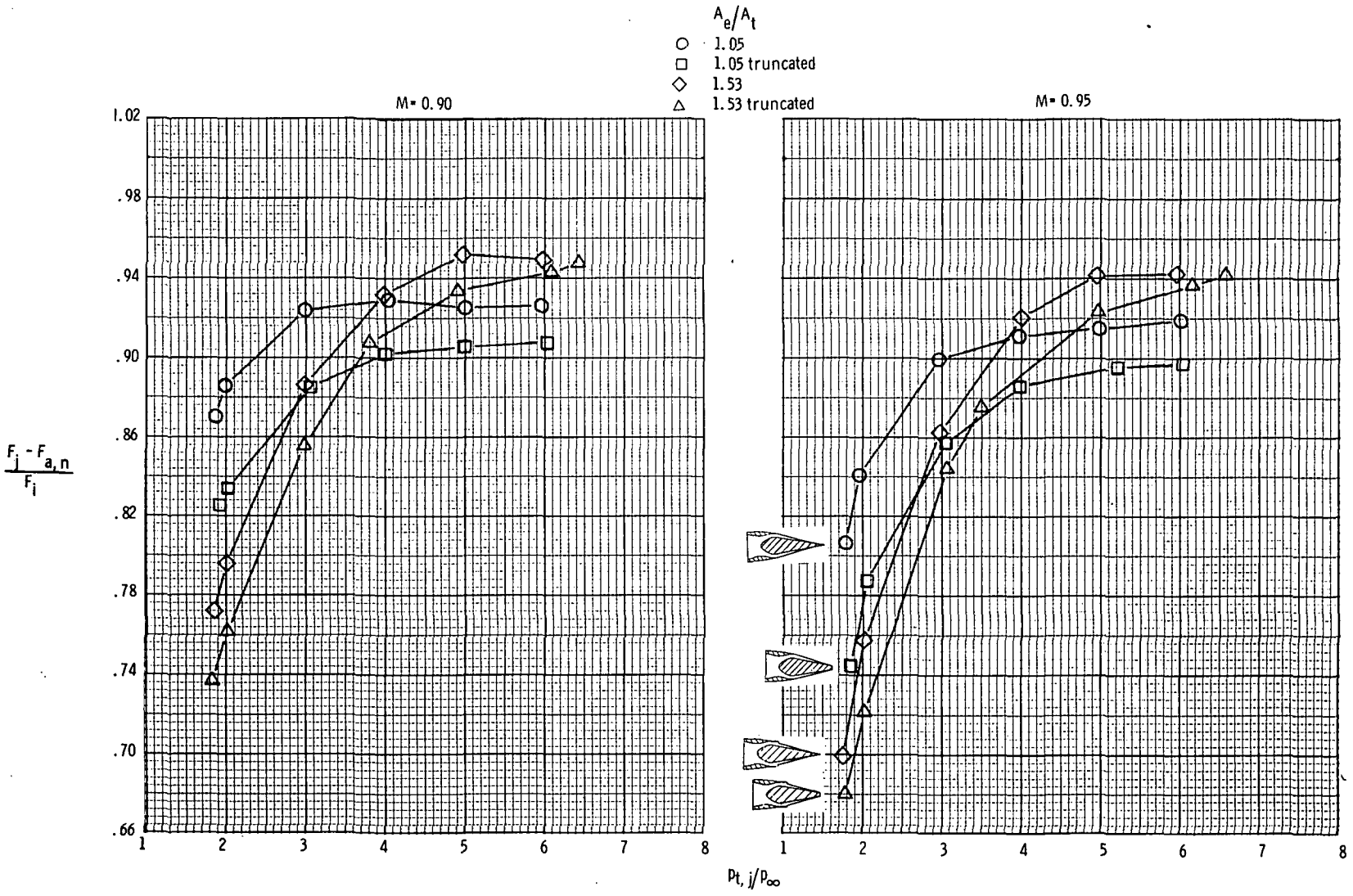

(b) M = 0.90 and 0.95.

Figure 11.- Continued.

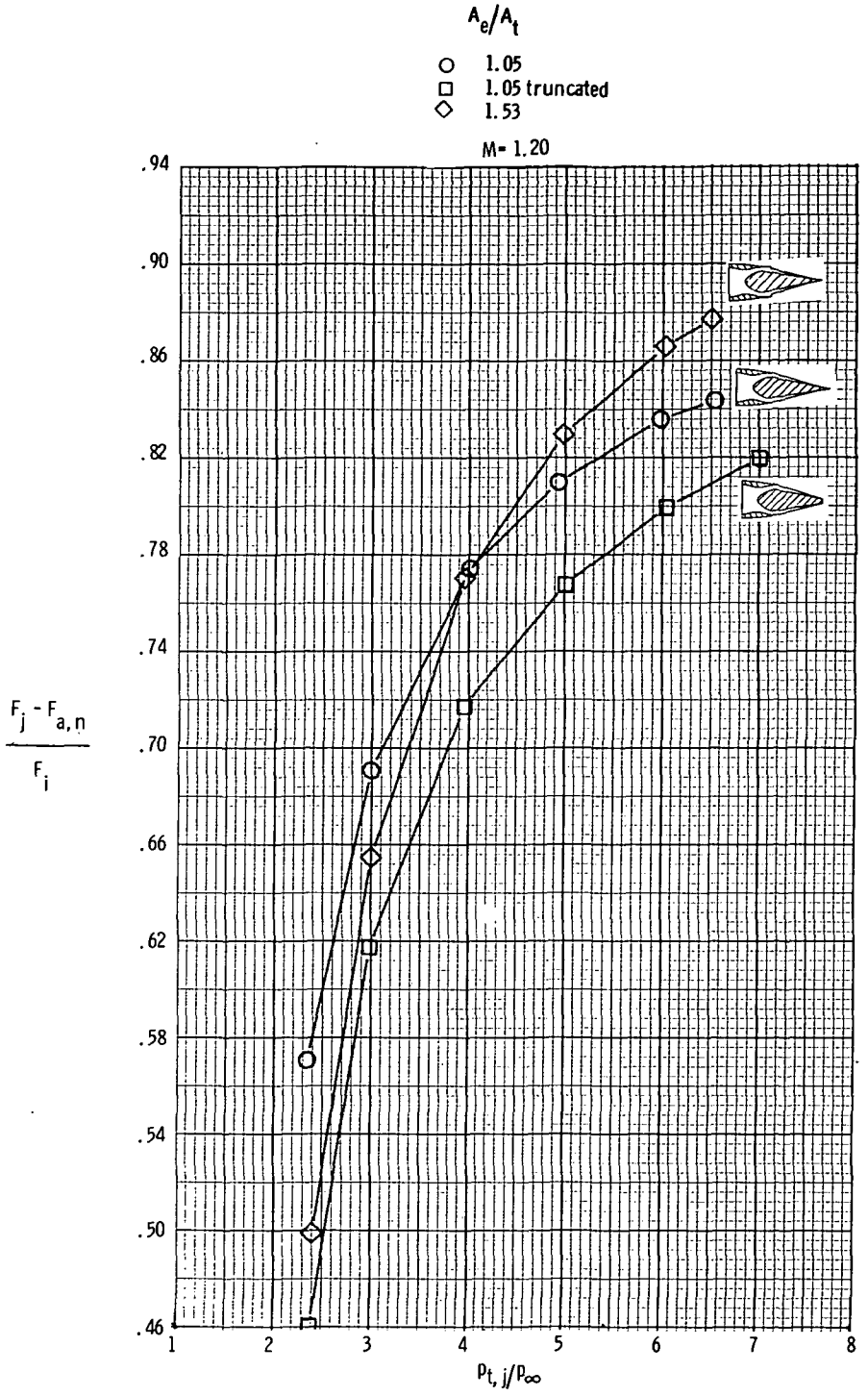

(c) M = 1.20.

Figure 11.- Concluded.

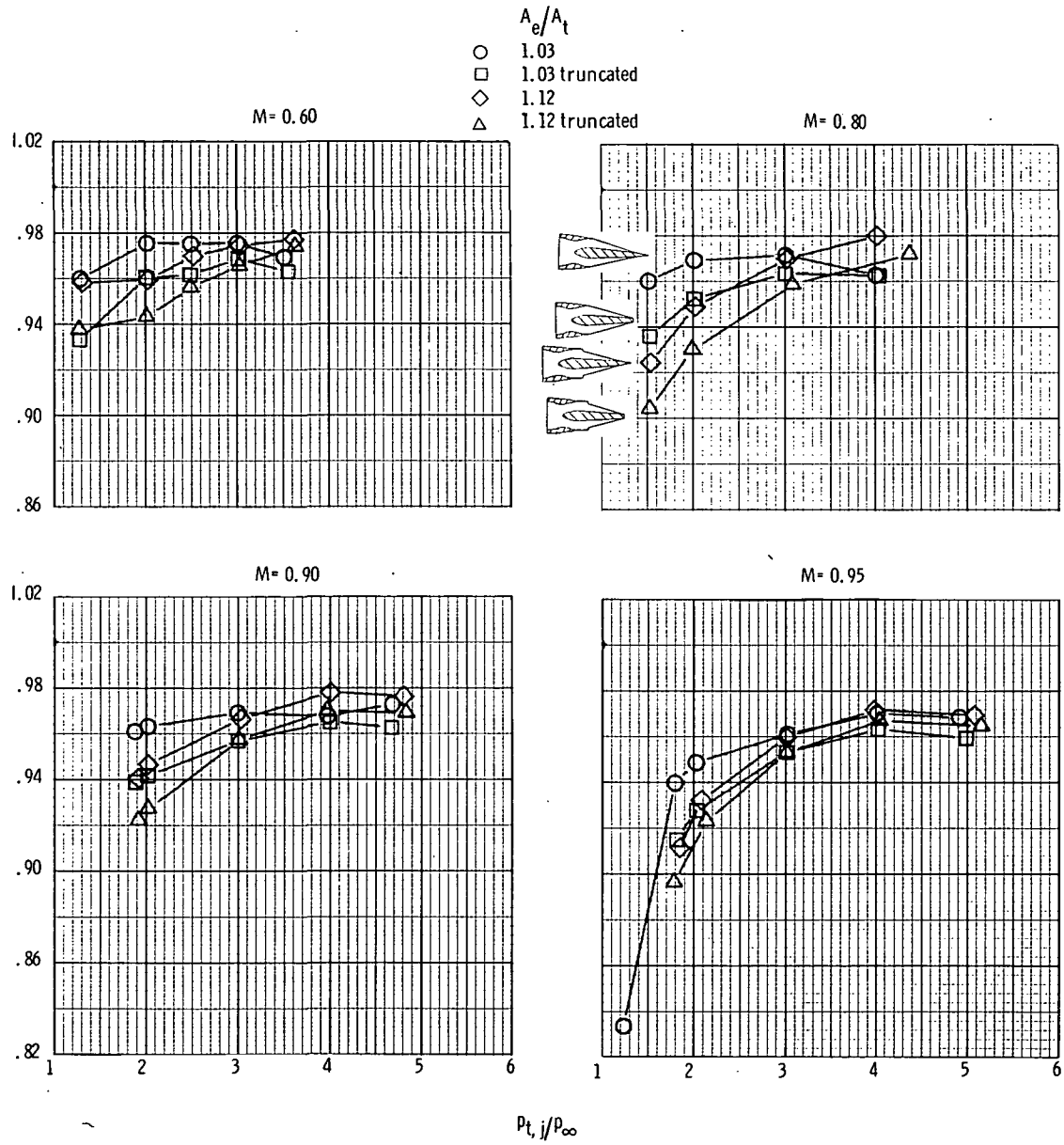

(a) M = 0.60, 0.80, 0.90, and 0.95.

Figure 12.- Variation of thrust-minus-axial-force ratio with jet total-pressure ratio for afterburner-power nozzle at several Mach numbers. $\alpha = 0^o$.

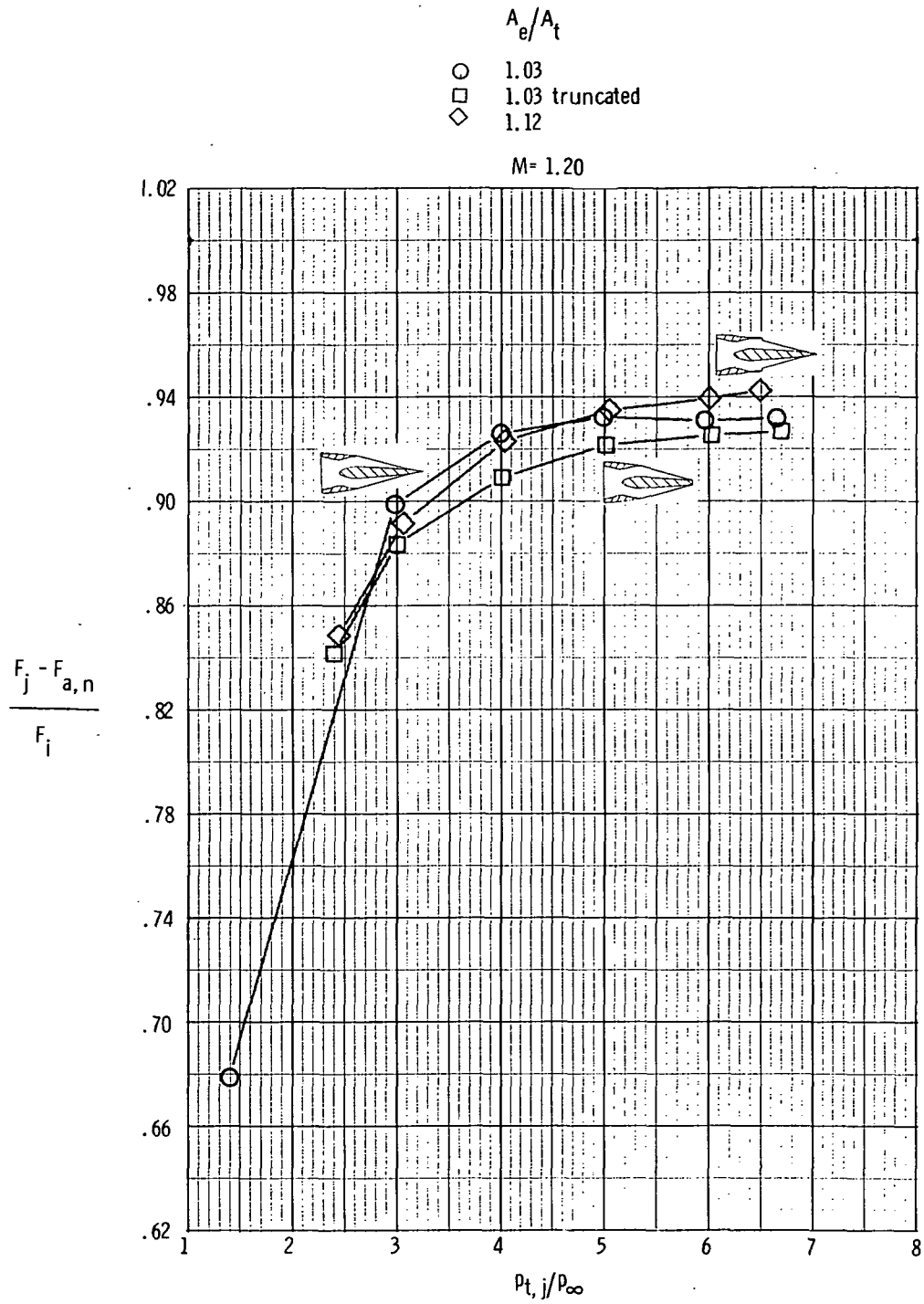

(b) M = 1.20.

Figure 12.- Continued.

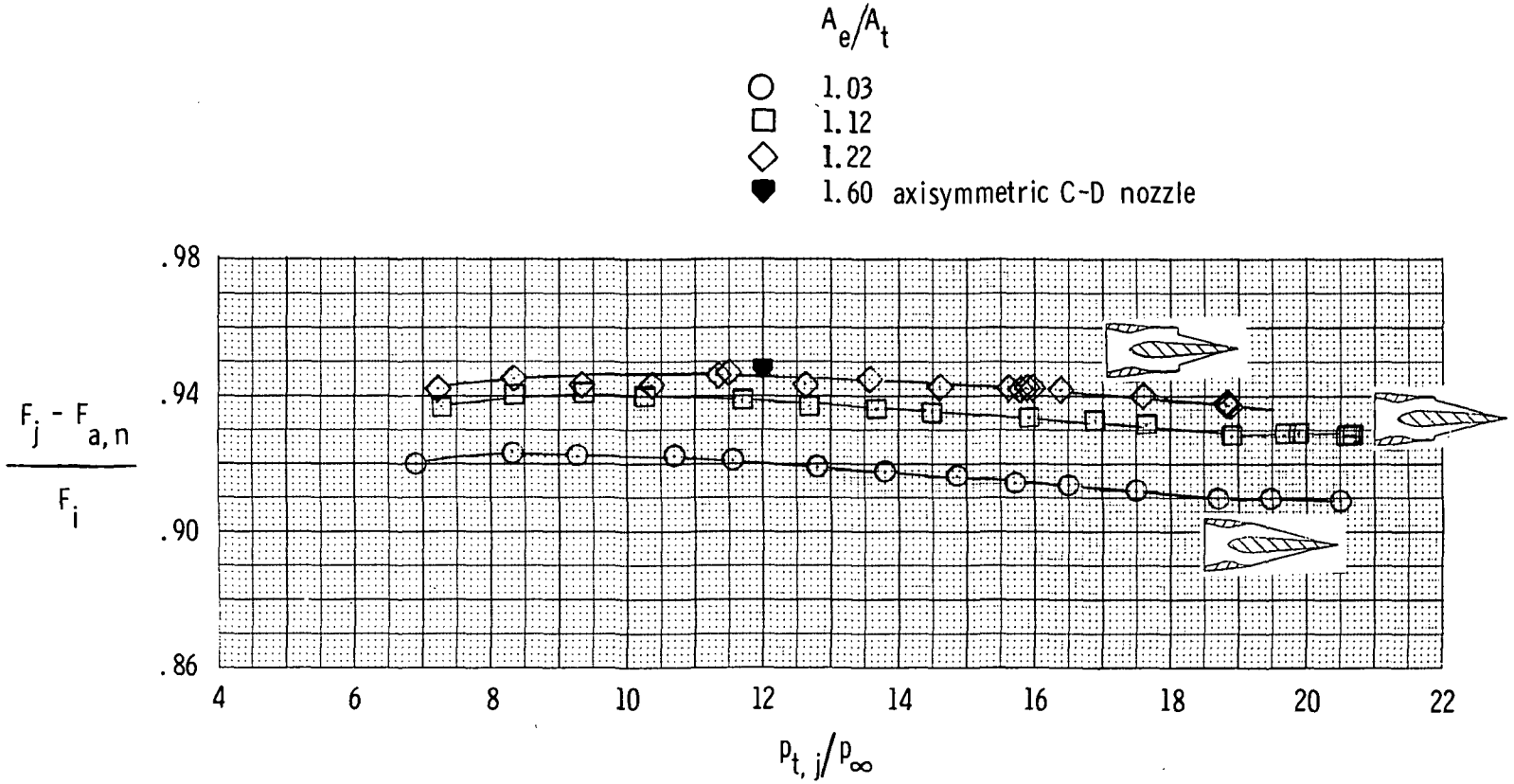

(c) M = 2.01.

Figure 12.- Concluded.

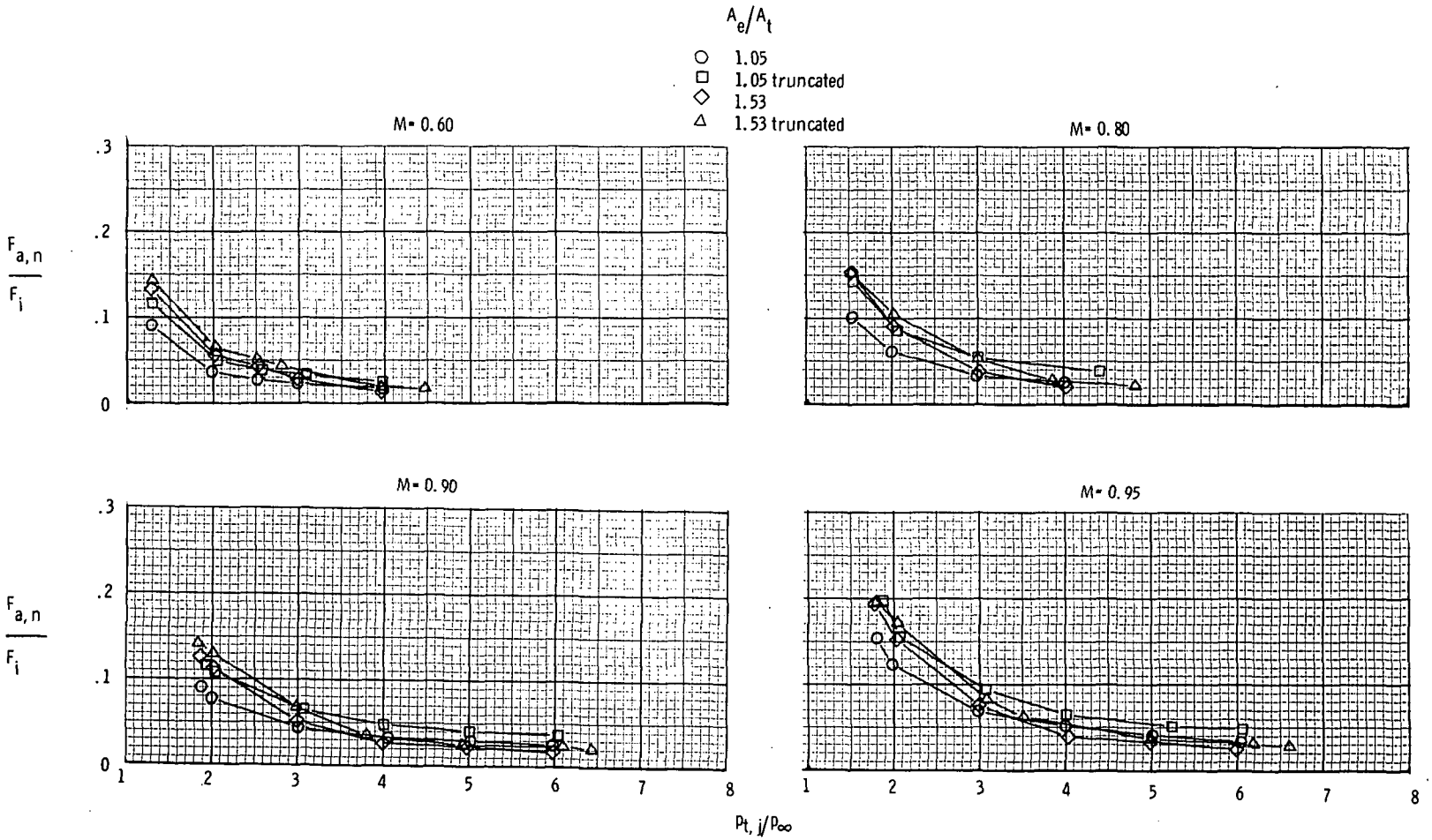

(a) M = 0.60, 0.80, 0.90, and 0.95.

Figure 13.- External flow effect on dry-power nozzle wedge and cowl axial-force ratio.

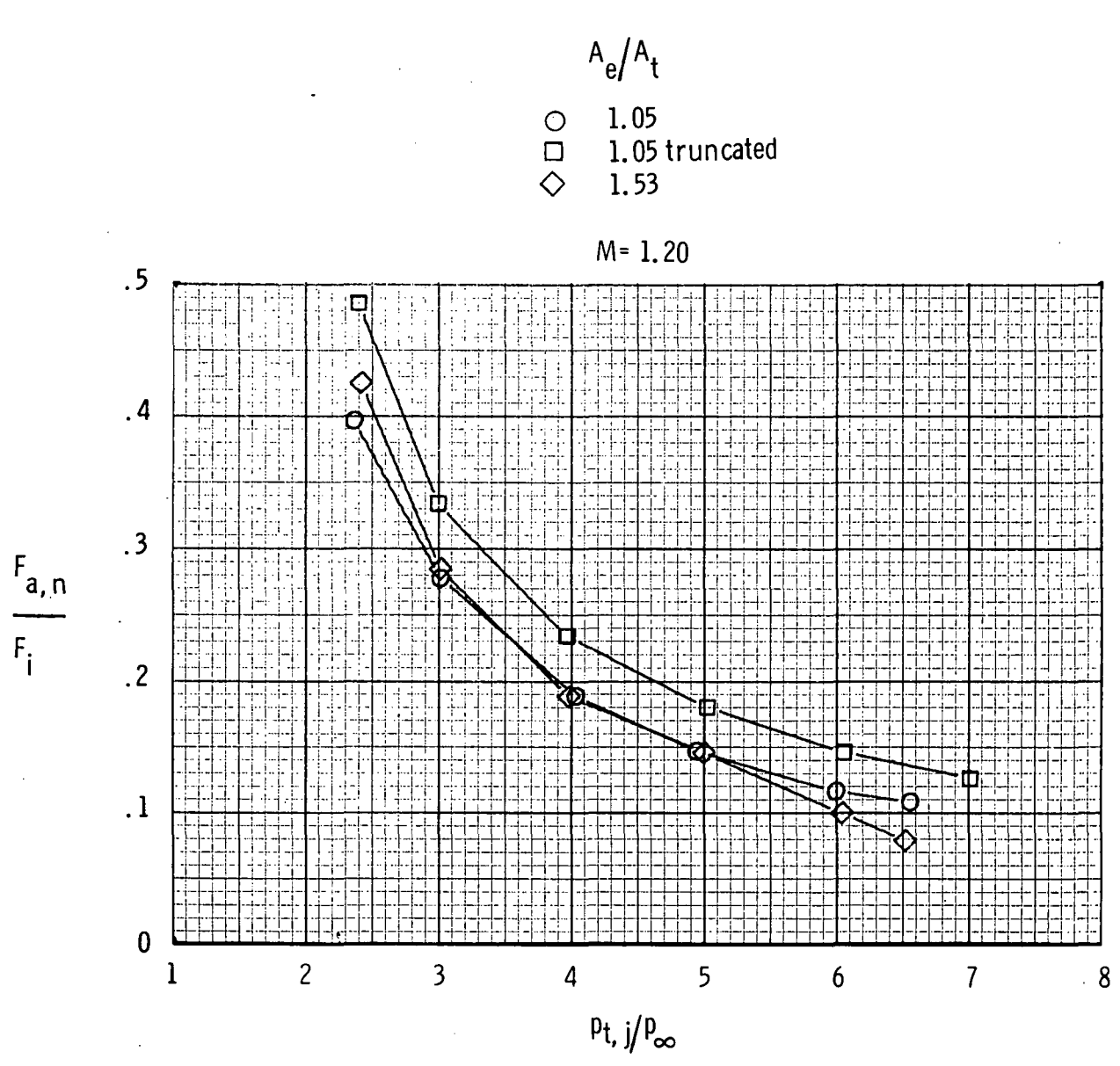

(b) M = 1.20.

Figure 13.- Concluded.

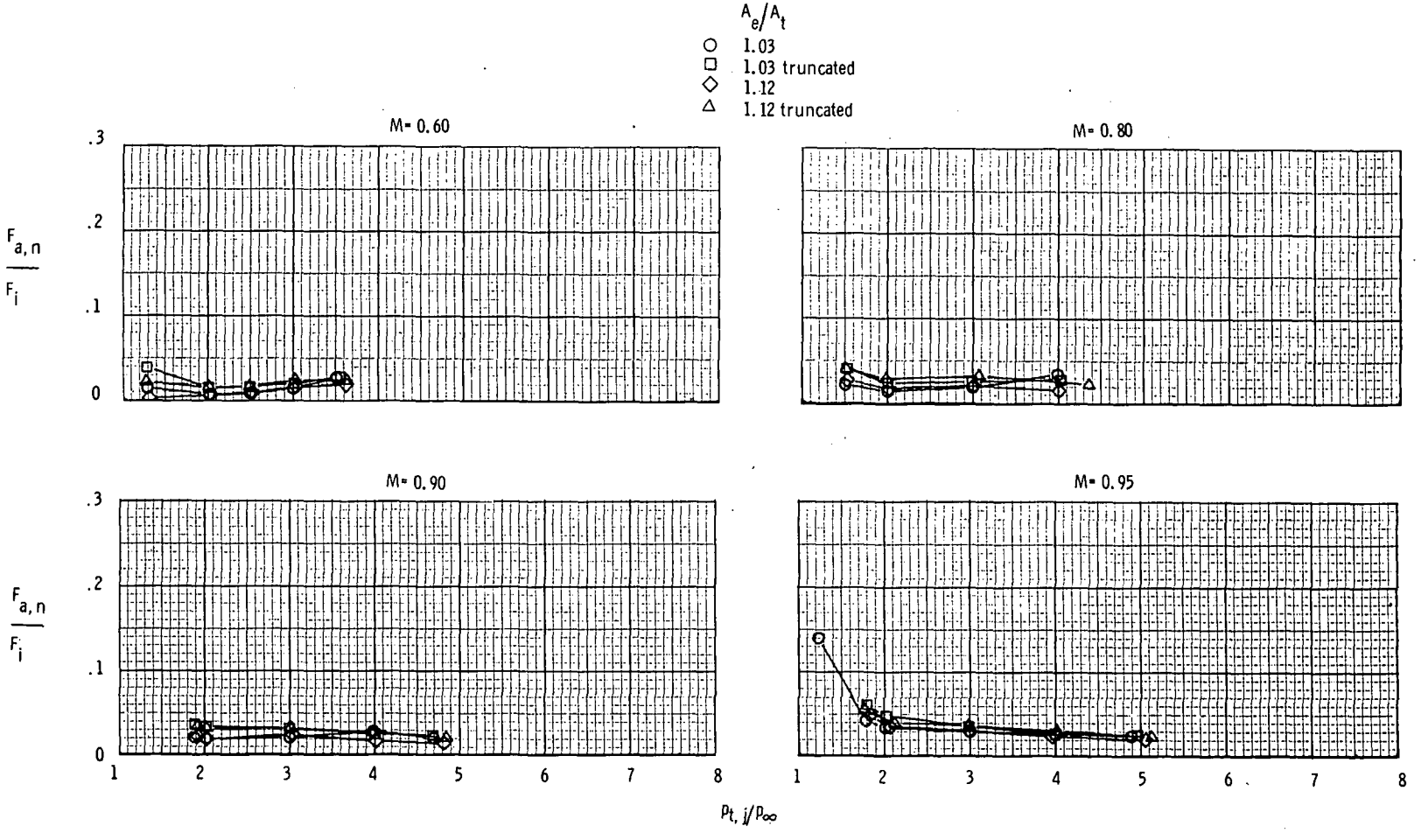

(a) M = 0.60, 0.80, 0.90, and 0.95.

Figure 14.- External flow effect on afterburner-power nozzle wedge and cowl axial-force ratio.

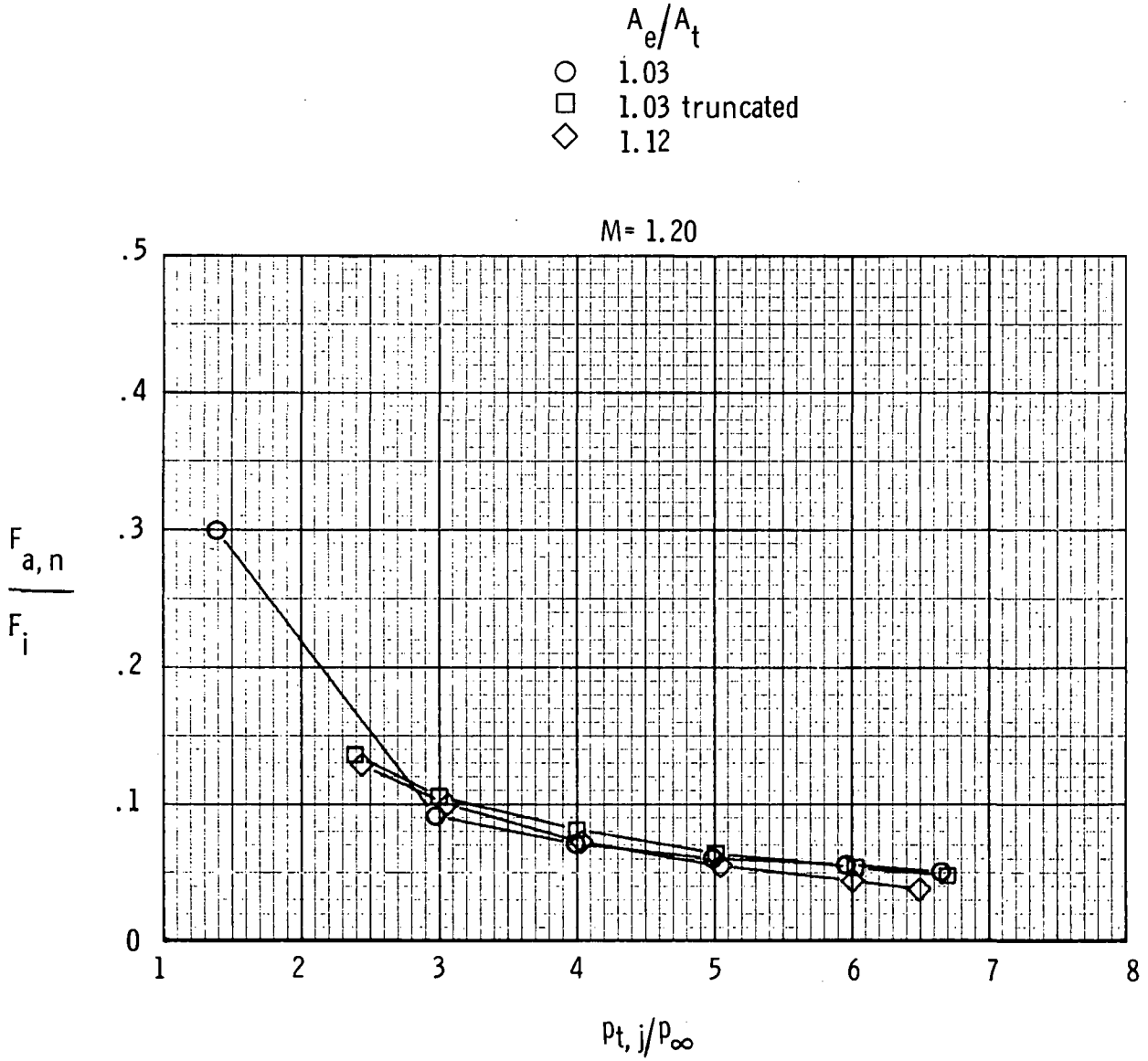

(b) M = 1.20.

Figure 14.- Concluded.

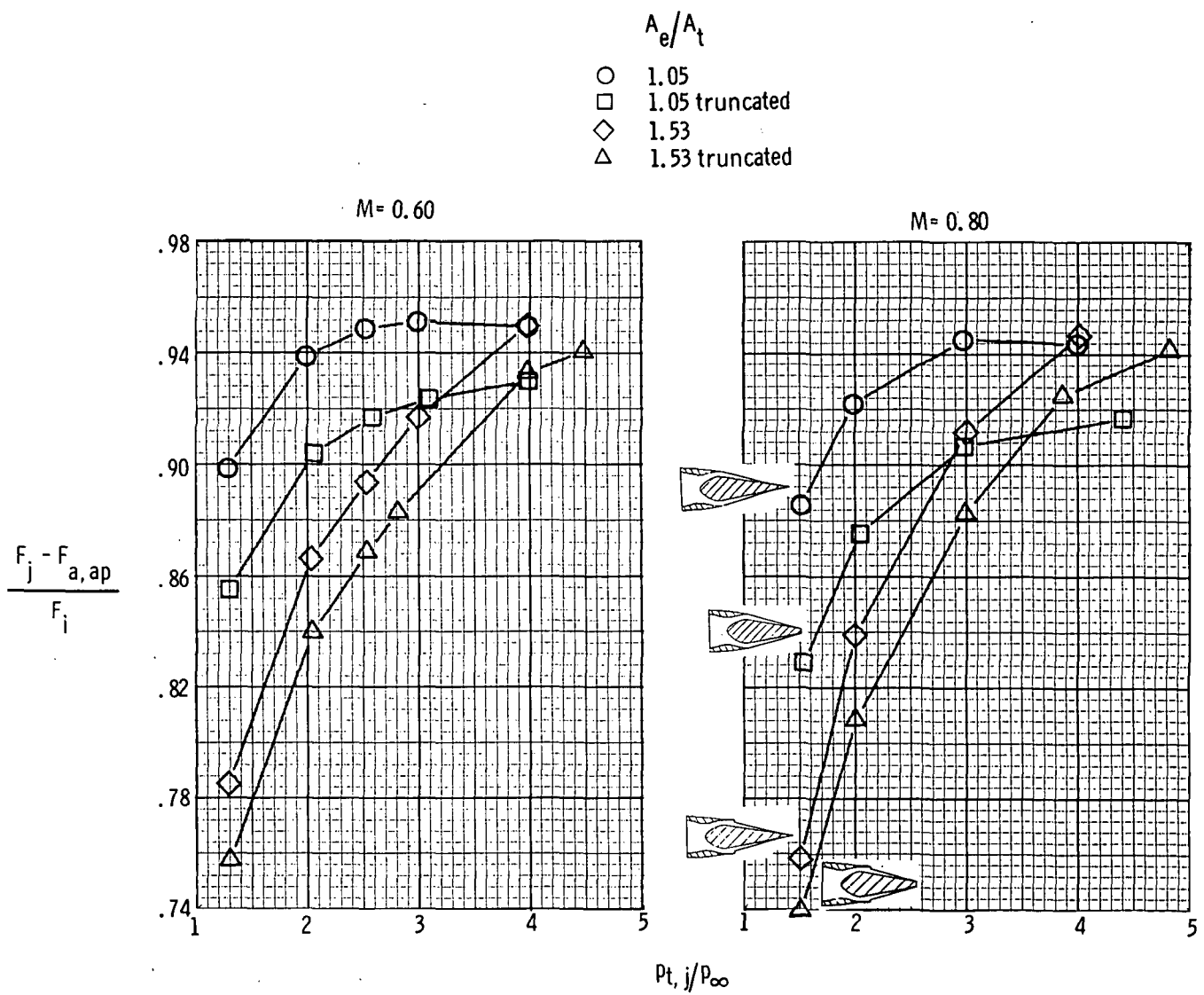

(a) M = 0.60 and 0.80.

Figure 15.- Variation of thrust-minus-axial pressure-force ratio with jet total-pressure ratio for dry-power nozzle at several Mach numbers. $\alpha = 0^o$.

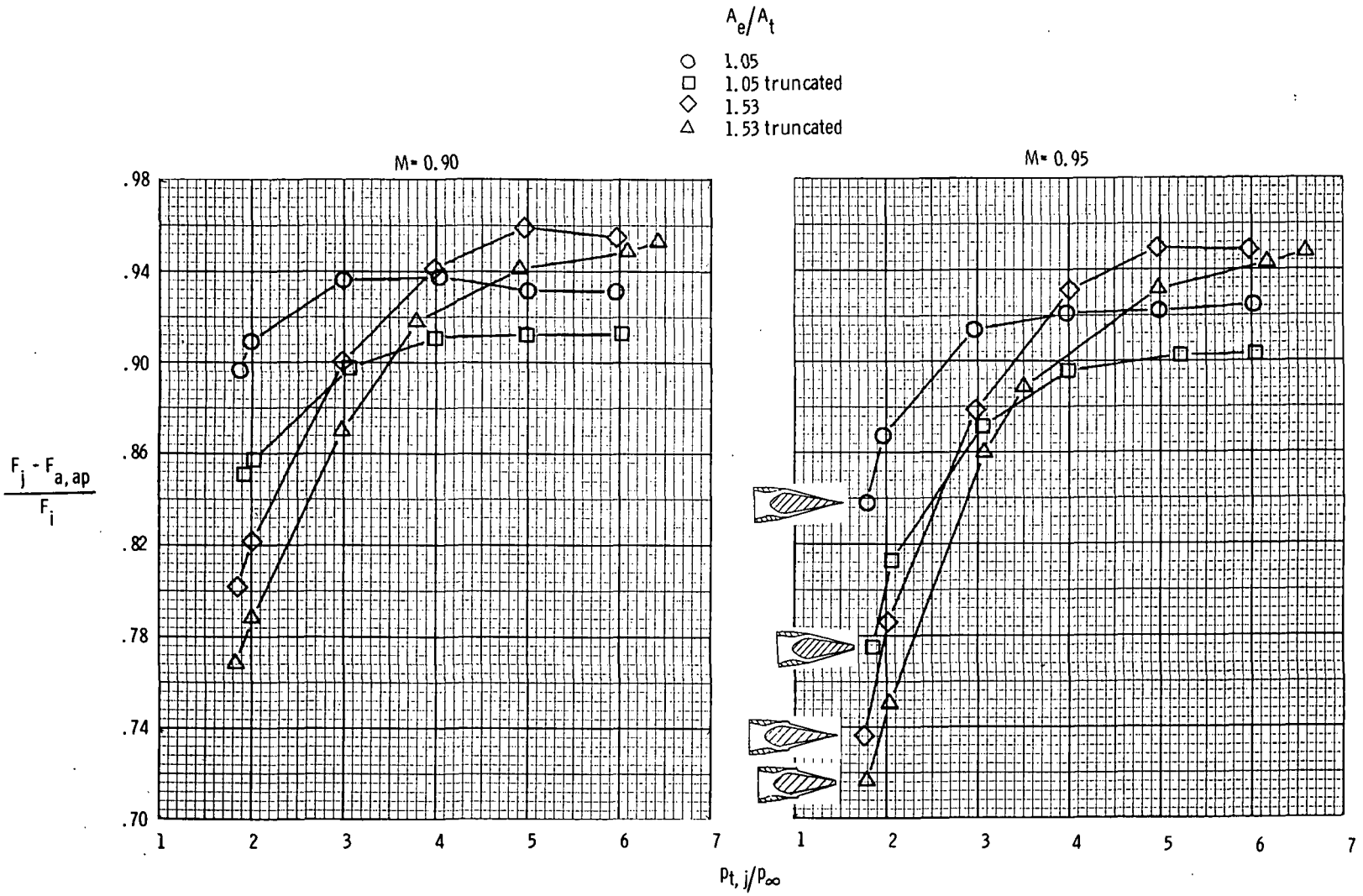

(b) M = 0.90 and 0.95.

Figure 15.- Continued.

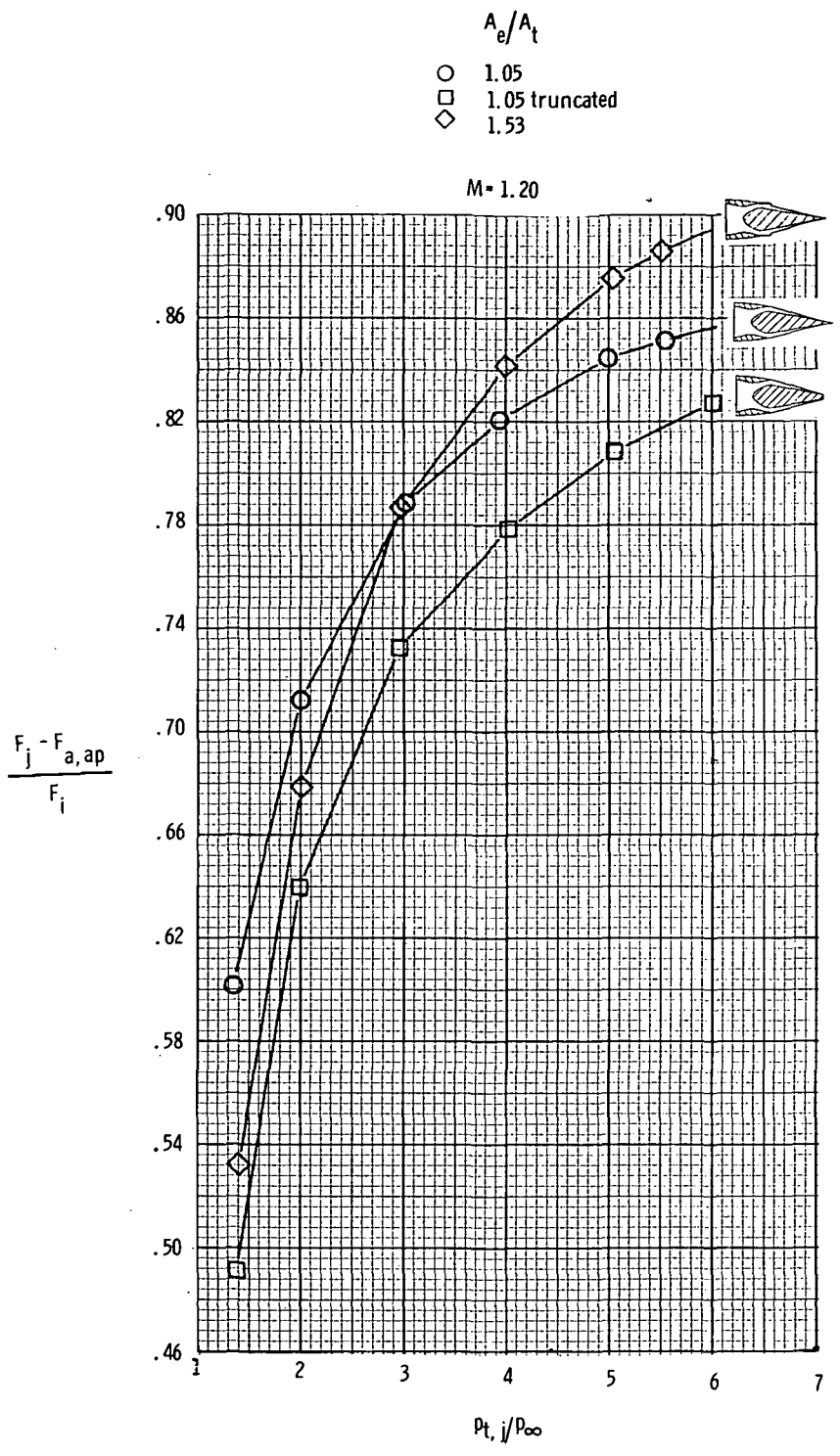

(c) M = 1.20.

Figure 15.- Concluded.

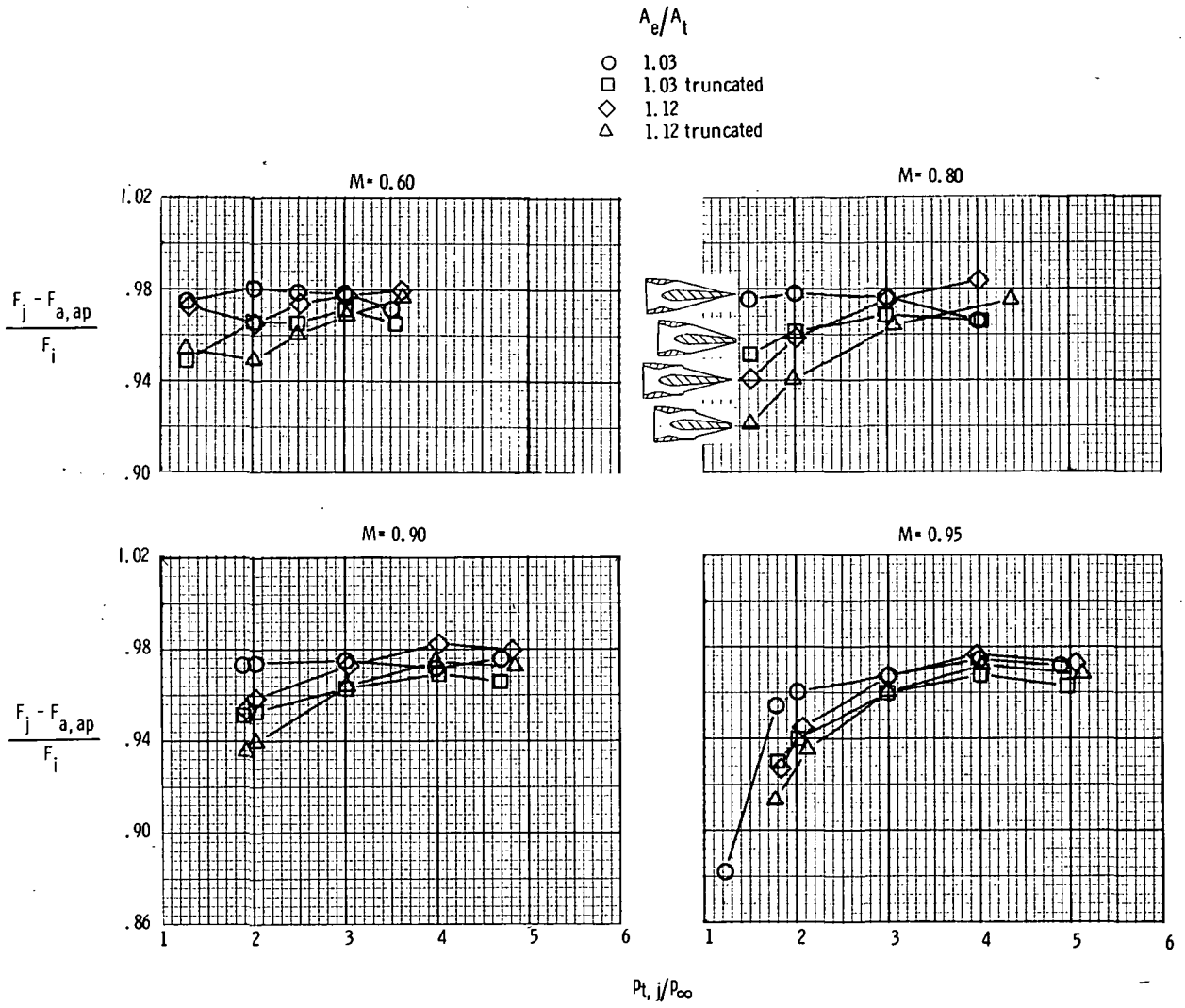

(a) M = 0.60, 0.80, 0.90, and 0.95.

Figure 16.- Variation of thrust-minus-axial pressure-force ratio with jet total-pressure ratio for afterburner-power nozzle at several Mach numbers. $\alpha = 0^o$.

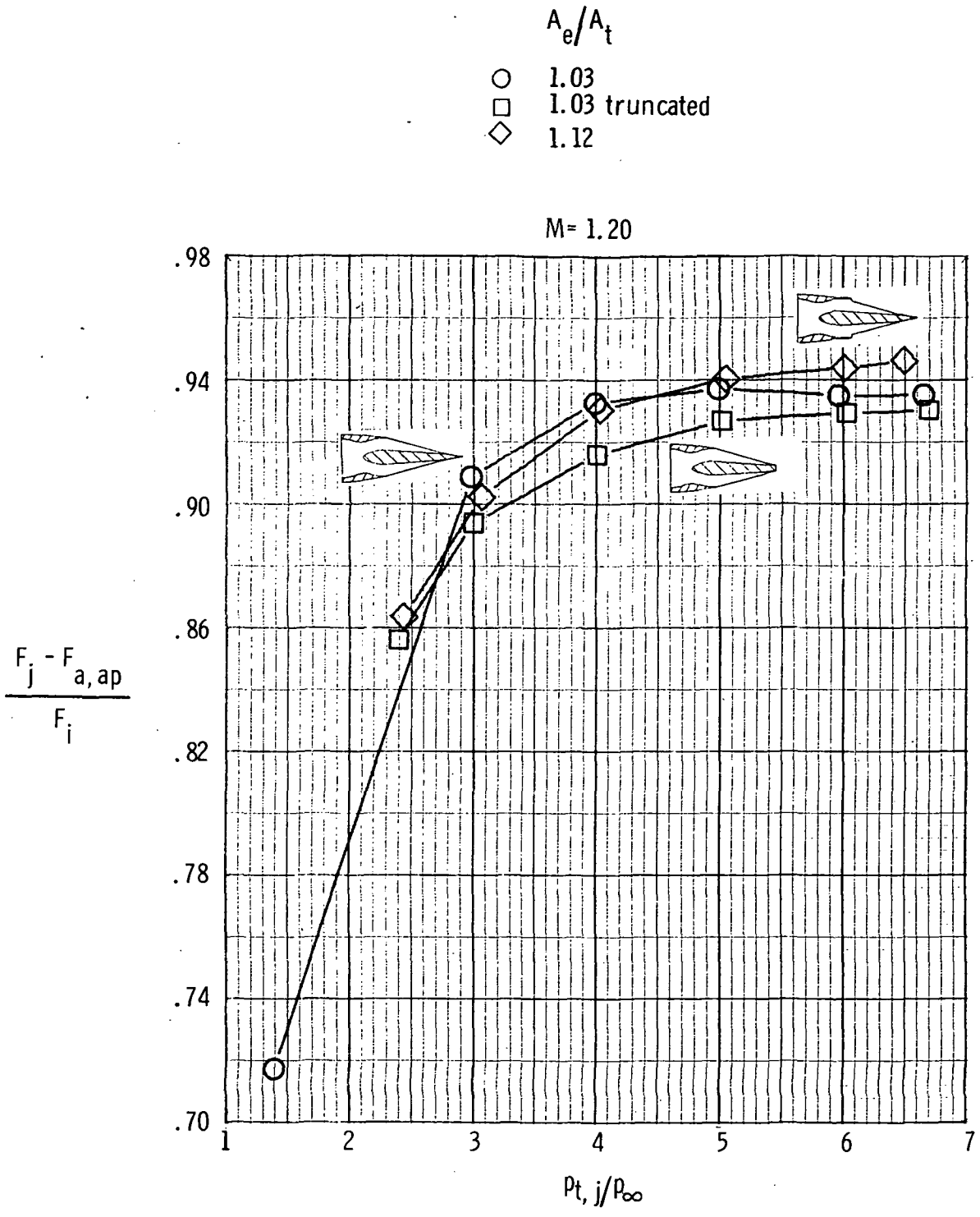

(b) M = 1.20.

Figure 16.- Continued.

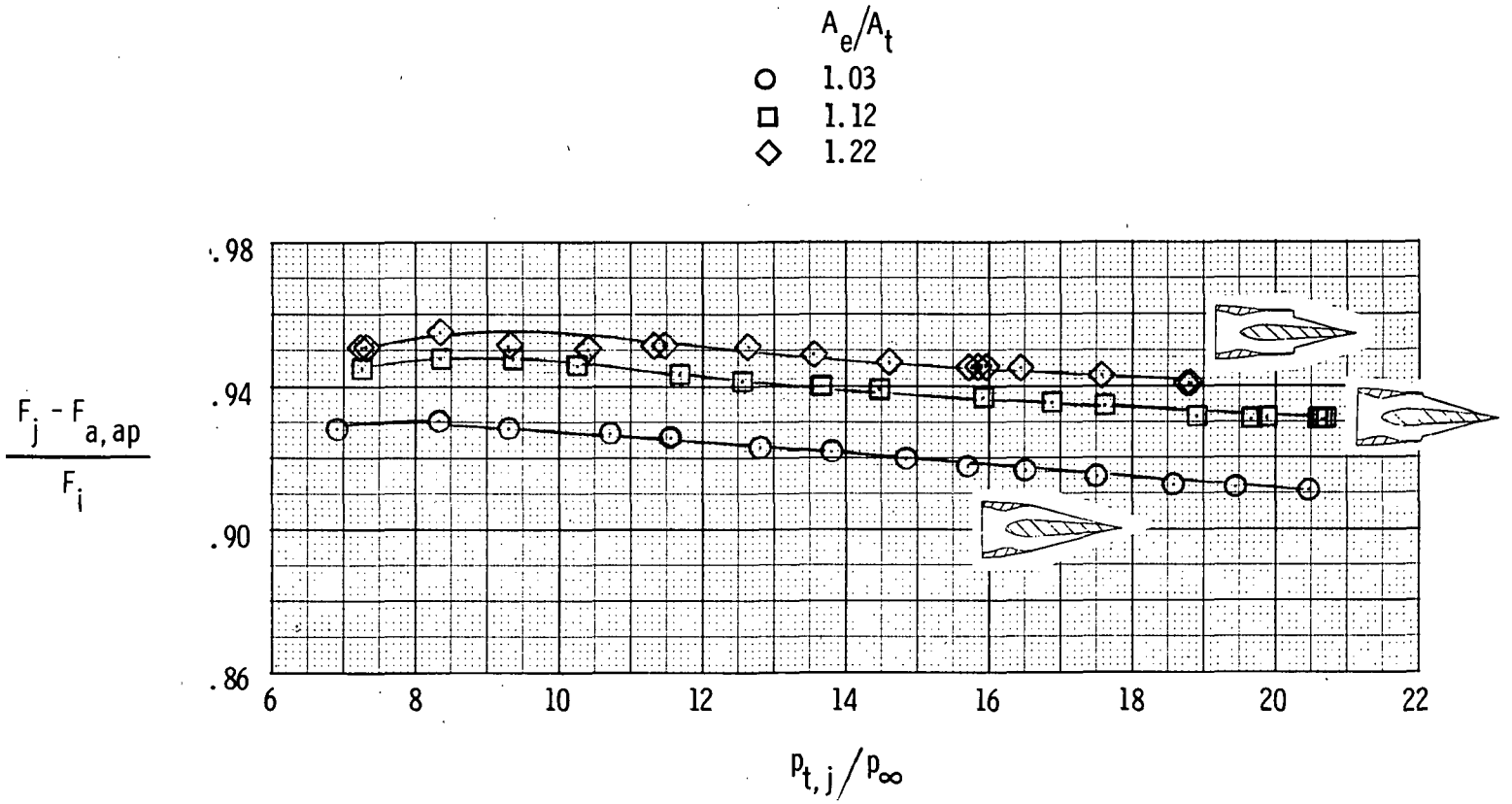

(c) M = 2.01.

Figure 16.- Concluded.

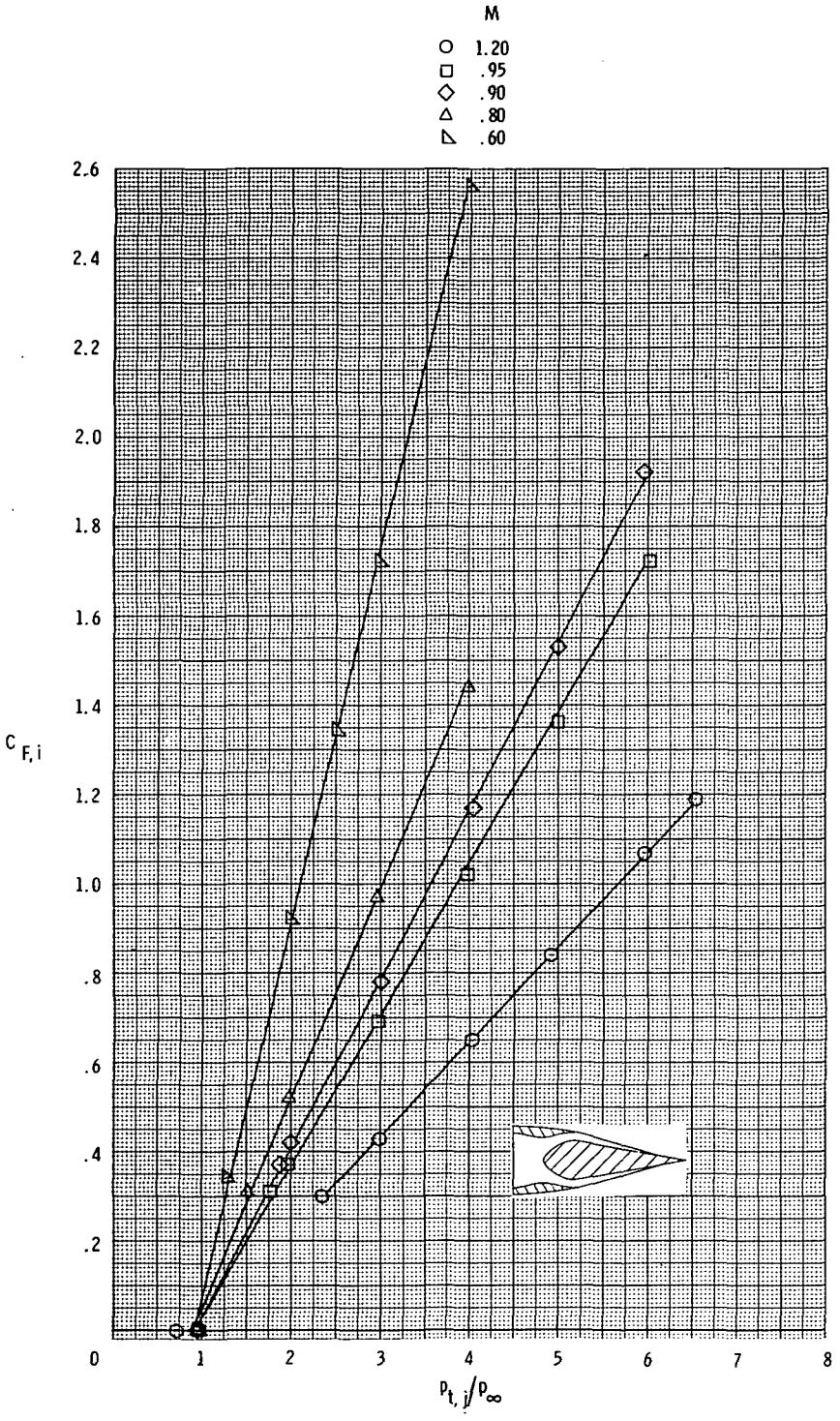

(a) Dry-power nozzle. $A_e/A_t = 1.05$.

Figure 17.- Variation of aerodynamic ideal thrust coefficient with jet total-pressure ratio for all configurations at several Mach numbers.

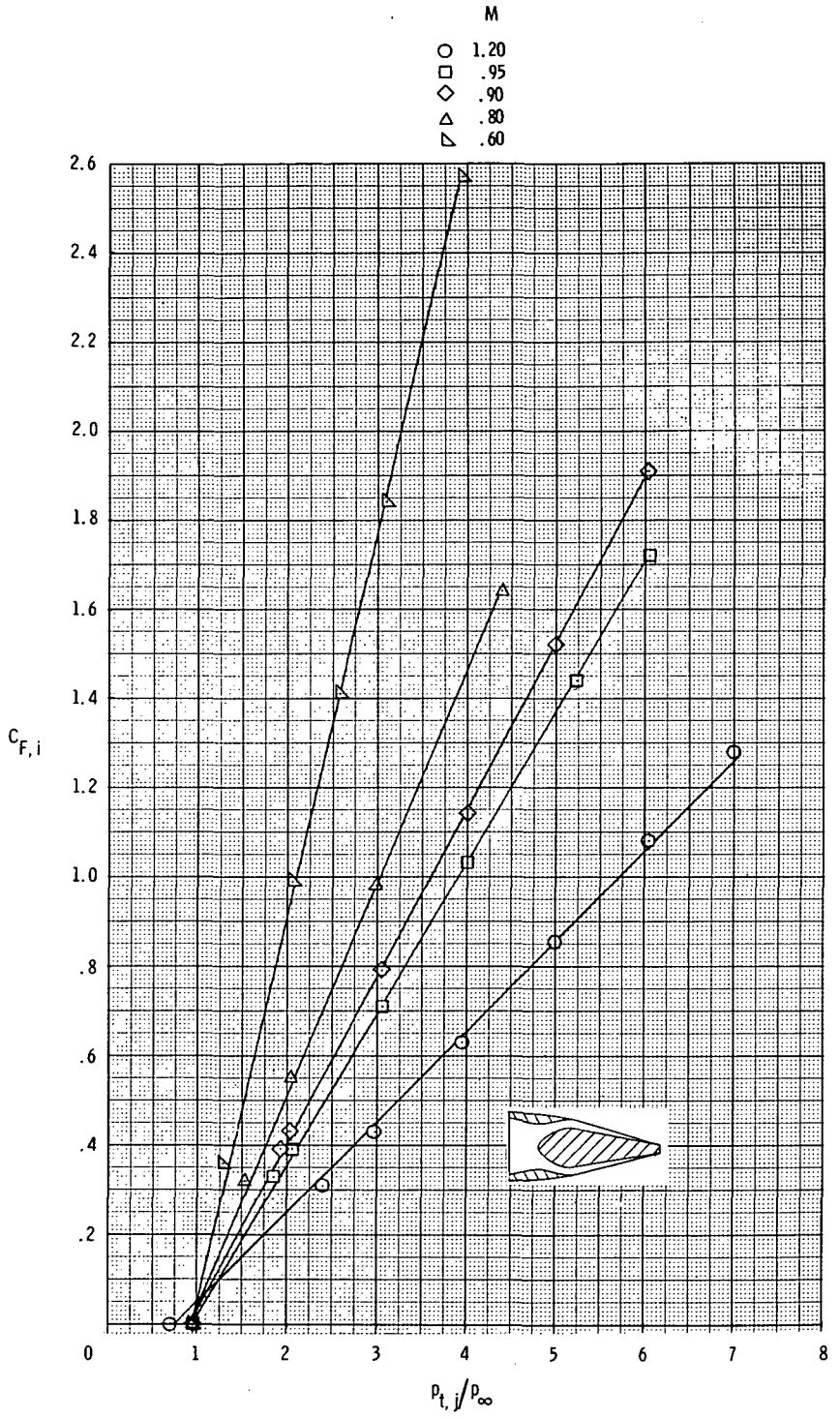

(b) Truncated-wedge dry-power nozzle. $A_e/A_t = 1.05$.

Figure 17.- Continued.

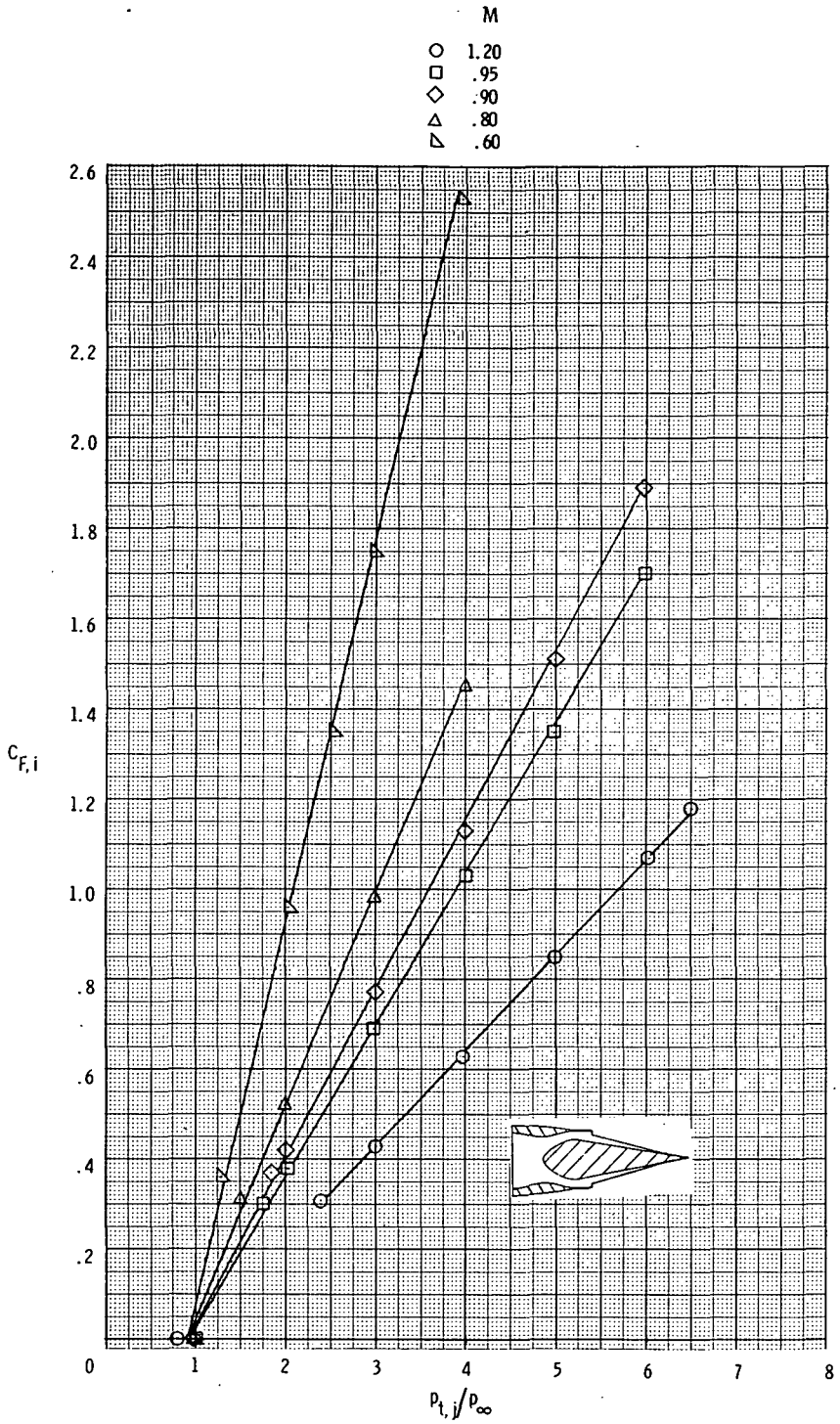

(c) Dry-power nozzle. $A_e/A_t = 1.53$.

Figure 17.- Continued.

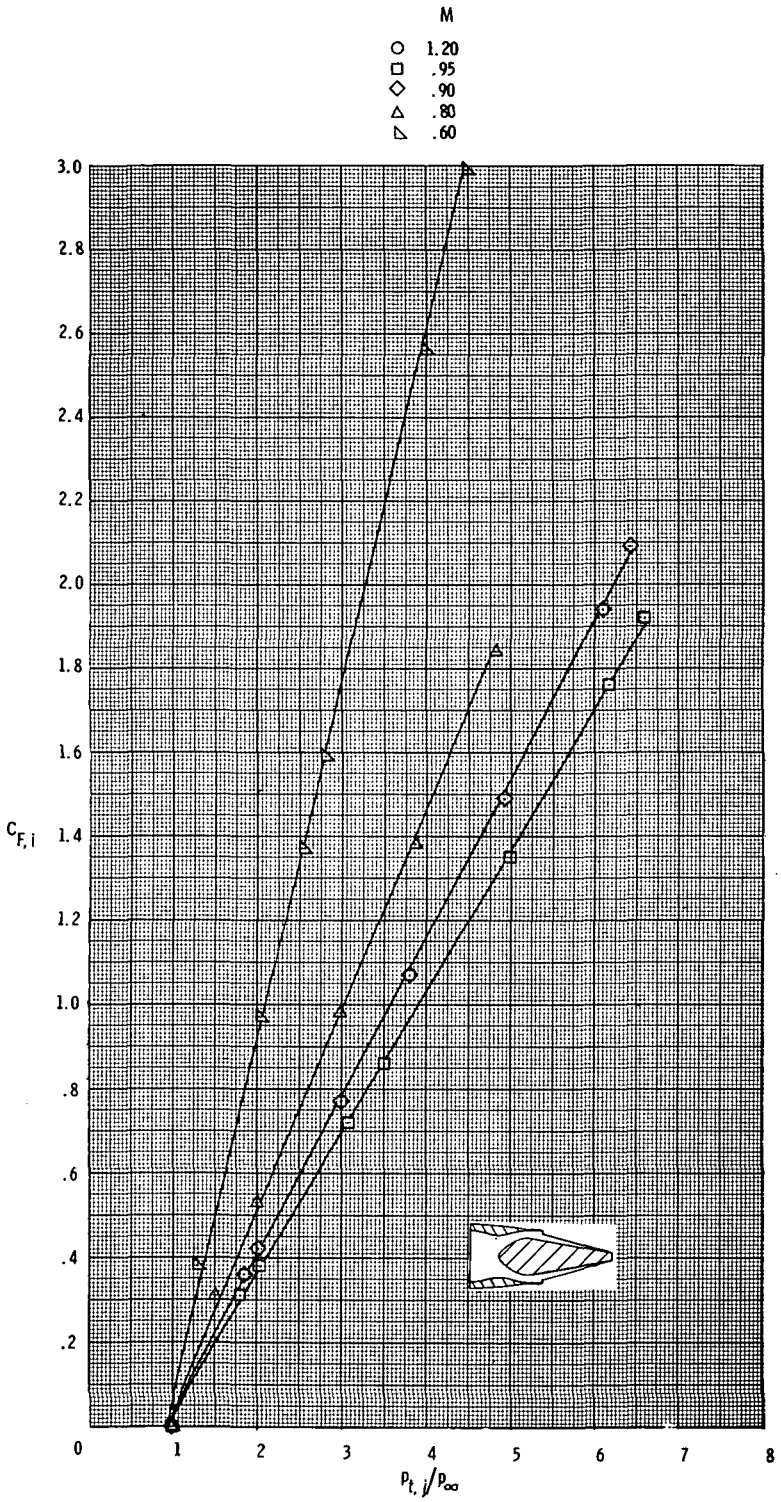

(d) Truncated-wedge dry-power nozzle. $A_e/A_t = 1.53$.

Figure 17.- Continued.

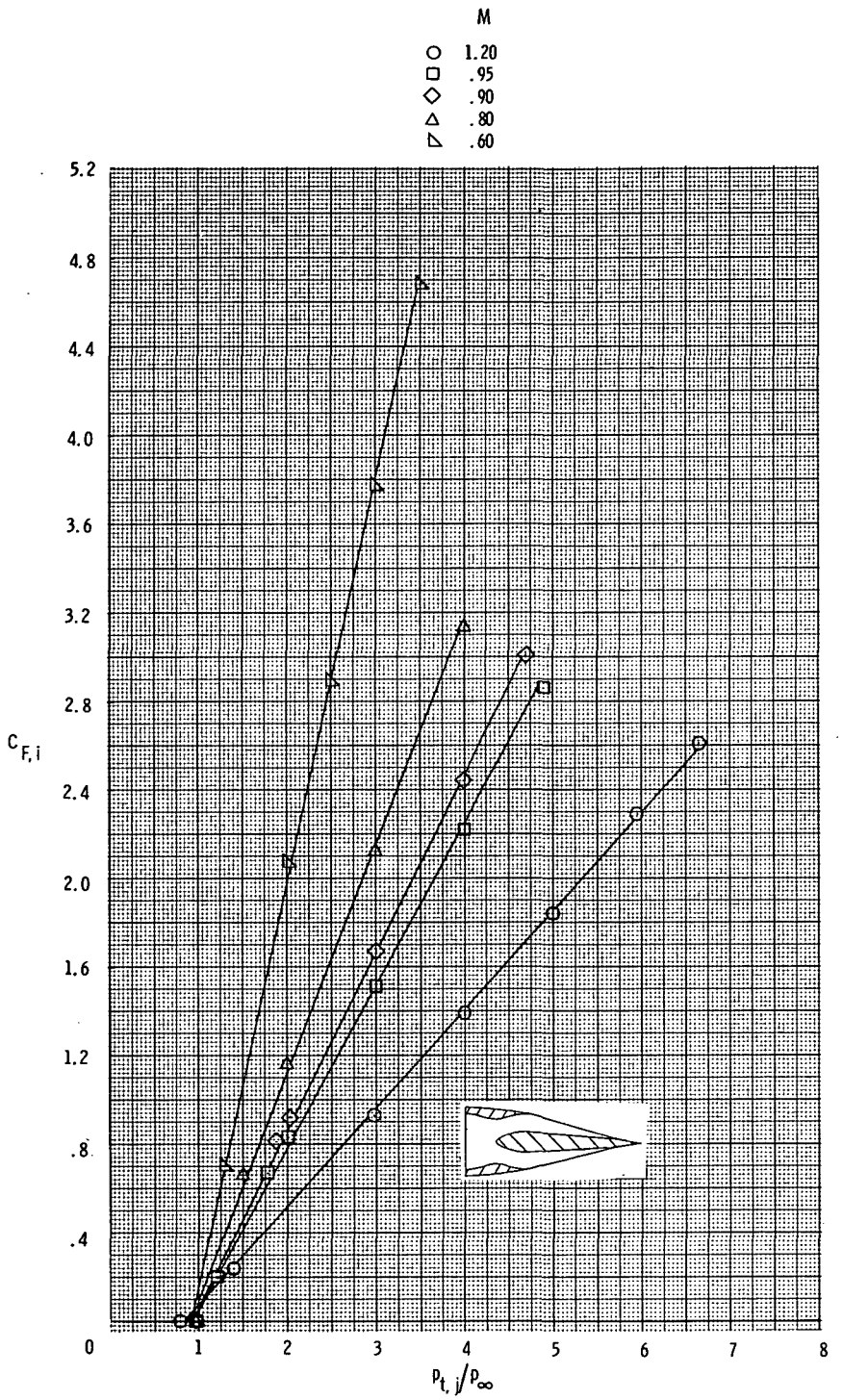

(e) Afterburner-power nozzle. $A_e/A_t = 1.03$.

Figure 17.- Continued.

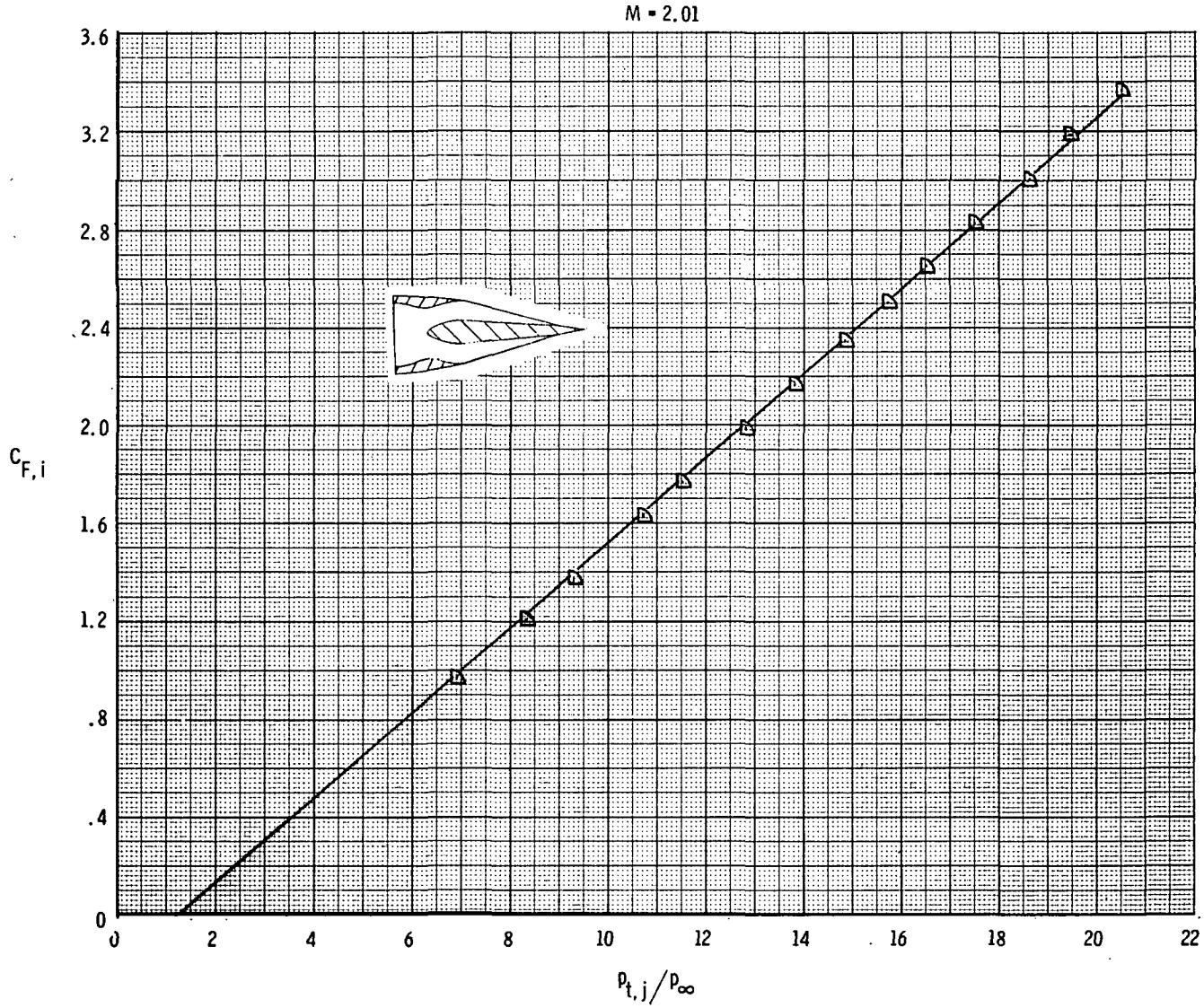

(e) Concluded. $A_e/A_t = 1.03$.

Figure 17.- Continued.

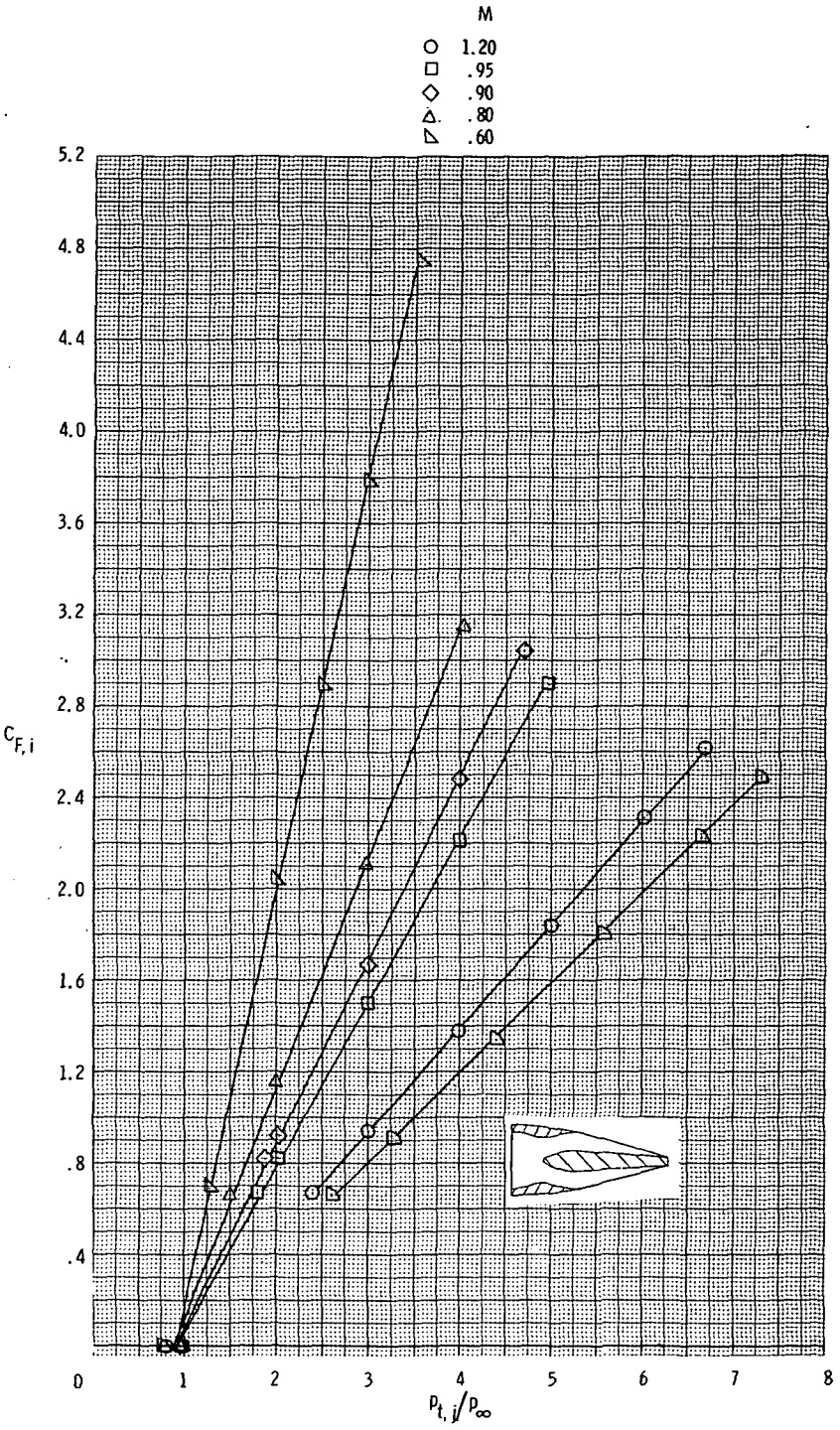

(f) Truncated-wedge afterburner-power nozzle. $A_e/A_t = 1.03$.

Figure 17.- Continued.

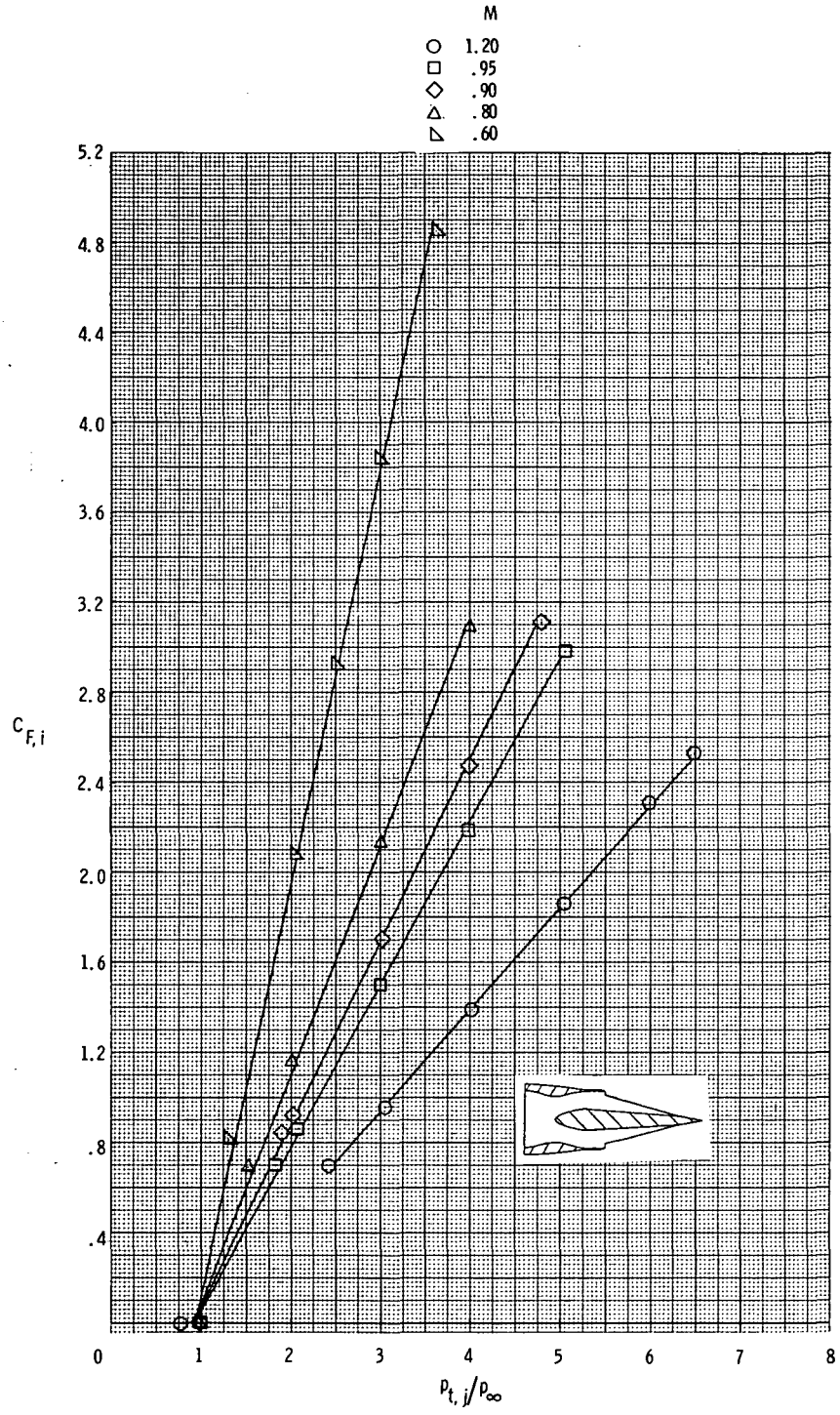

(g) Afterburner power nozzle. $A_e/A_t = 1.12$.

Figure 17.- Continued.

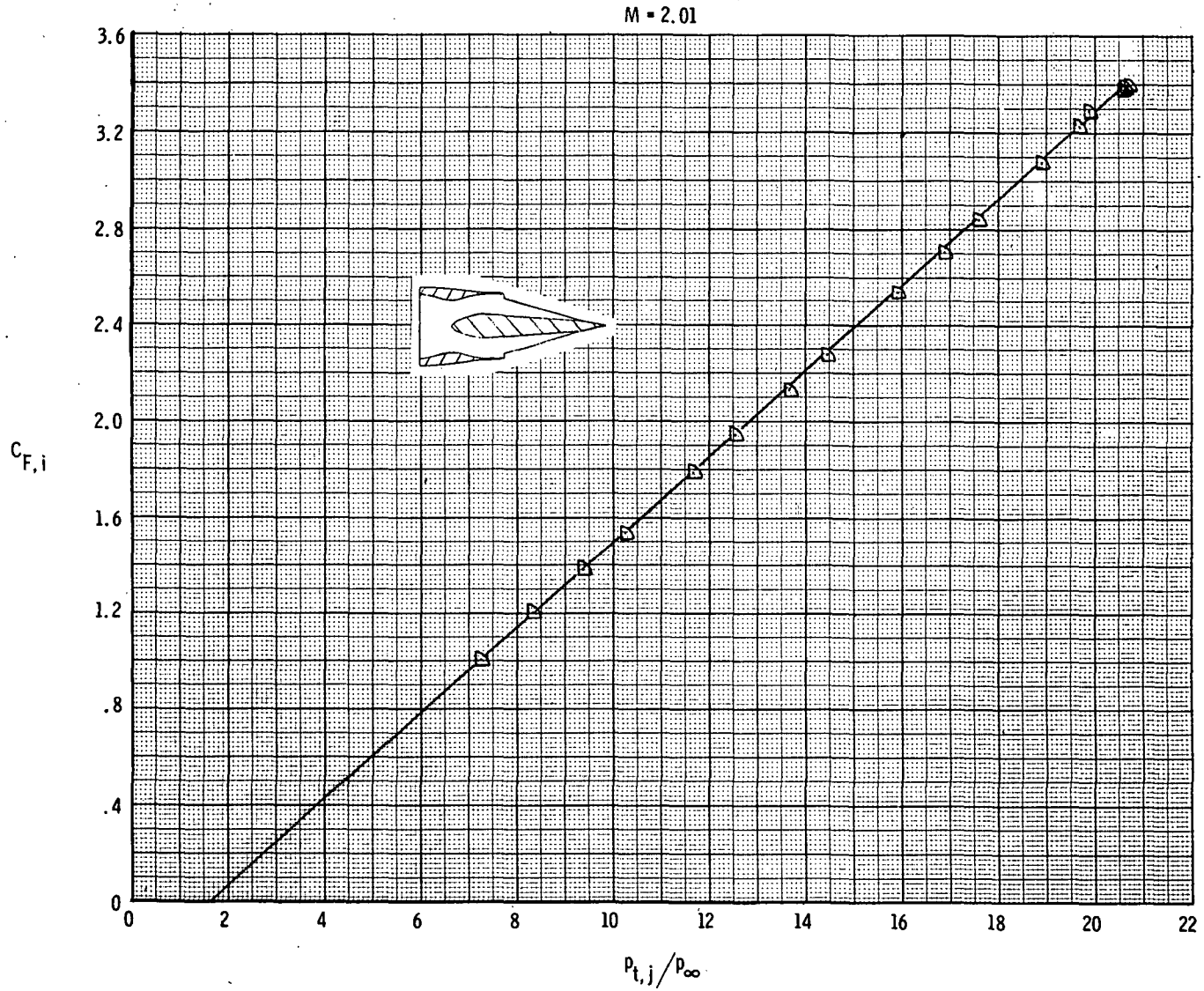

(g) Concluded. $A_e/A_t = 1.12$.

Figure 17.- Continued.

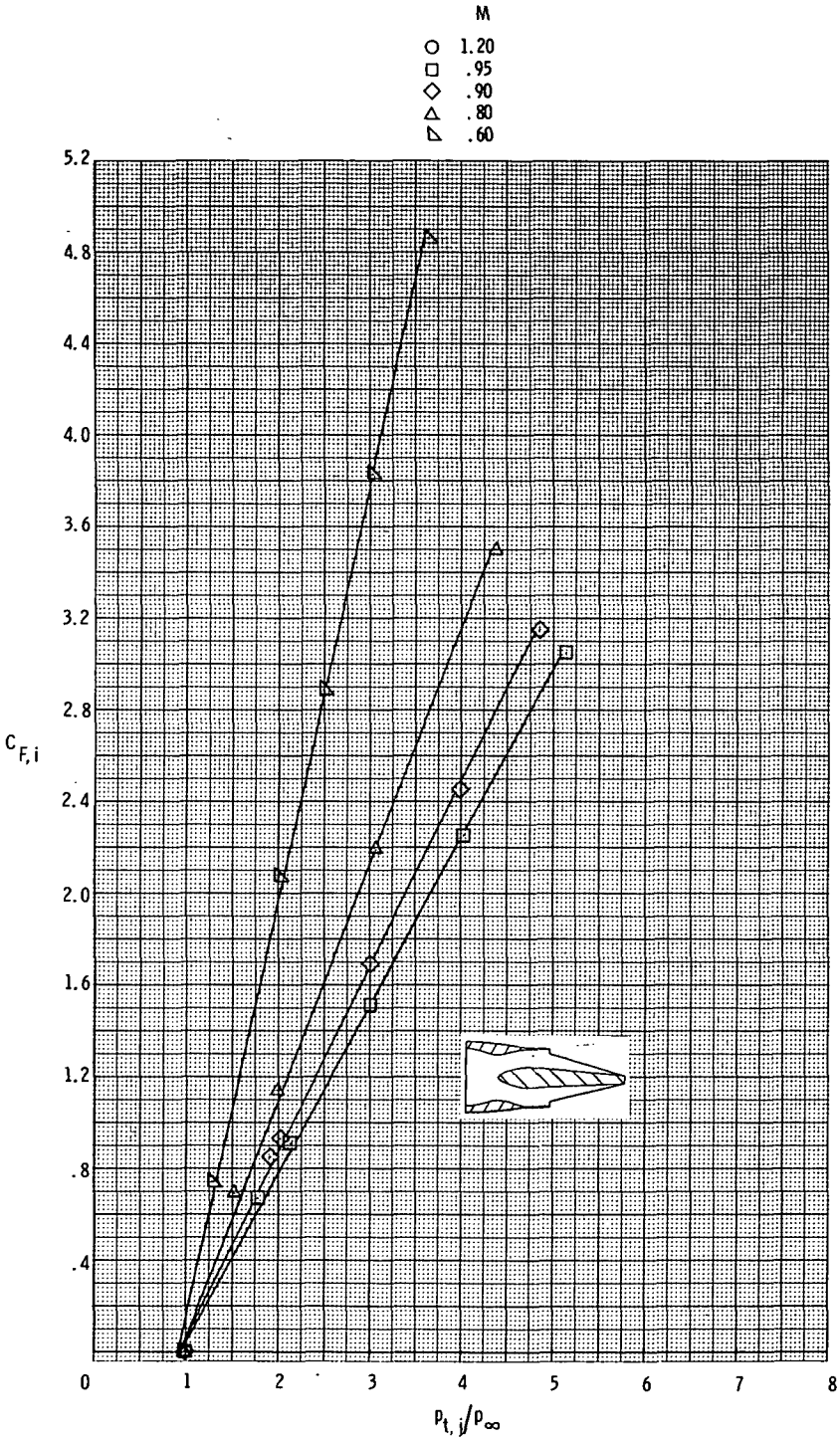

(h) Truncated-wedge afterburner-power nozzle. $A_e/A_t = 1.12$.

Figure 17.- Continued.

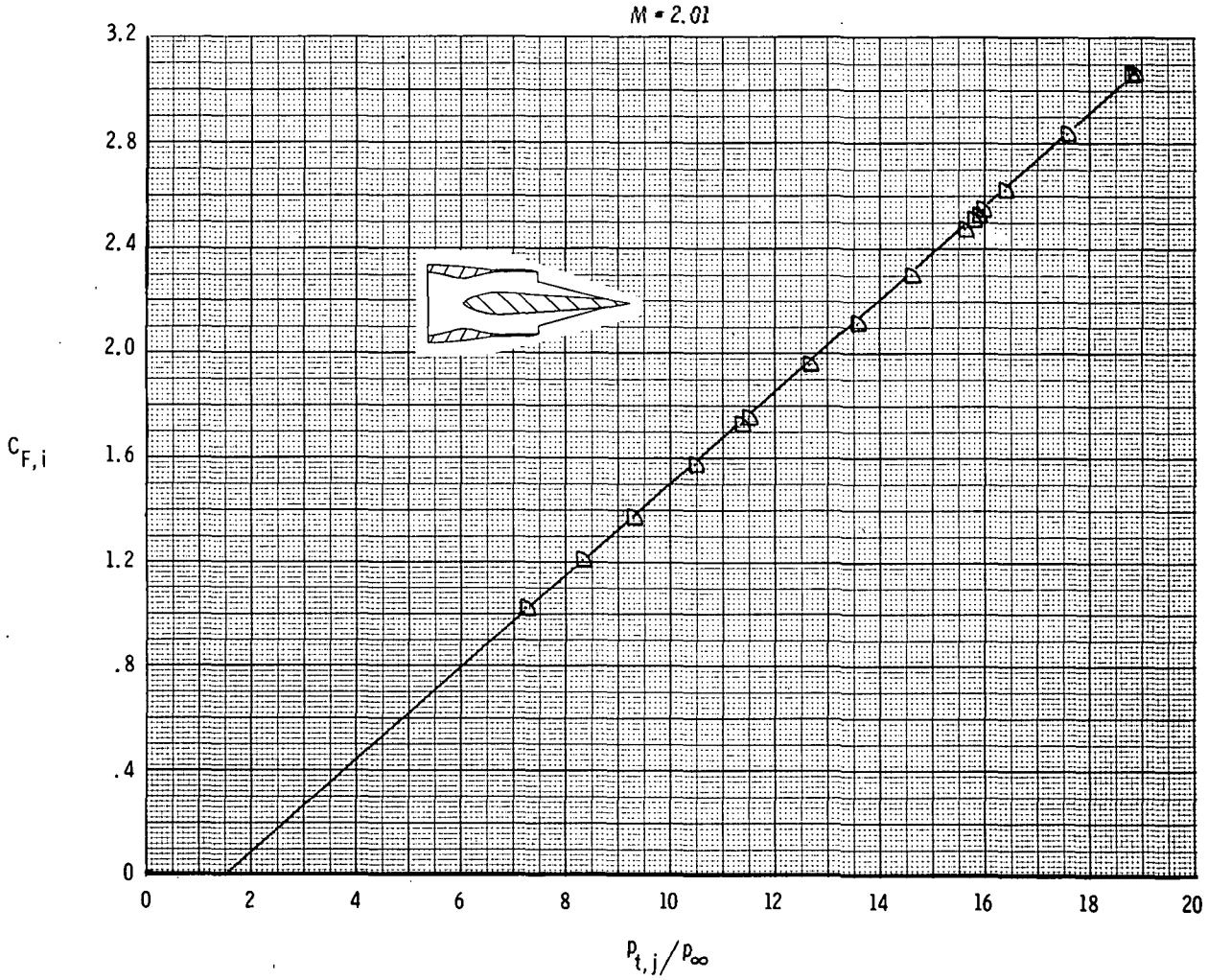

(i) Afterburner-power nozzle. $A_e/A_t = 1.22$.

Figure 17.- Concluded.

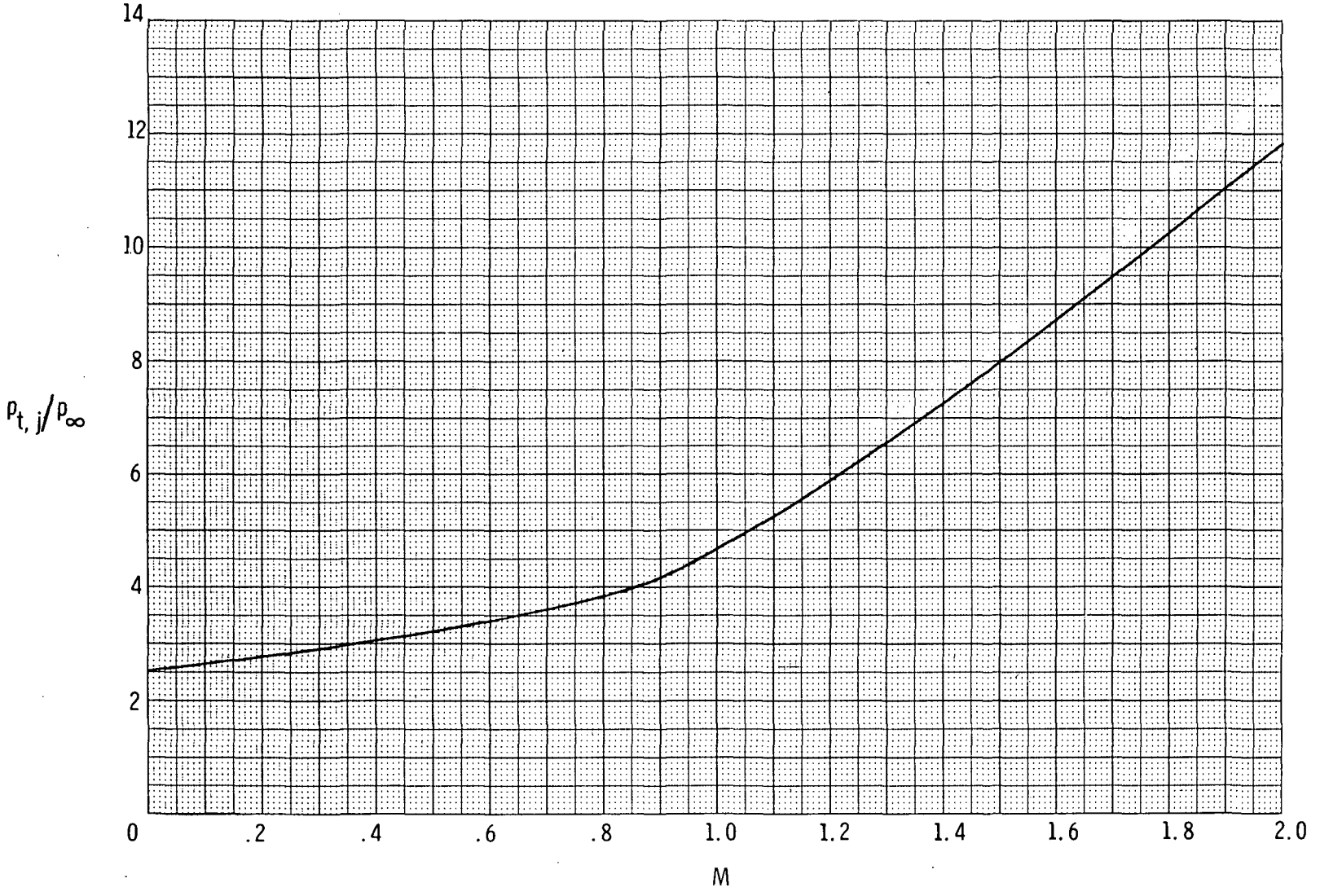

Figure 18.- Typical schedule of advanced engine total-pressure ratio with flight Mach number.

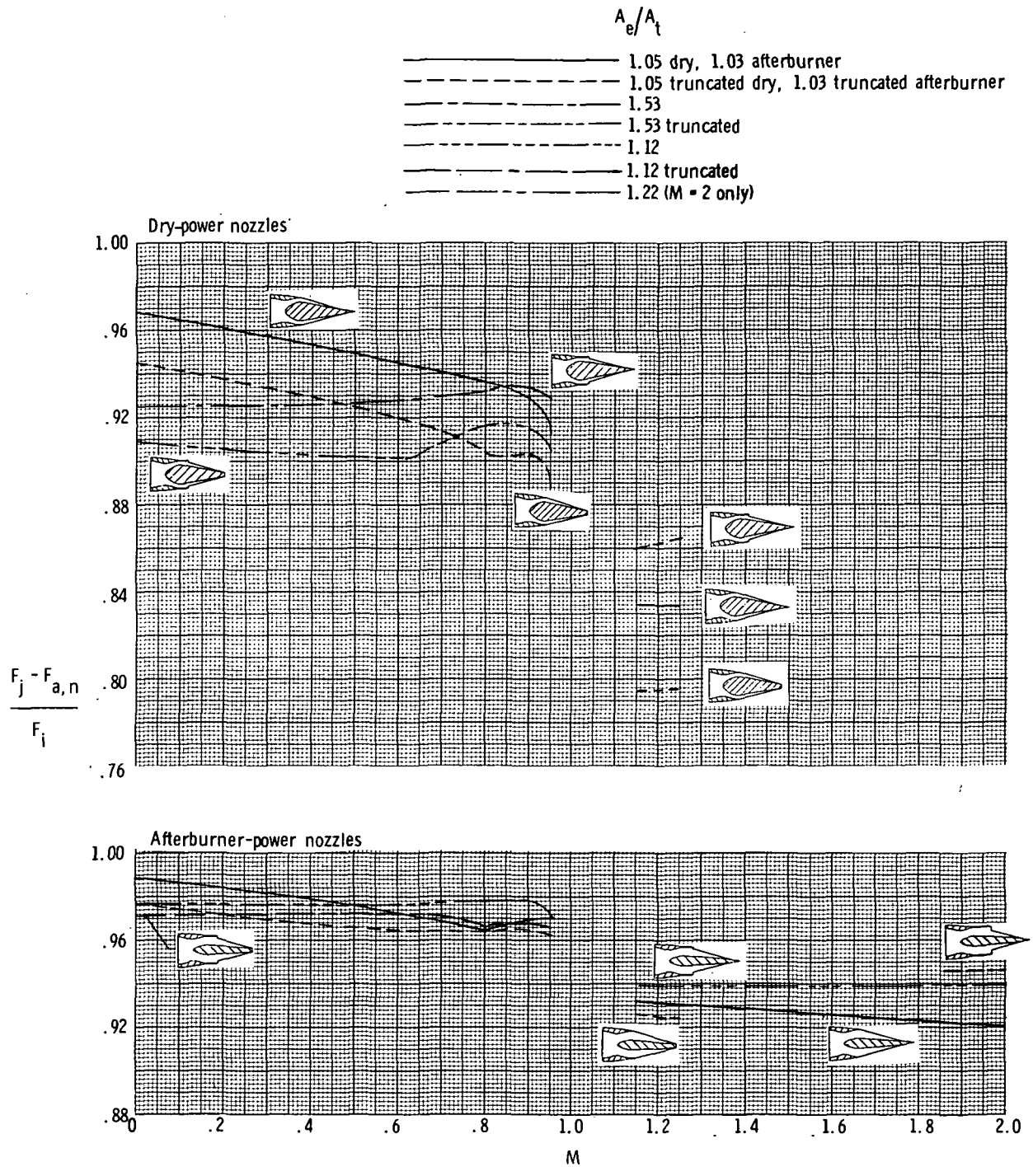

Figure 19.- Variation of thrust-minus-axial-force ratio with Mach number at a pressure ratio schedule for a high performance engine.

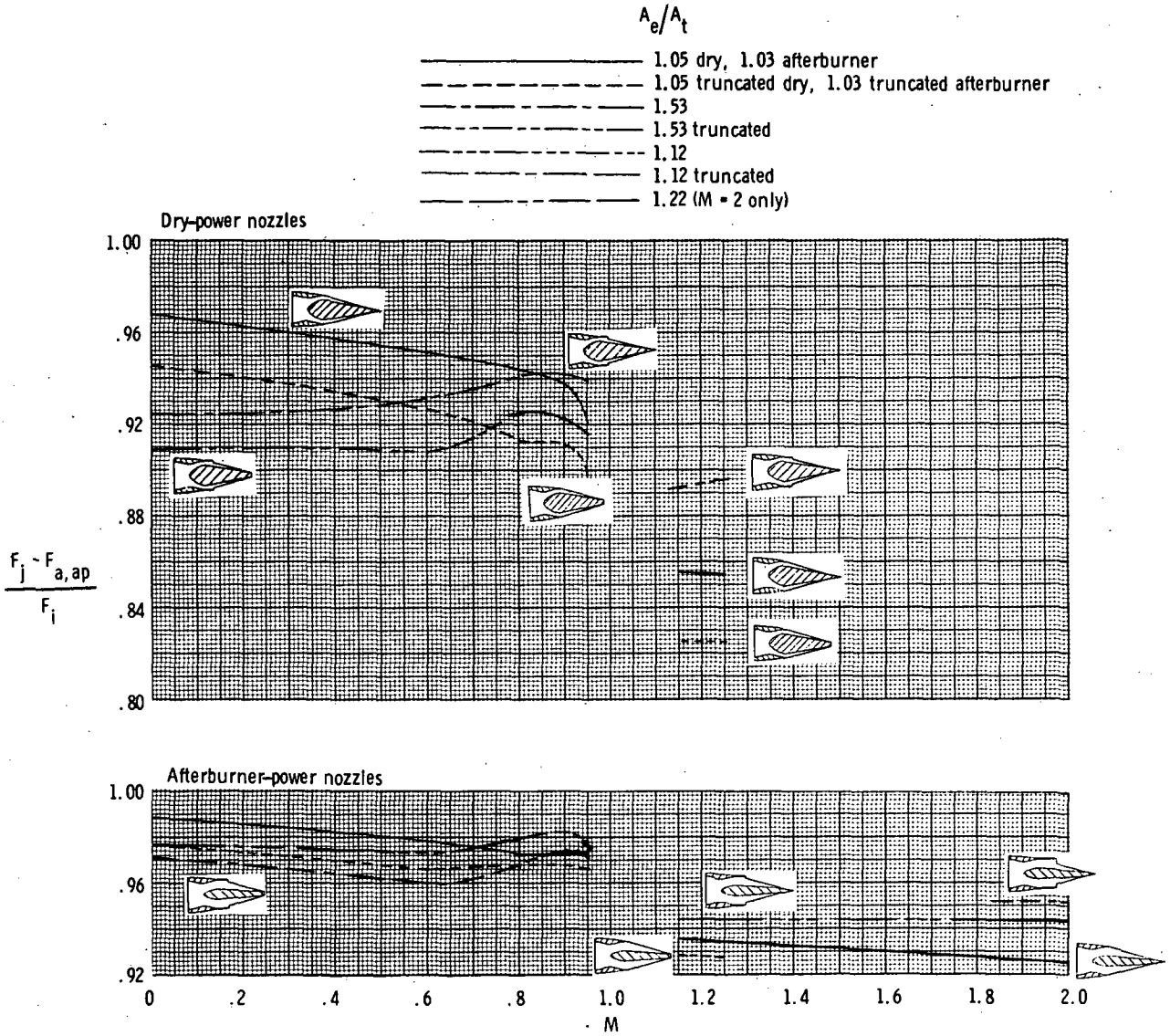

Figure 20.- Variation of thrust-minus-axial pressure force with Mach number at a pressure ratio for a high performance engine.

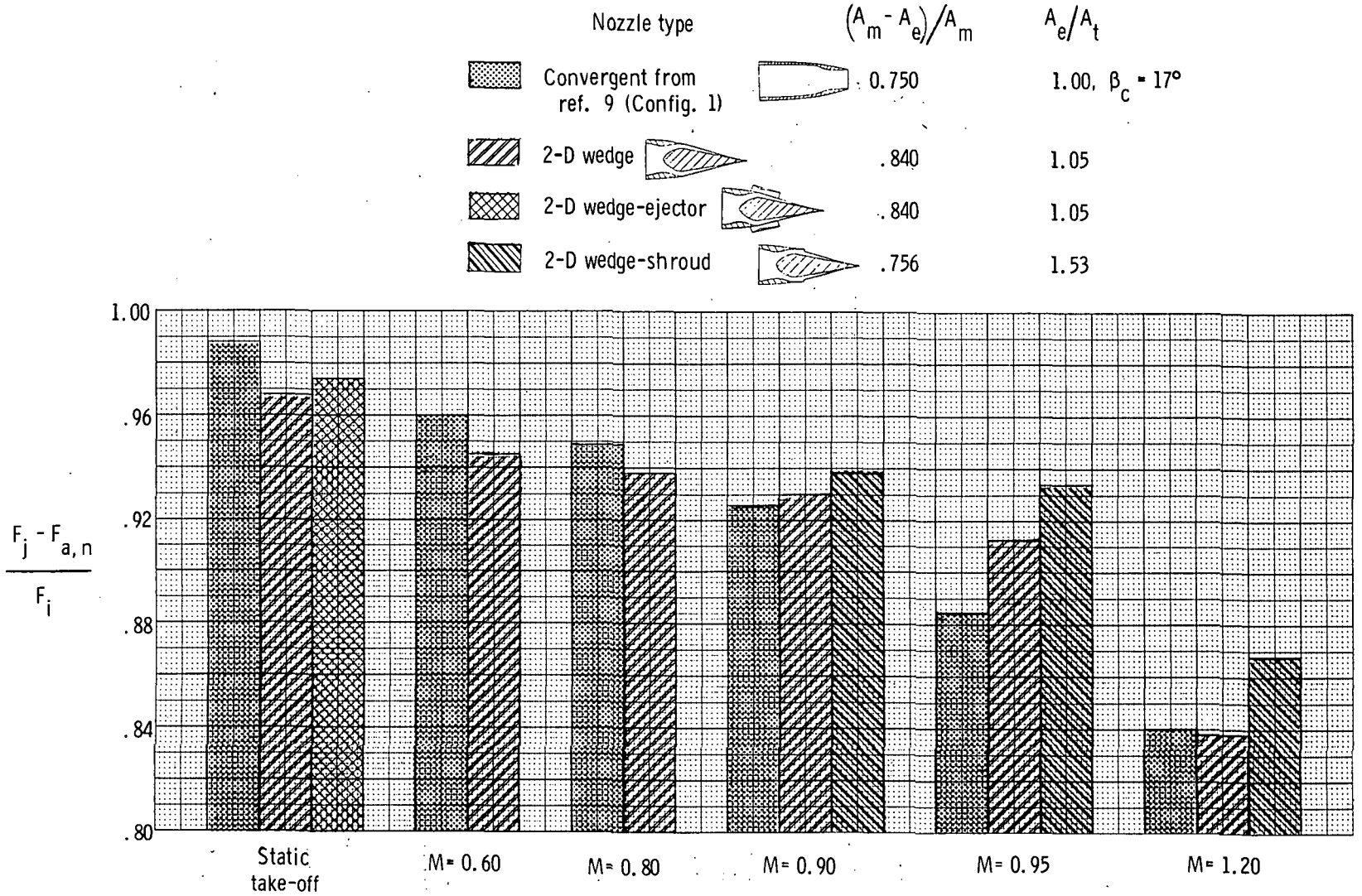

Figure 21.- Dry-power two-dimensional wedge nozzle and axisymmetric convergent nozzle performance for the jet total-pressure-ratio schedule.

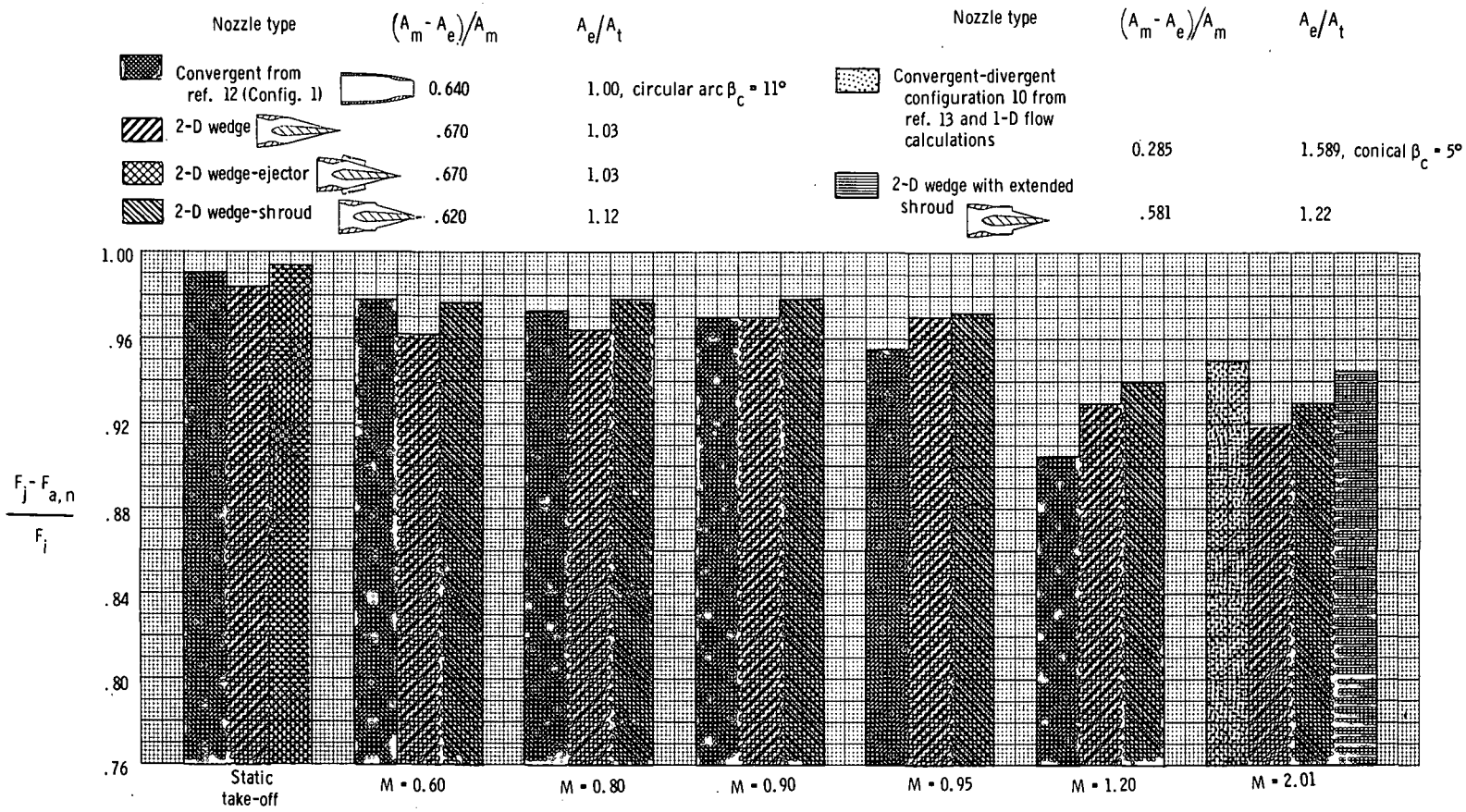

Figure 22.- Afterburner-power two-dimensional wedge nozzle and axisymmetric convergent nozzle performance for the jet total-pressure-ratio schedule.

"The aeronautical and space activities of the United States shall be conducted so as to contribute . . . to the expansion of human knowledge of phenomena in the atmosphere and space. The Administration shall provide for the widest practicable and appropriate dissemination of information concerning its activities and the results thereof."

—NATIONAL AERONAUTICS AND SPACE ACT OF 1958

NASA SCIENTIFIC AND TECHNICAL PUBLICATIONS

TECHNICAL REPORTS: Scientific and technical information considered important, complete, and a lasting contribution to existing knowledge.

TECHNICAL NOTES: Information less broad in scope but nevertheless of importance as a contribution to existing knowledge.

TECHNICAL MEMORANDUMS: Information receiving limited distribution because of preliminary data, security classification, or other reasons. Also includes conference proceedings with either limited or unlimited distribution.

CONTRACTOR REPORTS: Scientific and technical information generated under a NASA contract or grant and considered an important contribution to existing knowledge.

TECHNICAL TRANSLATIONS: Information published in a foreign language considered to merit NASA distribution in English.

SPECIAL PUBLICATIONS: Information derived from or of value to NASA activities. Publications include final reports of major projects, monographs, data compilations, handbooks, sourcebooks, and special bibliographies.

TECHNOLOGY UTILIZATION PUBLICATIONS: Information on technology used by NASA that may be of particular interest in commercial and other non-aerospace applications. Publications include Tech Briefs, Technology Utilization Reports and Technology Surveys.

Details on the availability of these publications may be obtained from:

SCIENTIFIC AND TECHNICAL INFORMATION OFFICE

NATIONAL AERONAUTICS AND SPACE ADMINISTRATION

Washington, D.C. 20546